REACTIONS OF SHORT-LIVED SPECIES IN A FLOWING AFTERGLOW

A thesis

presented for the Degree

of

Doctor of Philosophy in Chemistry

in the

University of Canterbury

by

J.P. Liddy

University of Canterbury

1976

CONTENTS.

PUBLICATION.

The following paper relating to the research described in this thesis has been published:

"Laboratory Measurements of some Ion-Molecule Reactions related to Sulphur Chemistry in Interstellar Clouds", J.P. Liddy, C.G. Freeman, and M.J. McEwan, Astrophys. Lett., 16, 155 (1975).

ABSTRACT.

A steady-state flowing afterglow method has been used to measure rate coefficients for a number of positive ion-molecule reactions. A description of the technique and the method of data analysis is given.

Rate coefficients for proton transfer from H_3^+ to neutral species XCN have been found to be in good agreement with those predicted by the ADO (or AQO) theory for X = H, CH_3, Cl, and CN. For X = Br, I, the experimental rate coefficients were lower than predicted by the ADO theory by 37% and 48% respectively.

Rate coefficients have been measured for a number of reactions relating to the formation and destruction of sulphur-containing molecules and of hydrogen cyanide in interstellar gas clouds. These new laboratory measurements produce no major changes in mechanisms proposed by other authors for the chemistry of these molecules in interstellar clouds.

A large rate coefficient has been measured for the endothermic charge-transfer reaction between S^+ and H_2S, and this is thought to indicate that significant amounts of excited S^+ are present in the afterglow when S^+ is formed by the reaction of He^+ with sulphur-containing molecules.

CHAPTER 1

REVIEW AND INTRODUCTION.

1.1 THE DEVELOPMENT OF ION-MOLECULE REACTION STUDIES.

Well before the turn of the century, conductivity measurements on flames, and gases subjected to electrical discharges, led scientists to conclude that ions must be present in such systems. The interaction between ions and neutral species in gases was considered in 1905 by Langevin, who derived a theory of the ion-neutral collision process.[1] The fact that chemical reactions take place between ions and neutral species was recognised in the early days of mass spectrometry. The first report of the effect of such a reaction was made by J.J. Thomson in 1912.[2] In his study of the mass spectrum of hydrogen he noticed the appearance of a line in the mass spectrum corresponding to a particle with a charge-to-mass ratio of three. The ion was correctly identified as H_3^+, and was recognised as arising from secondary processes in the mass spectrometer ion source.[3,4] In 1925, the process leading to the formation of H_3^+ was correctly suggested[5] to be

$$H_2^+ + H_2 \rightarrow H_3^+ + H \qquad (1.1)$$

although the rate of this reaction was not measured until 1957.[6] Other ion-molecule reactions were observed during this early period. For example, in 1928 both positive and negative ions arising from secondary reactions in iodine vapour were observed.[7]

In the years following 1930, the main interest of mass spectroscopists was in the primary processes in the ion source, and in the development of the mass spectro-

meter as an analytical device. A great improvement in high-vacuum technique and increases in the sensitivity of ion-detecting devices allowed mass spectra to be recorded at much lower pressures than were previously possible. At these lower pressures the extent of secondary reactions was greatly reduced, although such reactions were not completely eliminated. For example, attempts to determine the natural abundance of the hydrogen isotope HD at mass 3 by mass spectrometry were complicated by the presence of H_3^+ formed by reaction (1.1) [8,9]

Although there was little direct interest in the secondary reactions occurring in the mass spectrometer ion source during the period 1930-1950, new reactions continued to be discovered. Thus, for example, the ion H_3O^+ was observed in the mass spectrum of water vapour,[10] and the ion N_2H^+ in the mass spectrum of a nitrogen-hydrogen mixture.[11] A significant development during this period was the calculation of the rate constant for reaction (1.1) by Eyring et al.[12] using absolute reaction rate theory. Their calculated value of $2{\cdot}069 \times 10^{-9}$ cm^3 molecule^{-1} s^{-1} was later shown to be in excellent agreement with a value of $2{\cdot}1 \times 10^{-9}$ cm^3 molecule^{-1} s^{-1} determined by the ion cyclotron resonance method,[13] and values ranging from $1{\cdot}3$ to $2{\cdot}9 \times 10^{-9}$ cm^3 molecule^{-1} s^{-1} determined in mass spectrometer ion source measurements.[6,14-16]

Interest in the secondary processes occurring in the mass spectrometer ion source was re-awakened in the early 1950's. In Russia Tal'roze and Lyubimova [17] commenced a study of reactions of the type

$$XH^+ + YH \rightarrow XH_2^+ + Y \qquad (1.2)$$

where XH = YH = CH_4, C_3H_6, C_4H_8, and H_2O. About the same time, a number of groups in the U.S.A. measured rate constants for reactions of the general type (1.2).[18-20] A theory for calculating rate constants for reaction between charged and neutral species was also developed at this time.[21]

The large rate constants measured for many ion-molecule reactions led to the realization that such reactions could play an important role in such fields as radiation chemistry, flame chemistry, and the chemistry of gas discharges. A development of the late 1950's was the measurement of the composition of the ionosphere by rocket-borne mass spectrometers. Ion-molecule reactions played a fundamental role in interpretation of these measurements. To obtain more data of relevance to such systems, a number of new techniques for the study of thermal energy ion-molecule reaction rates were developed during the 1960's. These techniques, described in the following section, generally offered greater versatility than was possible in the mass spectrometer ion source.

Some idea of the rapid growth of interest in ion-molecule reactions may be gained from the number of publications dealing with the subject. In 1957, Field and Franklin devoted about seven pages of their book [22] to the secondary reactions occurring in mass spectrometer ion sources. This covered most of the information then available, and consisted mainly of observation of appearance potentials and pressure dependence of secondary ion intensities, with few rate constants being reported. The review of Lampe et al. [23], published in 1961, lists

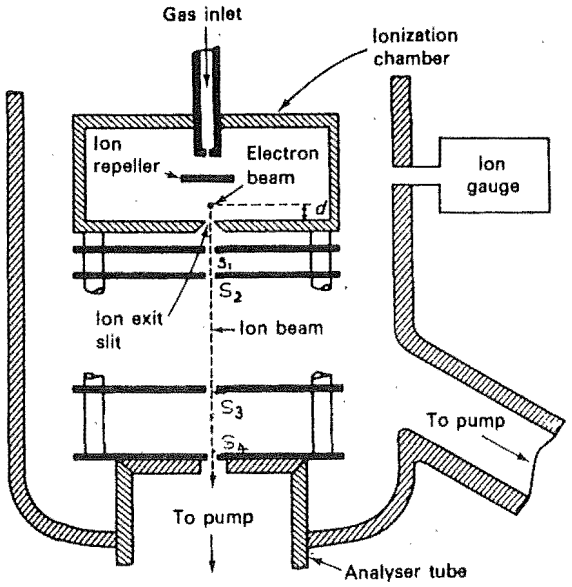

FIGURE 1.1 A typical mass spectrometer ion source used for ion-molecule reaction studies.

50 rate constants known at that time. Since the early 1960's however, review articles and compilations of data have been appearing at intervals of a year or two, and a number of books on the subject have been published. A selection of these reviews and books is listed in references 22-30. To date, rate constants have been determined for many hundreds of ion-molecule reactions.

1.2 METHODS FOR MEASUREMENT OF ION-MOLECULE REACTION RATE CONSTANTS AT THERMAL ENERGIES.

1.2.1 The Mass Spectrometer Ion Source

If the pressure in a mass spectrometer ion source is high enough (typically above 10^{-5} torr) some ions will undergo collision and possibly reaction with neutral species during their passage out of the ionization chamber. A typical mass spectrometer ion source used for reaction rate studies is shown in figure 1.1. The ionizing electron beam is confined by electric and magnetic fields to a narrow well-defined region of the ionization chamber. Ions produced by electron impact in this region are swept out of the ionization chamber through its exit slits by an electric field (the repeller field). The ions are accelerated and collimated in the slit system S_1- S_4 and then enter the mass analyser. Reaction is effectively quenched as the ions exit from the ionization chamber, due to the lower pressure and higher ion energies in the collimating and analyser regions. If the primary ion undergoes reaction in the ionization chamber, the relationship between the secondary ion current I_s, and the primary ion current, I_p, is given by

$$I_s/I_p = 1 - \exp(-N_m \bar{q} d) \qquad (1.3)$$

where N_m is the number density of the neutral reactant, $\bar{q}$ the average cross section for the reaction, and d the distance between the electron beam and the ionization chamber exit slit. If the ratio I_s/I_p is small, equation (1.3) may be approximated by

$$I_s/I_p = N_m\bar{q}d \qquad (1.4)$$

obtained by expanding the exponential, retaining only the first two terms.

The primary ions formed in the electron beam are moved out of the ionization chamber with a continuously increasing velocity, due to the presence of the repeller field. Since reaction cross sections are generally energy-dependent, the cross section $\bar{q}$ obtained from (1.4) represents an average of the cross section q(E) over the range of energies present, from thermal energies up to a value of Vd, where V is the strength of the repeller field. The measured quantity $\bar{q}$, obtained by application of equation (1.4), is referred to as the phenomenological cross section, and will not be directly applicable to reactions occurring at thermal energies.

To measure the rate constants for reactions in which both the ionic and neutral species have thermal distributions of kinetic energy, the pulsed ion source has been developed.[31] Ions are produced with a thermal distribution of velocities by a short pulse of electrons. Following this ionization pulse, there is a variable delay period during which no voltages are applied inside the ionization chamber, and ion-molecule reactions take place at thermal energies. At the end of the delay period a high repeller field pulse is applied to move ions from the ionization chamber into the analyser region in a time too short for

further significant reaction to occur. Rate constants are determined from the measured primary and secondary ion currents, the neutral reactant density, and the length of the delay period. The pulsed ion source technique, adopted by a number of different groups, [32-34] allows reaction time to be controlled independently, unlike the continuous widthdrawal technique in which decreasing the reaction time by increasing the repeller field strength necessarily alters the range of ion energies. A modification of the pulsed ion source technique permits rate constants to be measured as a function of reactant ion energy, from thermal energy up to about 3eV. [35]

A number of variations of the above techniques are possible. By employing fast differential pumping of the collimating and analyser regions, ion-source pressures of up to a few torr are possible. [36,37] At these pressures it has proved possible to determine equilibrium constants for three-body clustering reactions.[38] The conventional electron impact source has been replaced with a photoionization source, giving greater control over the state of ions formed. [14] Kebarle and co-workers have used α-radiation from Polonium to form ions in a field-free ion source at pressures of up to 200 torr. [39] Although uncertainties in reaction time do not allow accurate measurement of rate constants, a number of equilibrium constants have been determined by this latter method.[40]

A number of workers [41-44] have employed ion-trapping techniques, in which the ions formed by a short pulse of electrons are prevented from reaching the walls of the ion source (where they would be lost) by electric and magnetic fields. Ions may thus be trapped for relatively long

periods (up to several milliseconds). Because of the longer reaction times possible, lower source pressures may be used and thus reactions may be studied under conditions where the extent of collisional stabilization of intermediates is reduced.

The mass spectrometer ion source method for rate-constant determination has some shortcomings. Firstly, reactant ions may be formed in electronically or vibrationally excited states, and will not normally have sufficient time to relax to the ground state before undergoing reaction. Hence a measured reaction rate may involve an unknown distribution of reactant ion energy states. Secondly, two or more concurrent reactions may give rise to the same product, and separation of the component channels leading to that product may be difficult. An example is the simultaneous reactions occurring in an H_2 - CO_2 mixture.[45,46] The secondary ion CO_2H^+ is produced in the reactions

$$CO_2^+ + H_2 \rightarrow CO_2H^+ + H \qquad (1.5)$$

$$H_2^+ + CO_2 \rightarrow CO_2H^+ + H \qquad (1.6)$$

Thirdly, a particular ion may be produced by both primary and secondary processes, complicating the analysis. In studying charge transfer reactions,

$$A^+ + B \rightarrow B^+ + A \qquad (1.7)$$

the product ion B^+ would be readily confused with primary B^+ ion produced by electron impact on B, and a small difference current would have to be measured to determine the current due to the secondary ion. To some extent this problem has been solved by Cermak and Herman,[47] who have devised an ingenious method for preventing primary, but not secondary, ions from entering the analyser region of the mass spectrometer.

1.2.2 The Pulsed Stationary Afterglow

If a gas or gas mixture is subjected to a pulsed discharge, ions and other energetic species are produced. By monitoring the composition of the discharged gas as a function of time after cessation of the discharge, rate constants for the removal of ionic species can be found. Radiofrequency discharges or high energy (~MeV) electron beams are commonly used to produce the ions, and the discharge may be applied as either a single or repetitive pulses. The composition of the afterglow is usually determined by mass spectrometric sampling of the discharge through a small orifice at the wall of the reaction vessel.

Rate constants are obtained in the following manner. The loss rate of A^+ by reaction

$$A^+ + B \rightarrow \text{products} \qquad (1.8)$$

is given by

$$-d[A^+]/dt = k[A^+][B] \qquad (1.9)$$

where $[A^+]$ and $[B]$ are the concentrations of A^+ and B respectively, and k is the binary rate constant for the reaction. Integrating equation (1.9) between t= 0 and t= T, assuming [B] is constant, yields

$$\log_e ([A^+]_T / [A^+]_0) = - k [B] T \qquad (1.10)$$

Apart from reaction, the principal loss process for A^+ is ambipolar diffusion, neglected in this analysis. In practice, the diffusive loss is minimized by carrying out the reaction in a large excess of an inert buffer gas (usually helium). If it is assumed that a measured instantaneous ion current I is proportional to the concentration of that ion in the reaction vessel, then a decay constant λ is defined

$$\lambda = - \log_e (I_0/I_T)/T = - k [B] \qquad (1.11)$$

Determining λ as a function of [B] yields the reaction rate constant. The above method of data analysis is due to Dickinson and Sayers.[48] An alternative procedure has been devised by Fite et al.,[49] in which the ratio of product and reactant ion currents is used to cancel partially the effects of electron-ion recombination and ambipolar diffusion.

The stationary afterglow method suffers from some of the same disadvantages as the mass spectrometer ion source method. Reactant ions may be produced in vibrationally and electronically excited states, and will not have time to relax to the ground state before undergoing reaction. Since the neutral reactant must be subjected to the discharge, it too may be excited. One instance where this has lead to error is in the study of the atmospherically-important reaction

$$O^+ + N_2 \rightarrow NO^+ + N \qquad (1.12)$$

The rate of this reaction is strongly dependent on the N_2 vibrational temperature.[50] Rate constants measured in stationary afterglows showed considerable variation,[51-54] in one case being over an order of magnitude too large. This variation was due to vibrational excitation of nitrogen in the discharge pulse.

Impurities produced by reactions initiated by the discharge may pose a serious problem, particularly if the discharge is pulsed repetitively, e.g. repetitive pulsing of a nitrogen-oxygen mixture leads to a rapid build-up of a nitric oxide impurity. This may be overcome to a certain extent by renewing the gas after each discharge pulse.

1.2.3 The Flowing Afterglow

The flowing afterglow technique, described in detail in chapter two, was developed during the early 1960's in the laboratories of the National Oceanic and Atmospheric Administration (NOAA) at Boulder, Colorado, [27,55] and has since been adopted by a number of other groups.[56-59] It is an extension of the discharge flow technique used to study neutral-neutral reactions, [60,61] and replaces the temporal resolution of the pulsed stationary afterglow with spatial resolution, by carrying ions formed in the discharge region down a reaction tube in a rapidly flowing gas.

This spatial separation of the discharge and reaction regions gives rise to a number of advantages. Firstly, there is usually sufficient time between production and reaction of the primary ions to ensure that any ions produced in excited states will be de-excited before undergoing reaction. Secondly a great variety of reactant ions, either positive or negative, may be produced, including those which do not correspond to stable neutral species. Thirdly, the neutral reactant need not be subjected to the discharge used to produce the primary ions. Not only does this eliminate the problem of concurrent reactions, but also ensures that the neutral reactant is present in the ground electronic and vibrational states, with a thermal distribution of velocities. If desired, however, the neutral reactant may be subjected to a separate discharge, and this facility confers on the flowing afterglow a unique ability to study the reactions of unstable neutral species, or neutral species in carefully controlled excited states.

Such reactants which have been studied in the flowing afterglow include atomic nitrogen,[62-64] oxygen,[62,63,65] and hydrogen,[66] electronically excited oxygen,[67] and molecular nitrogen at a variable, controlled vibrational temperature.[50] The flowing afterglow is the only technique by which it has proved possible to study the reactions of such unstable neutral species. The flowing afterglow technique also readily permits continuous spectroscopic observation to be made at any stage of a reaction.

Normally reactions in the flowing afterglow are carried out at room temperature. The NOAA group have measured the temperature of the carrier gas, both by Doppler linewidth and He_2 rotational intensity distribution measurements, and found it to correspond to the temperature of the flow tube walls.[27] The electron temperature in the afterglow has also been measured spectroscopically,[27] and found to be within a few degrees of the wall temperature a few centimetres from the discharge region. The NOAA group have modified their flowing afterglow apparatus to permit rate studies to be carried out over the temperature range 80K to 900K.[27, 68]

The same group have also developed the flow-drift apparatus[69] which combines the chemical versatility of the flowing afterglow with the variable energy capability of the drift tube. Using this apparatus it has been possible to measure rate constants as a function of ion-molecule relative kinetic energy over the range 0.5 - 5 eV,

thus bridging the gap between thermal energy measurements and those obtained by molecular beam experiments.

The flowing afterglow is not able to readily and accurately determine branching ratios for a reaction giving two or more products, due to mass discrimination in the ion sampling and detecting systems. This mass discrimination does not affect the determination of the overall rate constant however. Another relative disadvantage of the flowing afterglow method is the rather limited total pressure range of between 0.1 and 2 torr which may be used.

In addition to its capability for making kinetic measurements, the flowing afterglow method may also be used for thermodynamic measurements. In a number of ion-molecule reactions, equilibrium is attained under the range of conditions of reaction time and reactant concentration available. In such cases, it is possible to measure the equilibrium constant for the reaction by analysis of the approach to, and attainment of, equilibrium.[70] Two methods may be used: measurement of the rates of the forward and reverse rate constants, or measurement of reactant ion: product ion ratios leading directly to the equilibrium constant. The measured value of the equilibrium constant yields a value for the free energy change for the reaction. Measurement of the equilibrium constant as a function of temperature enables the enthalpy and entropy of reaction to be determined.[71]

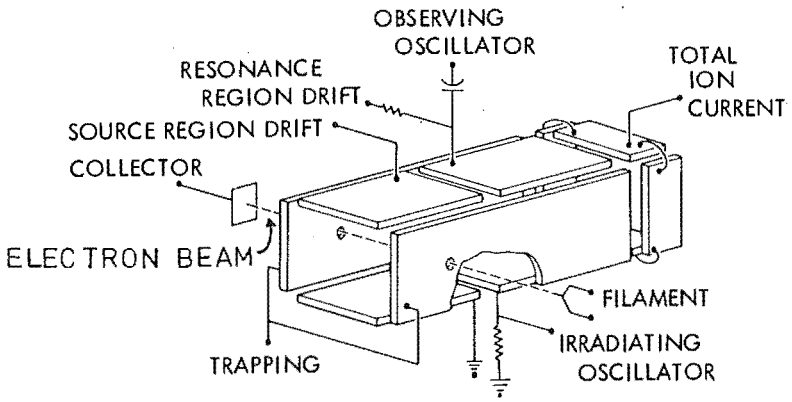

FIGURE 1.2 Schematic diagram of a drift mode cell for an ICR spectrometer.

1.2.4 Ion Cyclotron Resonance Spectroscopy.

The technique of ion cyclotron resonance spectroscopy (ICR), which has been reviewed by a number of authors,[72-74] is based on the motion of charged particles in electric and magnetic fields. An ion in a uniform magnetic field B is constrained in a circular orbit in a plane perpendicular to B, but is unrestricted parallel to B. The angular or cyclotron frequency ω_c of the orbital motion is independent of the ion velocity and is given by

$$\omega_c = q\ B/mc \qquad (1.13)$$

where q is the charge on the ion, m the mass of the ion, and c the speed of light. The radius of the orbit r is given by

$$r = mcv/qB \qquad (1.14)$$

where v is the velocity of the ion.

If an oscillating electric field of frequency ω is applied in a direction perpendicular to that of B, ions will absorb energy from the electric field when $\omega = \omega_c$, being accelerated to larger velocities and orbital radii. This absorption of energy will manifest itself as a change in the power drawn from the oscillator, and may thus be determined by using a load- sensitive oscillator. Since the cyclotron frequency for any singly-charged ion depends only on its mass and the strength of the magnetic field, a mass spectrum can be obtained by measuring the power absorbed from the oscillator as a function of magnetic field strength, while holding the oscillator frequency constant.

The cell of a conventional drift-mode ICR spectrometer is shown in figure 1.2. The direction of the magnetic field is parallel to that of the electron beam. The cell is

divided into three regions: source, analyser, and collector. Static voltages are applied to the top and bottom plates of the source and analyser regions to set up an electric field at right angles to the magnetic field. Ions are formed in the source region by electron impact and drift from there into the analyser region with a cycloidal motion under the combined influence of the electric and magnetic fields. Trapping voltages are applied to the side plates of the cell to prevent escape of ions with velocity components in a direction parallel to that of the magnetic field. The top and bottom plates of the analyser region form the capacitive element in the resonant circuit of the marginal oscillator used to apply the oscillating electric field. Resonant power absorption by ions in the analyser region of the cell will manifest itself as a change in the radiofrequency voltage level of the marginal oscillator. After drifting through the analyser region, ions enter the collector where the total ion current is measured.

At cell pressures below about 10^{-7} torr, the ICR spectrometer may be used as a mass spectrometer. Raising the pressure in the cell causes ions to undergo collision, and possibly reaction, in their passage through the cell. Since typical drift times are of the order of 10^{-3}s, a pressure of a few times 10^{-6} torr would be required to produce one reactive collision for a reaction with a rate constant of 1×10^{-9} cm^3 $molecule^{-1}$ s^{-1}.

The ICR technique was originally used for qualitative studies of ion-molecule reactions, particularly for identification of reaction channels in a complex reaction scheme,

using the technique of ion cyclotron double resonance.[75,76] A pulsed irradiating field is applied to the ICR cell at a frequency corresponding to the cyclotron frequency of the reactant ion of interest, thus increasing this ion's kinetic energy. Since an ion-molecule reaction rate normally varies with the kinetic energy of the reactant ion, the concentration of secondary ions produced by reaction of the irradiated primary ion will vary with the amplitude of the pulsed irradiating field. This variation may be detected by feeding the output of the analysing marginal oscillator into a phase-sensitive detector referenced to the pulsing frequency of the irradiating field. In this way, it is possible to establish reactant-product relationships where a particular product ion can be produced from a number of different reactant ions. This ICR double resonance technique has also been used to study the dependence of reaction rate on ion kinetic energy.[77,78] A further application of double resonance is the ion-ejection technique,[79] in which the irradiating field is used to supply sufficient energy to a particular reactant ion for its orbit to be increased to such an extent that it will strike one of the cell walls and be neutralized.

Absolute rate constants may be determined in the ICR drift cell, by measuring ion intensities as a function of drift voltage or neutral reactant pressure. Obtaining a rate constant from such data requires a detailed analysis of the integrated power absorption by primary and secondary ions in the analyser region of the ICR cell. The equations involved are complicated, and a resort to iterative techniques using a digital computer is required for exact

solution. Alternatively, various approximate solutions have been devised. Some of the approximate methods have been considered by McAllister,[80] while both exact and approximate methods have been reviewed in some detail by Anicich and Bowers.[81]

An alternative mode of operation of the ICR spectrometer is the ion-trapping mode devised by McIver.[82] Ions are produced by a short pulse of electrons and are trapped in the cell by electromagnetic fields while they undergo reaction with neutral species present. They are detected after a known and variable time delay, and then swept to the walls of the cell where they are neutralized so that the cycle can be repeated. The ion density is determined as a function of time by slowly sweeping the time delay between the ion production and detection pulses. Although McIver's original method required a specially designed ICR cell, it has since been possible to use a slightly modified drift cell for ion-trapping experiments.[83]

The ion-trapping mode of operation possesses a number of advantages over the drift mode. No calculation or measurement of the ion drift time is necessary. Also, the ion density is proportional to the instantaneous power absorption, and hence no approximations or complicated integrations of the power absorption equations are required. Rate constants may be obtained directly from plots of reactant ion density vs. time. Because long trapping times are available (up to about a second), reactions may be studied at very low pressures while ions still undergo many collisions. This reduces problems arising from pressure-broadening of the ICR absorption lines which leads to lowered mass resolution. At these low pressures

the time between collisions is long, compared with higher-pressure methods such as the flowing afterglow, and hence the effect of collisional stabilization of intermediates can be investigated.[84]

1.2.5 The Drift Tube

Although the drift tube was developed for the study of ionic mobility phenomena in gases, it has found some application in the determination of ion-molecule reaction rates. In the conventional drift tube, ions are formed in a pulsed source, often an electron impact source, and drift through the apparatus under the influence of a uniform applied electric field to an ion detector. The number of ions arriving at the detector is measured as a function of the time delay since formation of the ion pulse. The position of the maximum of such an arrival-time spectrum gives the drift velocity and mobility of the ions, while the width and shape of the spectrum is determined by the diffusion coefficients and reaction rate constant of the ions.

Although it has long been realised that impurities must be excluded from drift tubes because primary ions of interest could quickly be converted to ions of other types in ion-molecule reactions, the occurrence of such reactions in pure gases was overlooked until comparatively recently. For example, for many years it was assumed that the main ionic species detected in drift-tube studies of H_2 was H_2^+. It was not until 1960 that Varney[85] pointed out that the rapid reaction

$$H_2^+ + H_2 \rightarrow H_3^+ + H \qquad (1.1)$$

would convert essentially all the H_2^+ initially formed to H_3^+. This was confirmed by Barnes et al. a year later.[86]

Many different designs of drift tube have been developed, and are described elsewhere.[28, 87] Only three techniques will be discussed briefly here.

Beatty and Patterson [88, 89] used a drift tube to measure the rates of the reactions

$$He^+ + 2He \rightarrow He_2^+ + He \qquad (1.15)$$

and

$$Ne^+ + 2Ne \rightarrow Ne_2^+ + Ne \qquad (1.16)$$

Since the mobilities of the atmomic and molecular ions are different, the shape of the arrival time spectrum of the molecular ion will depend on the amount of drift time the molecular ion has spent as its atomic precursor. Hence rate constants for reactions (1.15) and (1.16) could be determined by fitting analytical expressions describing the combined drift-diffusion-reaction behaviour of the ions to the experimental arrival-time spectra.

McDaniel's group [90-91] have replaced the ion detector of the drift tube with a mass spectrometer, thus permitting positive identification and resolution of the ionic species present. Their drift tube is also equipped with a moveable ion source. Rate constants may thus be determined not only from the shape of the arrival-time spectra, but also from the dependence of ion signal on reaction length. A further modification of the drift-tube technique is that of Hasted's group, who have used a mass spectrometer to inject ions of a selected mass into the drift tube.[92]

Although ions will acquire some kinetic energy in their passage through the drift tube, this energy will be small compared to their thermal kinetic energy if the E/P ratio (the ratio of electric field strength to total gas pressure) is kept low, less than about $10 Vcm^{-1}$ $torr^{-1}$.[28]

It is possible to ensure that ions are in their ground state prior to reaction by imposing a delay period between their production and admission to the drift tube. The neutral gas will necessarily be in its ground state, since it is not subjected to the discharge producing the ions. The drift tube can thus be used for studying the rates of ground-state ion-molecule reactions as a function of ion kinetic energy from thermal energies upwards, by varying the E/P ratio.

1.2.6 Merging Beams

Beam techniques, in which a beam of ions of preselected mass and controlled energy is allowed to interact with a neutral species, yield much more detailed information about ion-molecule reactions than can be gained from the methods described previously. In addition to measurement of reaction cross sections, information such as the angular distribution of products and the partition of excess energy between internal and kinetic energy may be obtained. Such information is essential to the development of detailed theoretical models of reaction mechanisms. Conventional beam techniques are normally limited to ion energies in excess of a few electron-volts since the effects of space charge, spurious electric fields, and poor energy resolution become serious at low energies. Using the merging beam technique, beam measurements may be extended down to the near-thermal energy range.

In the merging-beam technique, a beam of ions is neutralized by charge transfer to give a beam of neutrals whose energy in the laboratory frame of reference is large ($\sim$ k eV). This beam is then merged with a beam of ions

travelling in the same direction and the two collinear beams are allowed to run together for a time. The ions are then separated out and detected. The interaction energy of the ion and neutral species in the centre-of-mass reference frame can be made very small by reducing the difference in energies of the two beams to a low value. The spread of the interaction energy is also very small, many times smaller than the energy spread of the individual beams. In addition to its capability for giving detailed kinematic information of ion-molecule reactions in general, the technique may be used for the study of symmetric charge transfer reactions at near-thermal energies. Further discussion of the method will not be given here. For more detailed information, the reader is referred to a review by Neynaber on the subject.[93]

1.3 APPLICATIONS OF ION-MOLECULE REACTION RATE DATA.

1.3.1 Radiation Chemistry, Flame Chemistry and the Chemistry of Gas Discharges

Rate constants for ion-molecule reactions are generally several orders of magnitude greater than those for the most rapid reactions involving neutral species, and hence ion-molecule reactions will play an important part in determining the properties of a gas in which ions may be formed. The field of radiation chemistry is one area of chemistry in which ion-molecule reactions play a large part. Prior to 1950, most chemists assumed that reactions of free radicals were of major importance in irradiated gases or gas mixtures. After the first ion-molecule reaction rate constants were measured in the mid-1950's, it was realised that such reactions could be invoked to explain the

observed product distributions in irradiated gases, [94] e.g. Thompson and Schaeffer showed that ion-molecule reactions involving H_3^+ as a chain propogator were important in determining the amount of HD formed on α-radiolysis of H_2-D_2 mixtures.[95]

Similarly ion-molecule reactions will play an important role in determining the characteristics of gas discharges and flames. The main loss mechanisms for ions in such systems are electron-ion recombination and ambipolar diffusion. Since the recombination coefficients of molecular ions are generally several orders of magnitude greater than those for atomic ions, the loss rate by recombination will depend on the nature of the ions present. Similarly the diffusive loss will be dependent on the mobility, and hence the type, of ions present. Thus transformation of an ion of one type into one of a different type in an ion-molecule reaction will affect not only the ionic composition but also the electron and ion loss rate.

1.3.2 Molecular Energetics

If an ion-molecule reaction rate constant is observed to be large (about one reaction per collision) it can be concluded that the reaction is not endothermic, and this may reveal new information on molecular energies. Thus if the charge-transfer reaction

$$A^+ + B \rightarrow B^+ + A \qquad (1.17)$$

is observed to be rapid, it can be concluded that the ionization potential of A is greater than that of B. Although ionization potentials are usually directly and accurately determined by other methods, electron affinities are not so well known and negative-ion charge transfer reactions may provide useful information in this regard.

One example where useful electron affinity data was obtained arose from the observation[96] that the reaction

$$NO^- + O_2 \rightarrow O_2^- + NO \qquad (1.18)$$

was rapid. This observation established that the electron affinity of NO was less than that of O_2, the latter quantity being fairly well known.[97] The upper limit thus placed on the electron affinity of NO was in disagreement with an earlier measurement.[98]

A scale of relative gas-phase acidities of some organic and inorganic Bronstead acids has been set up[99,100] by observing the preferred direction of reaction for reactions of the type

$$A^- + BH \rightarrow AH + B^- \qquad (1.19)$$

In a similar manner a scale of relative proton affinities has been established [101] by observing the preferred direction of reaction for reactions of the type

$$AH^+ + B \rightarrow BH^+ + A \qquad (1.20)$$

If it proves possible to measure an equilibrium constant for an ion-molecule reaction, the magnitude of the free energy change of the reaction may be determined from the relationship $\Delta G^\circ = - RT \ln K$. The enthalpy of reaction may then be calculated from the relationship $\Delta G^\circ = \Delta H^\circ - T\Delta S^\circ$ if a value of ΔS° is available, either calculated or determined from measurement of ΔG° as a function of temperature. The enthalpy of reaction, when combined with other thermodynamic information, can lead to values for various other thermodynamic quantities, e.g. suppose ΔH° has been determined for the reaction

$$A^- + BH \rightleftharpoons B^- + AH \qquad (1.21)$$

Then

$$\Delta H^\circ = \Delta H_f^\circ (B^-) + \Delta H_f^\circ (AH) - \Delta H_f^\circ (A^-) - \Delta H_f^\circ (BH) \qquad (1.22)$$

If the heats of formation of AH, BH, and A^- are known, then $\Delta H_f^\circ (B^-)$ is readily calculated. This leads directly to a value for the proton affinity of B^- for example, or combined with a value for $\Delta H_f^\circ (B^-)$, gives the electron affinity of B. For further discussion of studies of this type, see reference 56.

1.3.3 The Ionosphere

The chemical and physical processes occurring in the earth's ionosphere have been reviewed in detail elsewhere[102-105] and the subject will be touched upon only briefly here.

Ions are produced in the earth's upper atmosphere mainly by absorption of ultra-violet and X-radiation from the sun by the neutral species in the atmosphere. The main ionic species thus produced in the E and F regions of the ionosphere are O^+, O_2^+, and N_2^+, and these ions undergo charge-transfer and ion-atom interchange reactions with the neutral species present. Some examples of such reactions, together with their rate constants, are :

$$N_2^+ + O \rightarrow NO^+ + N \qquad (1.23)$$

$$k = 1.4 \times 10^{-10} \text{ cm}^3 \text{ molecule}^{-1} \text{s}^{-1} \quad 106$$

$$N_2^+ + O_2 \rightarrow O_2^+ + N_2 \qquad (1.24)$$

$$k = 5.0 \times 10^{-11} \text{ cm}^3\text{molecule}^{-1}\text{s}^{-1} \quad 106$$

$$O^+ + N_2 \rightarrow NO^+ + N \qquad (1.25)$$

$$k = 1.2 \times 10^{-12} \text{ cm}^3\text{molecule}^{-1}\text{s}^{-1} \quad 106$$

$$O^+ + O_2 \rightarrow O_2^+ + O \qquad (1.26)$$

$$k = 2.0 \times 10^{-11} \text{ cm}^3\text{molecule}^{-1}\text{s}^{-1} \quad 106$$

The rapid rates reactions (1.23) and (1.24) account for the low N_2^+ density observed in the E and F regions of the ionosphere in spite of its rapid production there. The slower reactions (1.25) and (1.26) are important in controlling the electron density of the ionosphere, since they convert atomicions, which have low electron-ion recombination coefficients, into molecular ions, which recombine rapidly with electrons.

In the D region of the ionosphere, below about 90 km, ion-molecule chemistry becomes very complex. Because of the higher pressure at these lower altitudes, the role of three-body reactions and reactions of minor neutral species becomes important. The occurrence of metal ions and negative ions further complicates the ion chemistry in this region. The cluster ion $H_3O^+ \cdot H_2O$ is the dominant ion up to about 80 km, and, as yet, no completely satisfactory model for its formation has been proposed.

Space probes of the atmospheres of Mars and Venus have lead to an interest in the ion-molecule reactions occurring there, and some reactions relevant to the predominantly-CO_2 atmospheres have been studied.[107,108]

1.3.4. Astrophysics

The clouds of gas between the stars consists mainly of hydrogen at densities ranging from 10^8 cm^{-3} down. The temperature of such clouds lies in the range 5 - 200 K. Until less than ten years ago it was believed that the only molecular species present in these clouds were simple diatomic molecules, such as CH, CN, and OH. In 1968, the polyatomic molecules NH_3 and H_2O were detected in interstellar clouds by radio astronomy [110], followed shortly after by the detection of formaldehyde.[111] To date more than twenty different molecules have been detected,[112] the most complex being organic molecules containing up to seven atoms. The most abundant molecule, after hydrogen, is carbon monoxide. For a typical cloud with a hydrogen density of 10^4 cm^{-3}, the CO density is about 1 cm^{-3}, with the densities of other molecules being two or more orders of magnitude below that of CO.

In the less dense interstellar clouds where appreciable ultra-violet radiation can penetrate, molecules will be destroyed by photo-dissociation in a period of 100-1000 years.[113] In more dense clouds, shielding by the dust grains found in such clouds will effectively eliminate photo-dissociation as a removal mechanism for molecular species. Dissociation by high-energy cosmic rays may still be important though, and adsorption onto the surface of the dust grains may become an important loss mechanism. At typical grain temperatures of a few tens of degrees Kelvin, the lifetime of a molecule against such adsorption has been calculated [113] to be about 10^5 years. Because of these loss mechanisms, there must be some process producing

molecules in these clouds.

Three-body reactions do not provide an adequate production mechanism, for the time scale for such reactions at the low interstellar densities is greater than the age of the universe. Reactions on the surfaces of dust grains have been postulated,[114] and could lead to formation of a number of the observed molecules. The mechanism of such reactions, the nature of the grain surfaces, and the mechanism for removal of molecules from the grain surfaces are all poorly understood however. Reactions between neutral species have been proposed,[115] but are unable to account for the formation of the more complex molecules observed. Also, such reactions often involve activation energy barriers, and will thus be exceedingly slow at the low temperatures prevailing in interstellar clouds.

Recently ion-molecule reaction schemes have been suggested to account for formation of molecules in interstellar clouds.[116-118] Although the degree of ionization is low (electron density is less than 10^{-4} of the neutral hydrogen density [109]) ion-molecule reactions are likely to be important for two reasons. Firstly, their rate constants are generally several orders of magnitude greater than those for reactions between neutral species. Secondly, ion-molecule reactions do not generally involve activation energy barriers and so will proceed rapidly at the low interstellar temperatures.

Rate constants for a number of ion-molecule reactions of relevance to postulated interstellar reaction schemes have been measured, principally by the flowing afterglow method.[59, 119-121] Although laboratory rate constants have usually been measured at a temperature of 300K, such

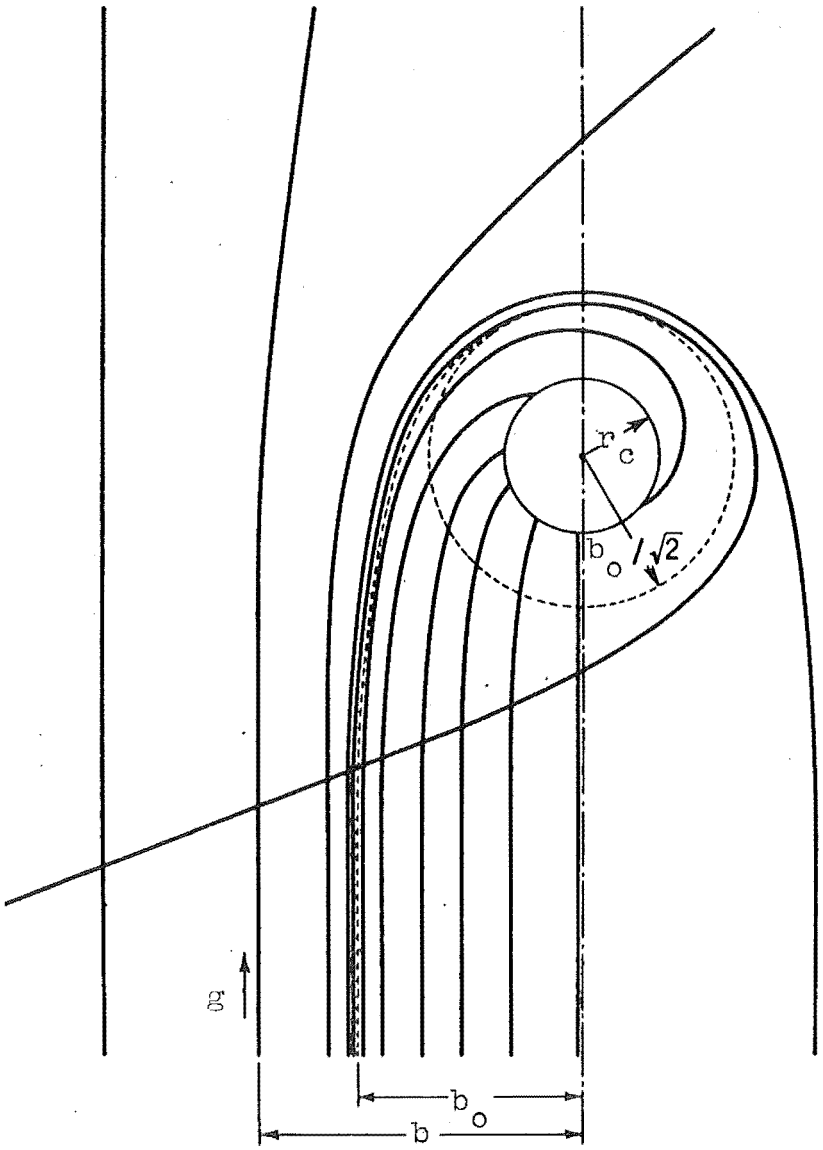

FIGURE 1.3 A typical family of trajectories for an ion-molecule encounter.

data will, in most cases, be directly applicable to reactions occurring at very low temperatures because fast ion-molecule reactions generally show little dependence of rate on temperature.

1.4 THEORIES OF THERMAL-ENERGY ION-MOLECULE REACTION RATES.

The first general approach to the calculation of ion-molecule reaction rate constants was that of Gioumousis and Stevenson,[21] who derived an expression for the rate constant for collision between a neutral species having a thermal distribution of velocities, and an ion having a velocity distribution corresponding to acceleration in the repeller field of a mass spectrometer ion source. The theory is based on the long-range attractive forces produced if the approaching ion is able to polarize the neutral molecule. The ion-induced-dipole potential V is given by

$$V(r) = - q^2\alpha/2r^4 \qquad (1.27)$$

where q is the charge on the ion, α the average polarizability of the neutral, and r the separation between the ion and the neutral species, both considered as point particles. The trajectories of particles moving under such a potential have been considered by Langevin.[1] (A translation of Langevin's paper appears as Appendix II of reference 87). A trajectory is initially characterized by two parameters, the relative velocity of the two particles, g, and the impact parameter b, which is the distance between the initial part of the trajectory and a parallel line drawn through the centre of the target molecule. A typical family of trajectories is shown in figure 1.3. There is a critical value b_o of the impact parameter such that for a

trajectory with $b=b_o$, the particles will enter a circular orbit of radius $b_o/\sqrt{2}$ about each other. For $b>b_o$, the two particles will approach no closer than $b_o/\sqrt{2}$, while for $b<b_o$, the two particles will spiral inwards towards each other, giving a long-lived orbiting collision complex. This inward spiralling will proceed only until short-range repulsive forces, not included in (1.27), become dominant. The value of the critical impact parameter leading to capture is given by

$$b_o = (4q^2\alpha/\mu g^2)^{\frac{1}{4}} \qquad (1.28)$$

where μ is the reduced mass of the ion-molecule pair, and g is the relative velocity of the two particles.

If it is assumed that reaction will occur whenever the particles approach within a certain critical distance r_c of each other, where $r_c < b_o$, and reaction will not occur if the distance of closest approach is greater than r_c, the cross-section for reaction, $\sigma(g)$, is given by

$$\sigma(g) = \pi b_o^2 = (\pi/g).(4q^2\alpha/\mu)^{\frac{1}{2}} \qquad (1.29)$$

The general relationship between rate constant k and cross-section is

$$k = \int_o^\infty \int_o^\infty f_1(v_1) f_2(v_2) g\sigma(g) dv_1 dv_2 \qquad (1.30)$$

where v_1 and v_2 are the velocities of the two reactants, $g = v_1 - v_2$ their relative velocity, and f_1 and f_2 the distribution functions of v_1 and v_2, respectively. For a reaction occurring at thermal energy, f_1 and f_2 will be given by the Maxwell-Boltzmann distribution law. From (1.29) the term $g\sigma(g)$ is independent of v_1 and v_2, hence (1.30) is readily integrated to give

$$k = 2\pi q(\alpha/\mu)^{\frac{1}{2}} \qquad (1.31)$$

Equation (1.31) gives the capture rate constant, commonly termed the Langevin rate constant, and it is expected to

provide an upper limit to the reaction rate constant if the polarization attraction is the only significant long-range force. The analysis is limited to low energies where the polarization energy is large, or at least comparable to, the relative kinetic energy of the ion-molecule pair.

If long-range forces other than polarization attraction are operative then the Gioumousis-Stevenson analysis must be modified. For example, if the neutral molecule possesses a permanent dipole moment there is an additional term V_D in the ion-molecule potential energy expression, due to the ion-permanent dipole attraction, given by

$$V_D = -(q\mu_D/r^2)\cos\theta \qquad (1.32)$$

where μ_D is the permanent dipole moment and θ the angle between the dipole and the line of centres of the two reactants. This case was first considered by Moran and Hamill,[122] who pointed out the two extremes possible. Firstly, if the orientation of the dipole was completely random, the potential described by equation (1.32) would average out to zero, and hence the capture cross-section would be given by the Langevin expression. Secondly, if there was complete alignment or "locking in" of the dipole with the incoming ion then $\theta=0^\circ$ and the ion-molecule potential would be the sum of the ion-induced dipole and ion-permanent dipole terms:

$$V(r) = -(q^2\alpha/2r^4) - (q\mu_D/r^2). \qquad (1.33)$$

Gupta et al.[123] have derived an expression for the capture cross-section for the system whose potential is described by equation (1.33). The cross-section $\sigma(g)$ is given by

$$\sigma(g) = (2\pi q/g)(\alpha/\mu)^{\frac{1}{2}} + (2\pi q\mu_D/g^2\mu) \qquad (1.34)$$

The rate constant k is related to the cross-section by the expression

$$k = \int_0^\infty g\,\sigma(g)\,f(g)\,dg$$
$$= 2\pi q(\alpha/\mu)^{\frac{1}{2}} + (2\pi q\mu_D/\mu)\int_0^\infty (f(g)/g)\,dg \qquad (1.35)$$

where $f(g)$ is the distribution function for the ion-molecule relative velocity g. At thermal energies, $f(g)$ will be given by the Maxwell-Boltzmann distribution law, and (1.35) may be integrated to give

$$k = (2\pi q/\mu^{\frac{1}{2}})[\alpha^{\frac{1}{2}} + \mu_D(2/\pi k_B T)^{\frac{1}{2}}] \qquad (1.36)$$

where k_T is the thermal-energy rate constant at temperature T, and k_B is Boltzmann's constant.

Reactions between ions and polar molecules have been studied by a number of groups,[122-128] and it has gnerally been found that although the measured rate constants are greater than those given by the Langevin theory, they are substantially less than predicted by the locked-dipole theory, equation (1.36). This suggests that although there is some attraction between the permanent dipole and the incoming ion, locking-in does not occur. A similar conclusion has been reached by Dugan and Magee,[129] who solved numerically the equations of motion for interaction between an ion and a rotating polar molecule. Two different initial rotational energies of the dipole were assumed, and for each energy a number of random impact parameters were chosen. A trajectory was calculated for each value of the impact parameter, and capture was assumed to have occurred if the ion and the molecule approached within a certain arbitrary minimum separation. The capture cross-sections thus derived were larger than predicted by the Langevin theory, but smaller than predicted by the locked-dipole

theory.

To account for these results, a classical model for ion-polar-molecule collisions has been developed by Su and Bowers.[130] Known as the average dipole orientation (ADO) theory, it considers the effect that the thermal rotational energy of the dipole has on the degree of dipole locking. The theory assumes that the angle θ between the dipole and the line of centres of the reactants may be treated as an average angle $\bar{\theta}$ which will be a function of the ion-dipole separation r only, at a constant temperature. This average angle $\bar{\theta}(r)$ is evaluated using the expression

$$\bar{\theta}(r) = \int \theta P(\theta) d\theta \; / \int P(\theta) d\theta \qquad (1.37)$$

when $P(\theta)$ is the probability that the dipole will be orientated at an angle θ to the line of centres of the reactants. Integration of (1.37) yields $\bar{\theta}(r)$ as a complicated function of the ion-dipole potential and the initial distribution of rotational energies of the dipole. The effective potential [87] of the ion-dipole pair, which includes a term for the centrifugal effect, is given by

$$V_{eff}(r) = (L^2/2\mu r^2) - (\alpha q^2/2r^4) - (q\mu_D/r^2)\cos\bar{\theta}(r) \qquad (1.38)$$

where $L = \mu b g$ is the translational angular momentum of the system. $V_{eff}(r)$ is at a maximum at some critical value r_k of the ion-dipole separation r, and capture will occur if $r \leq r_k$. Consideration of the energy requirements for surmounting the potential energy maximum at r_k leads to an expression for the largest impact parameter, b_k, for which capture can occur. The capture cross-section σ is then given by πb_k^2, and is a function of r_k, $\cos\bar{\theta}$ at $r = r_k$, and g. By specifying r_k (i.e. when $\partial V_{eff}/\partial r = 0$) and using the value of $\bar{\theta}$ from equation (1.37), σ may be determined as a function of g. The thermal-energy rate

constant is then calculated by numerical integration of equation (1.39):

$$k = \int_0^\infty g\sigma(g)\, f(g)dg \qquad (1.39)$$

where $f(g)$ is the Maxwell-Boltzmann distribution of relative velocity g.

To facilitate ready calculation of rate constants by the ADO theory, Su and Bowers have parameterized the theory as follows.[131] The capture rate constant for reaction between an ion and a polar molecule may be written, by analogy with equation(1.36), as

$$k = (2\pi q/\mu^{\frac{1}{2}})[\alpha^{\frac{1}{2}} + c\mu_D(2/\pi k_B T)^{\frac{1}{2}}] \qquad (1.40)$$

where c is a parameter with a value between 0 and 1 which has been introduced to account for the effectiveness of locking-in of the dipole.

A number of typical random values of μ, μ_D and α were taken, and the corresponding values of k calculated from equation (1.39). This value of k was then inserted into equation (1.40) and the value of c was obtained. It was found that, at a constant temperature of 300K, c was a function of μ_D and α only, and a graph of c vs. $\mu_D/\alpha^{\frac{1}{2}}$ was plotted. Thus for any molecule whose dipole moment and polarizability are known, a value of c is readily obtained from this graph and may be used in equation (1.40) to calculate the thermal energy rate constant.

There have been a number of modifications and extensions to the original ADO theory. The parameter c is temperature-dependent, since the effectiveness of dipole locking depends on the rotational energy of the polar molecule. Values of c have been calculated as a function of $\mu_D/\alpha^{\frac{1}{2}}$ over the temperature range 50K-650K.[132] The original model, which calculated the average dipole

potential as a function of $\cos\bar{\theta}$, has been modified[133] to allow direct calculation of the average dipole potential by replacing $\cos\bar{\theta}$ with $\overline{\cos\theta}$. Although rate constants obtained from the $\overline{\cos\theta}$ model are almost identical with those given by the $\cos\bar{\theta}$ model, the former is both more justified theoretically and more simple algebraically. The ADO theory treats both the ion and the dipole as point particles. Allowance has been made[134] for the finite size of the dipole, giving negligible change in the rate constant. A number of authors [43,135,136] have suggested that, for anisotropic molecules, the average polarizability α should be replaced by the maximum component of the polarizability tensor. This has been tried[137] with near negligible effect on the rate constant.

Several comparisons have been made between experimental rate constants and those predicted by the ADO theory,[56,134,138] and the agreement is generally good. The theory has also been used to predict the dependence of rate constant on ion kinetic energy in one case,[139] again giving good agreement with experimental results.

If the neutral molecule does not possess a permanent dipole moment, ion-quadrupole attraction may play a significant part in determining the capture rate constant.[140] The ion-quadrupole potential V_Q is given by

$$V_Q = Qq(3\cos^2\theta - 1)/2r^3 \qquad (1.41)$$

where Q is the static quadrupole moment of the molecule, q the ionic charge, r the ion-quadrupole separation, and θ the angle between the quadrupole axis and the line of centres of the reactants.

The ion-molecule potential will then be given by the sum of the ion-induced dipole potential and the ion-quadrupole potential. There are two cases to be considered. In the even case, where Q and q have the same sign, V_Q is at a minimum when $\theta = 90^o$ and a maximum when $\theta = 0^o$. In the odd case, where Q and q have opposite signs, V_Q is at a minimum when $\theta = 0^o$. Rate constants calculated assuming that thequadrupole locks in i.e. setting $\theta = 90^o$ (even case) or $\theta = 0^o$ (odd case), are substantially larger than experimentally-determined values. Numerical calculations of trajectories for ion-quadrupole interactions, performed by Dugan and Palmer,[141] also indicate that complete alignment of ion and quadrupole does not occur.

Su and Bowers have developed the average quadrupole orientation (AQO) theory to account for the above observations.[142] The initial assumptions and derivation of the AQO theory are analogous to those of the ADO theory. Treatment of the angle in an average sense allows numerical calculation of thermal-energy capture rate constants k. The values of k calculated numerically for a range of values of Q, q, α and μ at 300K are then fitted to empirical expressions for k in terms of these variables. Using these parameterized equations, ion-quadrupole capture rate constants may be readily calculated.

All the above theories are purely physical theories, and make no allowance for chemical effects. Thus, for example, the presence of an activation energy barrier will cause a reaction rate constant to be less than the capture rate constant. The above theories give no information on the nature of the reaction products, except that product channels must be exothermic if the reaction efficiency

is to be unity.

An extension to the collisional theories has been developed by Light and co-workers.[143] Their theory, known as the phase-space theory, may be used for predicting product ratios where more than one reaction channel is available, and also for predicting the vibrational and electronic states of products. The theory assumes formation of an intermediate complex at a rate given by the capture rate constant. This complex then rapidly decomposes statistically into the available reaction channels. Light's original postulate [144] was that "the probability of formation of any given product in a 'strong coupling' collision is proportional to the volume of phase-space available to that product divided by the total phase-space available with conservation of energy and angular momentum." The arbitrary 'strong coupling' condition is necessary to ensure that the intermediate complex "loses all memory" of the initial state of the system so the decomposition will be statistically governed.

The phase-space theory, like the capture-rate theories, considers only the classical features of the ion-molecule interacton, completely neglecting quantum effects. Thus, for example, phase-space theory predicts [145] that the rate constant for the reaction

$$O^+ + N_2 \rightarrow NO^+ + N \qquad (1.42)$$

should be close to the capture limit at thermal energy, while experimentally it is found [50] to be about three orders of magnitude below this value for ground-state N_2. The fact that spin is not conserved in formation of an N_2O^+ doublet-state intermediate has been postulated [26] as a possible reason for the very low reaction efficiency.

Details of curve crossings between the various states of the N_2O^+ intermediate may also be important.[146]

A qualitative approach to charge-transfer reactions which takes into account chemical effects is the Massey adiabatic hypothesis.[147] The basis of the hypothesis is that, since orbital electronic velocity is much greater than the ion-molecule relative velocity, the interaction between the ion and the molecule will change so slowly that the electrons will have time to readjust themselves to the perturbation produced by the interaction without electron transfer occurring. The characteristic period of an electronic transition is given by $h/|\Delta E|$, where h is Planck's constant and ΔE the energy defect for reaction, which was originally defined as the difference in ionization potentials of the two ground-state reactants. The duration of the ion-molecule interaction is given by a/g, where a, known as the adiabatic parameter, is the collision length and g the ion-molecule relative velocity. Therefore, according to the adiabatic hypothesis, the probability of charge transfer occurring will be small if $h/|\Delta E| << a/g$. Since the adiabatic parameter is expected to be large for a spiralling Langevin-type collision, the probability of an electronic transition (i.e. charge transfer) occurring will be small unless the energy defect is close to zero. Experimental results for ion-atom charge transfer reactions support Massey's hypothesis i.e. such reactions are very slow unless they are near-resonant. However many exothermic non-resonant ion-molecule charge-exchange reactions proceed with high efficiency at thermal energy.

These results can be explained in terms of the adiabatic hypothesis if it is assumed that the product ion is formed in an excited electronic and/or vibrational state, thus reducing the energy defect. Bohme et al.[148] have explained a number of charge-transfer reactions on this basis. Recent studies [149] have suggested, however, that another factor to be considered is whether the resonant energy level of the excited product ion has a favourable Franck-Condon factor with the ground state of its neutral precursor.

It has been observed [126,130,150] that a number of charge-transfer reactions proceed with a rate greater than that expected for a capture collision process. This suggests there may be a mechanism by which electron transfer can take place at distances outside the critical impact parameter for capture. The fact that one such reaction has been observed [151] to proceed without momentum transfer is further evidence of such a process.

1.5 INTRODUCTION TO THE PRESENT WORK.

In this work, thermal -energy rate constants for a number of ion-molecule reactions have been measured by the flowing afterglow technique at a room temperature of 300K $\pm$ 2K

In chapter two, the apparatus and techniques used in making these measurements are described, and in chapter three the method for extracting rate constants from the raw experimental data is described. Chapters four to six contain results of the rate constant determinations, and dicussion of their significance. The results of this work are summarized in chapter seven, together with suggestions for further work. The rate constants reported in chapters

four to six are the averages of values determined in a number of runs. Details of the individual kinetic runs are collected in Appendix I, and Appendix II contains a listing of the computer program used in the data analysis.

The reactions studied may be divided into three broad groups. Chapter four reports the study of reactions involving proton transfer from H_3^+ to neutral species XCN where X = H, CH_3 , CN, Cl, Br, and I. All these neutral reactants, with the exception of C_2N_2, have large dipole moments and exhibit a range of polarizabilities, while the reduced mass of the ion-dipole pair varies only slightly. The experimentally-determined rate constants are compared with those predicted by the ADO and other collisional theories. Chapter five deals with the study of the reactions of a number of sulphur-containing molecules and ions. Some of these reactions are of relevance to the chemistry of sulphur in interstellar gas clouds. Chapter six reports measurements on reactions of various cyanide-containing species. Again these results are of relevance to processes occurring in interstellar clouds.

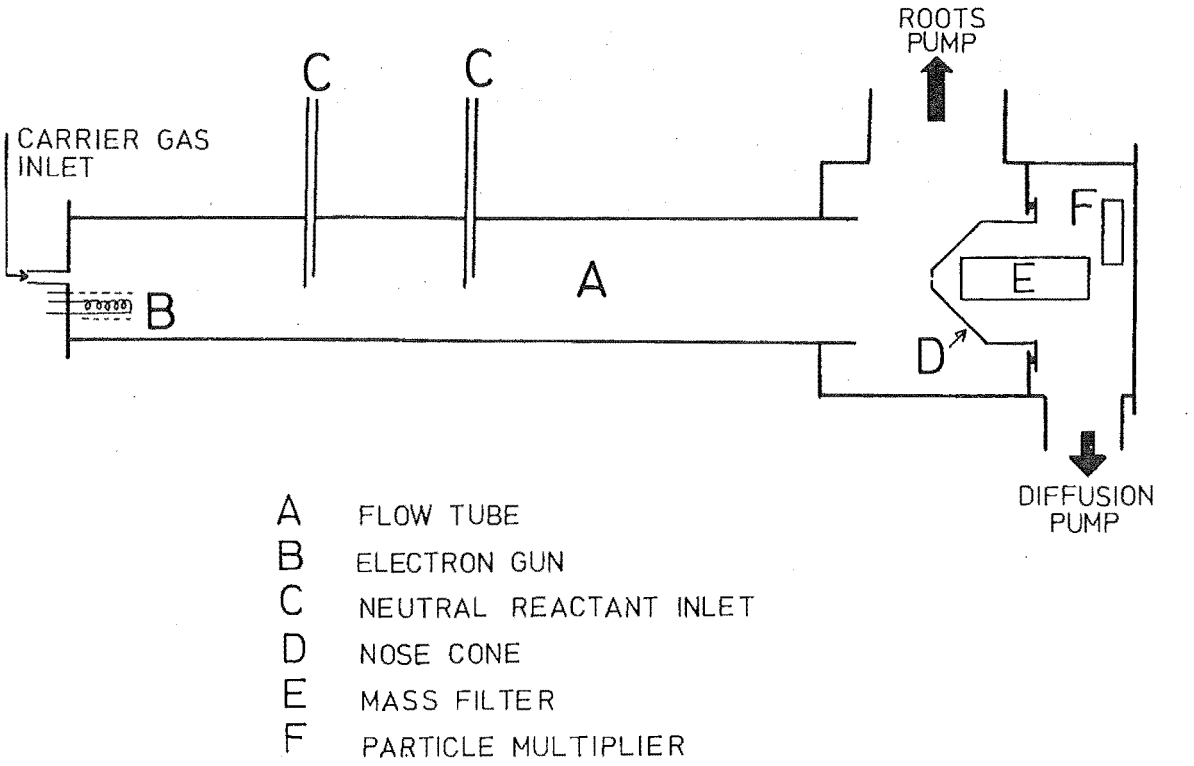

A FLOW TUBE
B ELECTRON GUN
C NEUTRAL REACTANT INLET
D NOSE CONE
E MASS FILTER
F PARTICLE MULTIPLIER

(a)

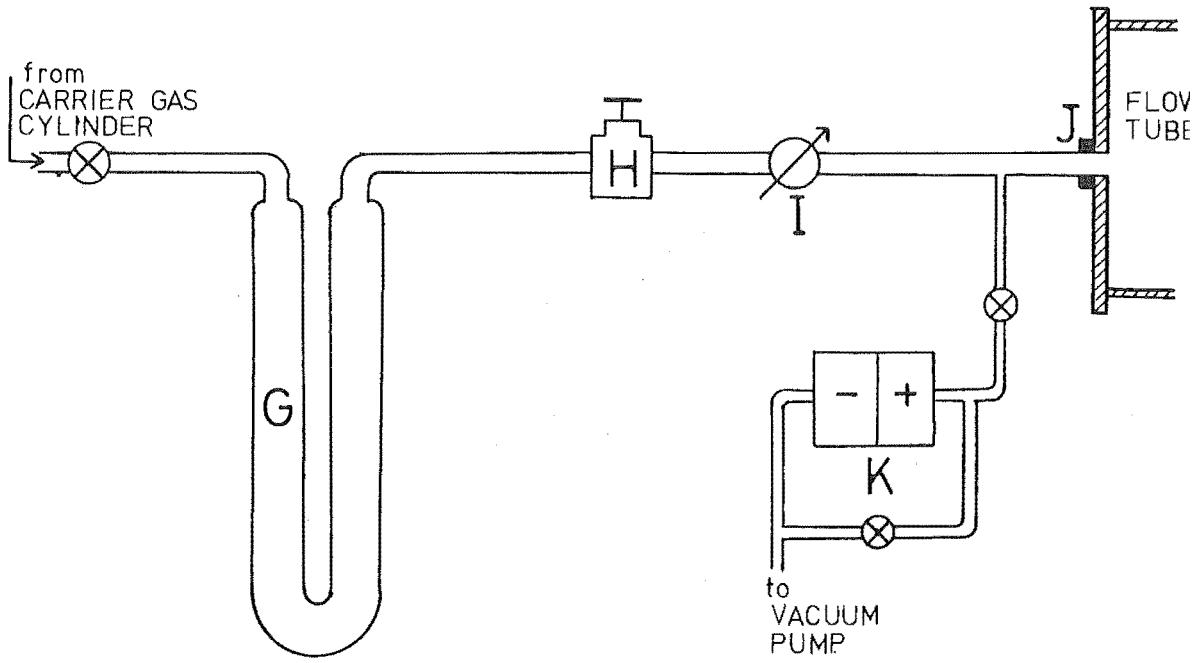

G ZEOLITE TRAP
H PRESSURE REGULATOR
I NEEDLE VALVE
J SWAGELOCK COUPLING
K PRESSURE TRANSDUCER
STOPCOCK

(b)

FIGURE 2.1 Schematic diagram of (a), the flowing afterglow apparatus, and (b), the carrier gas inlet line.

CHAPTER 2

EXPERIMENTAL.

2.1 APPARATUS.

2.1.1 General Description

The flowing afterglow apparatus is illustrated schematically in figure 2.1a. A fast flow of a suitable carrier gas (hydrogen, helium or argon in this work) is established in the flow tube A by a Roots-type blower backed by a large mechanical pump. Under typical operating conditions the pressure in the flow tube lies in the range 0.2 to 0.6 torr, with an average gas flow velocity of the order of 10^4 cm s^{-1}. Primary ions are produced in the carrier gas by means of an electron impact source B situated at the upstream end of the flow tube. The desired reactant ions are then produced by secondary reactions early in the afterglow. These ions are carried down the flow tube in the carrier gas pastthe neutral reactant inlet jets C, where a neutral reactant is added at a known rate. Reaction between ions and the neutral species takes place downstream from C. Reactant and product ions are sampled at the end of the reaction region through a small orifice at the apex of the nose cone D. The ions are then mass analysed by a quadrupole mass spectrometer, E, and detected with a particle multiplier, F.

By monitoring the intensity of the reactant ion signal as a function of the neutral reactant flow rate, the rate constant for the reaction may be determined, as outlined in chapter 3.

2.1.2 The Flow System

The flow tube is a copper tube 93 cm in length with an internal diameter of 9.48 cm. It is terminated a distance of about 9 cm from the tip of the nose cone. The gas flow in the tube is smoothly separated by the conical sides of the nose cone and exhausted through a 6-inch gate high vacuum valve (Japan Vacuum Engineering model VGH-06) and 20 cm diameter pipe to a Roots-type blower backed by a mechanical pump. The Roots blower (Japan Vacuum Engineering model PMB-020) has a maximum pumping speed of 570 l s^{-1} at 0.1 torr. The backing pump (Japan Vacuum Engineering model PKS-030) has a pumping speed of 50 l s^{-1}. Both pumps are automatically isolated from the flow tube in the event of power failure by an air-operated 8-inch gate valve (Japan Vacuum Engineering model VLP-0801).

Neutral reactants may be added into the afterglow through either of two inlet jets in the flow tube. The jets, situated 30 cm and 52.5 cm from the upstream end of the flow tube, consist of lengths of 0.7 cm o.d. glass tubing terminating on the flow tube axis. The ends of these jets are bevelled at an angle of 45^{o} to aid mixing. Some idea of the rapidity with which mixing occurs may be gained if the ion-molecule reaction taking place produces visible emission. Such studies have been carried out by Fehsenfeld et al.[55] The mixing characteristics of the type of inlet jet used in this work are illustrated in fig. 3c of reference 55.

Observation ports are fitted immediately downstream of each of the neutral reactant inlet jets. Each of these ports consists of two glass windows about 6 cm in diameter

mounted diametrically opposite each other on the walls of the flow tube.

All joints in the system are sealed with Viton A or Buna N O-rings.

2.1.3 Control and Measurement of Flow and Pressure

To obtain accurate rate constants from the flowing afterglow , it is necessary to be able to control and to measure accurately both the average flow velocity of the carrier gas and the flow rate of the neutral reactant.

The average flow velocity of the carrier gas is calculated from its measured volume flow rate and the pressure in the reaction tube. The latter is measured by an untrapped McLeod gauge whose sampling port is situated mid-way between the downstream neutral reactant inlet jet and the end of the flow tube.

The volume flow rate of the carrier gas is measured by using the carrier gas inlet port as a sonic nozzle. This method of flow measurement is outlined in reference 152. Briefly, if the pressure difference across a nozzle through which a gas is flowing exceeds a certain critical value, the gas velocity in the throat of the nozzle reaches a limiting value of the local speed of sound. Under these conditions, the volume flow rate of the gas is dependent only on the pressure upstream of the nozzle, and not on that downstream.

The carrier gas inlet line is shown in figure 2.1b. The carrier gas is widthdrawn from its cylinder and passes in turn through a refrigerated zeolite trap G, a pressure regulator H (Edwards model VPC 1), and a teflon-glass needle valve I, and then enters the flow tube through a

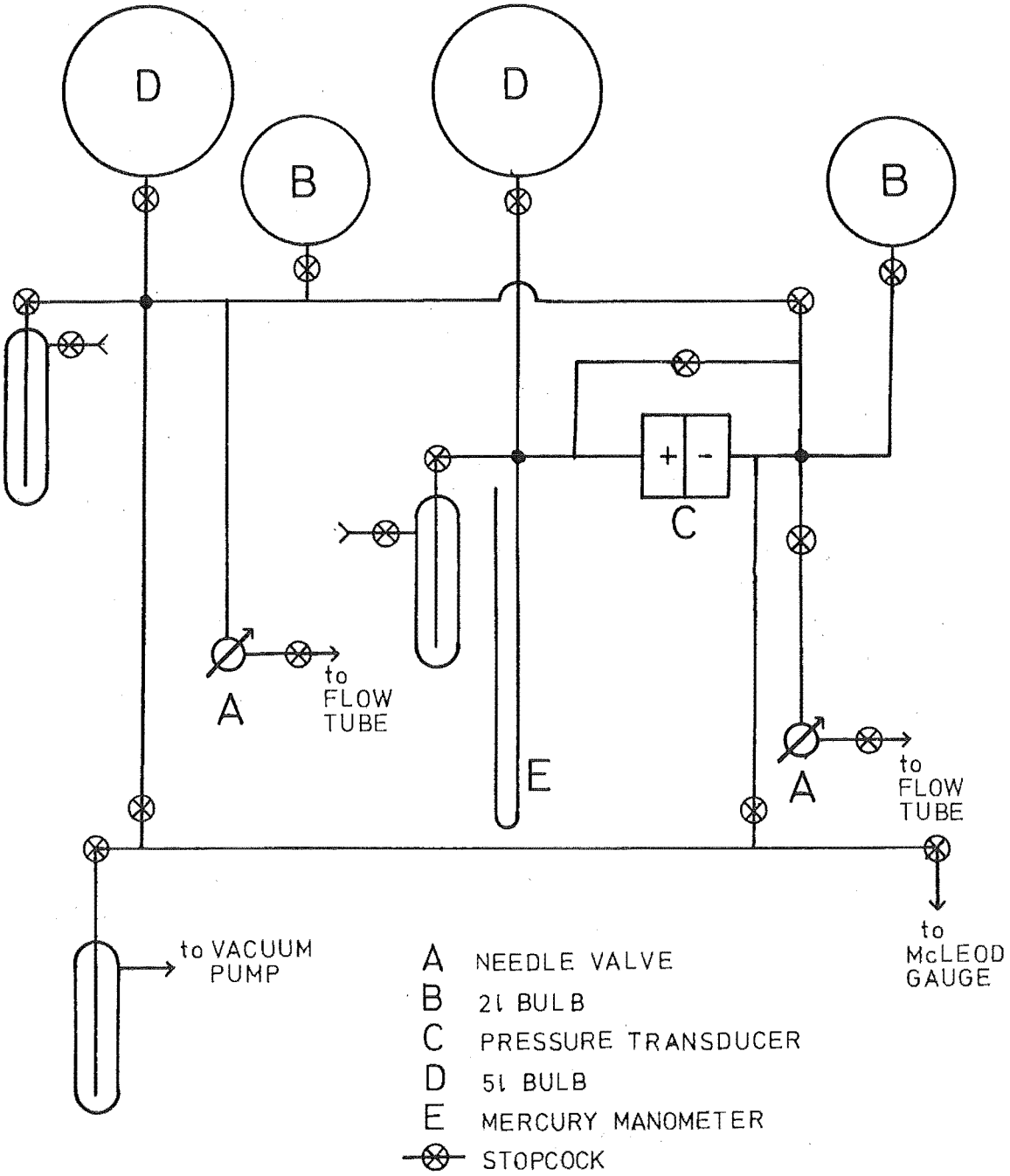

FIGURE 2.2 Schematic diagram of the neutral reactant gas handling line.

standard $\frac{1}{4}$ inch Swagelock coupling J welded to the end flange of the flow tube. No special design of the inlet nozzle was found to be necessary to achieve sonic flow conditions. The pressure is measured about 4 cm. upstream of the nozzle by a differential pressure transducer K (Celesco Industries model P7D). The reference side of this transducer was evacuated to a pressure of the order of 10^{-3} torr by a mechanical vacuum pump.

The sonic nozzle flow-meter was calibrated by connecting a commercial dry-test meter (UGI Meters Ltd.) in series in the carrier gas line and measuring with a stopwatch the time taken for the passage of a given volume of gas under steady flow conditions. For each observed flow rate, the corresponding voltage output of the transducer was noted. In this way , a linear relationship was found between the carrier gas flow rate and the transducer output, over the range of flow rates of interest. The transducer output at maximum carrier gas flow rates used in this work corresponds to a pressure immediately upstream of the nozzle of about 40 torr.

The neutral reactant is added through either of the two inlet jets from the glass line depicted schematically in figure 2.2. This line is evacuated by a mechanical vacuum pump (Hitachi model 4VP-CG) to a base pressure of 10^{-3} torr. The neutral reactant flow is controlled by Edwards type LB 1B needle valves A, and measured by monitoring the pressure drop in a constant calibrated volume. For each inlet, two calibrated volumes are available. One consists of a 2 litre bulb B, the other of the tubing between the bulb and the

needle valve, a volume of about 200 cm^3. The pressure drop in the chosen calibrated volume is measured with a differential pressure transducer C (Celesco Industries model P7D) whose output is displayed on a strip chart recorder. The neutral reactant flow can then be calculated from the linear pressure-time plots. Flow rates ranging from 1×10^{16} particles s^{-1} to about 5×10^{19} particles s^{-1} could be measured to within a few percent by this procedure.

Constant flow rates of neutral reactant can not be maintained for sufficient time for a measurement if the pressure of the reactant upstream of the needle valve is less than about 200 torr. In dealing with reactants whose vapour pressure at room temperature is less than 200 torr, the following procedure is adopted. The reactant is admitted to a 5 litre bulb D in the line at a pressure below its saturated vapour pressure at room temperature, this pressure being measured with the pressure transducer. High purity helium is then admitted to a 2 litre bulb in the line to fill it to about atmospheric pressure, this pressure being measured with a mercury manometer E. The contents of the two bulbs are then allowed to mix. The composition of the gas mixture is determined from the known pressures and volumes, assuming no condensation of the neutral reactant takes place. Condensation should not occur as the reactant pressure is chosen to correspond to its saturated vapour pressure at a temperature about $10^{o}C$ below room temperature. Once the composition of the gas mixture is known, the neutral

reactant flow rate can be determined from the measured flow rate of the mixture.

The transducer used in this work was calibrated against a quartz-Bourdon differential pressure gauge (Texas Instruments model 144) and checked periodically against a mercury manometer. The circuit diagram of the transducer control unit is shown in Appendix III.

2.1.4 The Ion Source

Ions are produced in the carrier gas by means of an electron impact source mounted on the end flange of the flow tube. This source consists of a heated filament surrounded at a distance of about 3 mm by a helical grid. The grid is maintained at earth potential while the filament has a negative voltage applied to it.

The filament consists of a 5 cm length of platinum - 13% rhodium wire 0.033 cm in diameter, and is coated with barium zirconate to improve its electron emission characteristics.[153] The coating is prepared by mixing about 5% of each of barium and strontium carbonates with barium zirconate and applying this mixture in suspension in acetone to the filament, which is then heated electrically.

The filament bias voltage can be varied from 18 to 100 V, and the emission current from 0 to 10 mA. The source is usually operated at about 2 mA emission with a filament bias of 80 to 100 V. At these electron energies, electron impact cross sections are at a maximum.

The circuit diagram of the emission control unit is shown in Appendix III.

2.1.5 Ion Sampling and Detection

Ions are sampled from the flowing plasma through a small orifice at the tip of the nose cone. They pass through one focussing electrode and then enter the quadrupole mass filter. The focussing electrode, a circular stainless steel plate with a 5 mm diameter hole at its centre, is situated about 7 mm in front of the mass filter assembly. In detecting positive ions, both the nose cone and the focussing electrode are usually maintained at a potential of about -4 V with respect to the tube walls (earth potential). The axis of the mass filter assembly is maintained at about -10 v with respect to earth by application of this bias voltage to all four rods in the filter assembly. After passing through the mass filter, the ions are detected with a particle multiplier.

The nose cone, made from stainless steel, is a 90^{o} truncated cone 9.7 cm in diameter at its base. At its front end is a disc of molybdenum 1.2 cm in diameter and 0.01 cm thick in which the sampling orifice is drilled. In this work a 0.03 cm diameter orifice was used. The nose cone is electrically insulated from the walls of the mass spectrometer chamber by teflon washers. A Viton A O-ring provides a vacuum seal between the reaction tube and the mass spectrometer chamber.

Molybdenum is the material used for the tip of the nose cone for the following reason. A variation in the sampling efficiency of the mass spectrometer has been found [27,58,65] when the material of the sampling orifice is gold, stainless steel, copper, brass, or rhodium. This variation

is particularly serious when oxygen atoms are present. The only two materials which have been found to give reliable sampling are molybdenum and carbon,[27] the latter in the form of a coating applied as an alcohol suspension of graphite.

The distance between the tip of the nose cone and the end of the reaction tube is about the same as the diameter of the flow tube. This geometry is expected to give a smooth separation of the flowing gas, and thus the gas near the front of the nose cone will characterize the central portion of the flowing plasma in the reaction tube. Ferguson and co-workers have confirmed qualitatively that the gas flow is uniformly intercepted by the nose cone, by observation of its appearance after performing experiments with metal ions.[27] These workers have also replaced the truncated nose cone with one which tapered to a sharp knife edge at the orifice.[154] Results obtained using this nose cone were identical to those obtained using truncated nose cones. It has thus been established that a stagnant sampling layer does not exist at the blunted face of the nose cone.

The stainless steel quadrupole mass filter has a length of 15.2 cm and a field radius of 0.273 cm. The power supply for the mass filter is of the voltage-scanning type and covers the mass range 1-150 amu, or 10-300 amu, depending on which of two constant frequencies is chosen. It is capable of giving unit resolution over the whole mass range. The design of the power supply is based on that of the EAI - Quad 150 A.

After passing through the mass filter the ions are

detected with a particle multiplier. In the early part of this work, a 15 - stage multiplier with Be - Cu dynodes was used (EMI model 9603/2B). It was mounted immediately behind the exit aperture, and in line with the axis, of the mass filter assembly. Positive ions were drawn into it by a voltage of - 3 kV applied to the first dynode.

This arrangement suffered from the disadvantage of a relatively high background current arising from radiation from the reaction tube reaching the first dynode of the multiplier. To eliminate this problem, the multiplier was replaced in later stages of this work with a continuous dynode particle multiplier (Galileo Electro-optics model 4219). The smaller size of this device permitted it to be mounted with its axis at right angles to the axis of the mass filter assembly. The multiplier's entrance aperture is situated about 2.5 cm behind the exit aperture of the mass filter assembly, and about 1.5 cm. from its axis. Ions are drawn into the multiplier by a voltage of - 3kV applied to its front aperture.

The output of the particle multiplier is measured with a high-speed picoammeter (Keithley model 417). The gain of the multipliers is typically 10^5 - 10^6, and their maximum output currents of the order of 10^{-7} amperes. The lowest detectable current is about 10^{-11} amperes.

The mass spectrometer chamber is evacuated to a pressure less than 5×10^{-5} torr during operation by a 4 - inch oil diffusion pump (Edwards model E04) backed with a mechanical pump (Edwards ES 150). There is a liquid-air-cooled trap between the diffusion pump and the mass spectrometer chamber. The pumping speed of the diffusion pump-cold trap combination is 400 l s^{-1} for hydrogen over the

pressure range 10^{-3} - 10^{-6} torr. Pressure is measured with an ionization gauge (Veeco RG 75 head and RG 21X controller).

One problem sometimes encountered in ion sampling was that of a reduction in the sampling efficiency with time, presumably due to a build up of charge on the surfaces of the nose cone and focussing electrode. To minimize this change in sampling efficiency the nose cone and focussing electrode are cleaned periodically. The cleaning procedure adopted consists of a vapour degreasing in trichloroethylene followed by overnight soaking in a 5% solution of Decon 90 surface active agent, and thorough rinsing in distilled water.

2.2 REACTANT ION PRODUCTION.

Reactant ions of interest are formed in the flowing plasma by adding a suitable parent gas to the afterglow downstream of the electron gun, and allowing it to react with the energetic species (ions or metastable atoms) produced by electron impact in the carrier gas. Ions of the carrier gas will produce reactant ions by charge transfer e.g.

$$Ar^+ + O_2 \rightarrow O_2^+ + Ar \qquad (2.1)$$

or dissociative charge transfer, e.g.

$$He^+ + CO \rightarrow C^+ + O + He \qquad (2.2)$$

while metastables produce ions by Penning ionization reactions e.g.

$$He\ (2^3S) + O_2 \rightarrow O_2^+ + He$$

If these reactions are rapid, only very small flows (0.1 - 1 cm^3 atm. s^{-1}) of the reactant ion parent gas are

required.

Reactant ions may also be produced by direct electron impact. In this case, the reactant ion parent gas is mixed with the carrier gas upstream of the electron gun. Relatively large flows ($\sim$10 cm^3atm. s^{-1}) of the reactant ion parent gas are required.

By varying the bias voltage applied to the filament of the electron gun, the electron energy can be controlled, and thus ion production can be selectively controlled. For example, if electron energies of less than 24.6 eV (but greater than about 20 eV) are used in a helium carrier gas, metastable helium atoms, but no helium ions, will be produced. Subsequent reaction with a neutral species such as CO will produce CO^+ ions, but no C^+ ions, which would have been produced had helium ions been present.

It is generally assumed that the reactant ions are in their ground electronic state at the point of neutral reactant addition. In a limited number of cases, other workers have shown this to be so. For example, the molecular ion N_2^+ is formed in a radiating state in the flowing afterglow by the Penning reaction

$$He(2^3S) + N_2 \rightarrow N_2^+(B^2\Sigma_u^+) + e + He(1^1S) \qquad (2.4)$$

Spectroscopic observation of the radiation emitted in the transition

$$N_2^+ (B^2\Sigma_u^+) \rightarrow N_2^+ (X^2\Sigma_g^+) \qquad (2.5)$$

showed that the N_2^+ ions radiate largely into the ground electronic and vibrational states before the neutral reactant inlet is reached.[27] Another example is offered by the atomic ion Kr^+. This ion has been produced in the flowing afterglow in the Penning reaction

$$He\ (2^3S) + Kr \rightarrow Kr^+ + He\ (1^1S) \qquad (2.6)$$

and, to some extent, by electron impact. Chemical evidence has been offered that the $^2P_{\frac{1}{2}}$ state of the Kr^+ ion has been largely de-excited by superelastic collisions with electrons before the neutral reactant inlet is reached.[155]

Such direct evidence has been obtained only in special cases. However, as the ions exist in the flowing plasma for a few milliseconds before reaching the neutral reactant inlet, there is normally sufficient time for them to be de-excited to the ground electronic state by radiative transitions or superelastic collisions with electrons. In the latter case, de-excitation cross sections need only be about 10^{-15} cm^2 for almost all the excited states to be removed. If, however, there are low-lying metastable energy levels of the ion available, then an appreciable fraction of the ions arriving at the neutral reactant inlet jet may be electronically excited. This possibility will be further discussed in chapter five in connection with the ion-molecule reactions of S^+.

2.3 THE ROLE OF IMPURITIES.

Impurities, which can confuse or falsify the data from the flowing afterglow, can arise from a number of sources. They may be released from the walls of the flow tube, or be added in with the carrier gas, the reactant ion parent gas, or the neutral reactant.

Impurities from the first two sources will be a problem if they are present in sufficient quantity to seriously deplete the reactant ion signal. Water vapour was one such impurity commonly encountered in this work.

For this reason, the carrier gases are purified by passing them through a refrigerated zeolite trap. This trap has a diameter of 3.5 cm, a total length of 200 cm, and is packed with Union Carbide type 5A molecular sieve. Impurities released from the walls of the flow tube are minimized by regularly baking the tube to about 80°C.

Impurities added with the reactant ion parent gas will not be a problem, unless they give rise to an ion signal at the same mass-to-charge ratio as the reactant ion.

More serious is the effect of impurities in the neutral reactant, although the extent to which these affect a rate constant determination depends on the particular reaction being studied. An impurity which is uniformly mixed with the neutral reactant and which reacts rapidly with the reactant ion will lead to a systematic decrease in the reactant ion signal which would mimic reaction with the added neutral reactant. If the reaction being studied is fast (reaction on almost every collision) such an effect will not be large. For slower reactions, which require large flows of the neutral reactant, the effect may be serious. In fact the rates of many slow reactions measured in the flowing afterglow can be determined only as upper limits, due to the uncertain effect of impurities.

In all rate constant determinations, a mass scan of the ions present is carried out before and after addition of the neutral reactant. Since any reactive impurity will usually give rise to an ion signal distinguishable from the products of the reaction being studied, the presence of an impurity is unlikely to go undetected and lead to an erroneous rate constant determination.

2.4 MATERIALS.

2.4.1 Carrier Gases

Three different carrier gases were used during the course of this work. They were hydrogen, helium, and argon.

Hydrogen: industrial or dry grade, supplied by New Zealand Industrial Gases Ltd. It was purified by passage through a zeolite trap cooled with liquid air.

Helium: obtained from two sources, Airco Industrial Gases, N.J., and Canadian Helium Ltd. Stated purity 99.995%. It was dried by passage through a zeolite trap cooled with liquid air.

Argon: welding grade, 99.99% pure, obtained from New Zealand Industrial Gases. It was dried by passage through a zeolite trap cooled in a dry ice-ethanol bath.

2.4.2 Reactant Ion Parent Gases, and Neutral Reactant Gases

Ammonia: supplied by the Christchurch Gas Co., 99.97% pure, and used without further purification.

Carbon Monoxide: C.P. grade, supplied by the Matheson Company, 99.5% pure. It was purified by passage through a liquid-air-cooled zeolite trap.

Cyanogen: supplied by the Matheson Company, 98.5% pure. It was purified by repeated freeze-pump-thaw cycles.

Hydrogen Cyanide: prepared by the action of phosphoric acid on sodium cyanide. It was dried over phosphorus pentoxide and further purified by trap to trap distillation.

Cyanogen chloride: prepared by admitting chlorine to a bulb containing an excess of sodium cyanide, and allowing reaction to proceed for 24 hours. Unreacted chlorine was removed by distillation at dry ice temperatures. The cyanogen chloride was then dried over phosphorus pentoxide and further purified by trap to trap distillation.

Cyanogen bromide: prepared by reacting bromine with excess mercuric cyanide. The cyanogen bromide was collected in a trap cooled to -78C, and purified by subliming it from trap to trap.

Cyanogen iodide: prepared by the method of Goy et al.[156] in which iodine was mixed with an excess of mercuric cyanide and sealed in an evacuated tube. The tube was heated fully immersed in a water bath for a few hours until reaction was complete, and was then heated partially immersed to sublime the iodine cyanide to the top of the tube. The iodine cyanide was purified by pumping under vacuum and by subliming it from trap to trap.

Methyl cyanide: analytical grade, supplied by Koch-Light Laboratories. It was purified by repeated freeze-pump-thaw cycles.

Hydrogen: dry grade, supplied by New Zealand Industrial gases. It was purified by passage through a de-oxo catalytic purifier (Englehard Industries Ltd.) and a zeolite trap cooled with liquid air.

Hydrogen sulphide: prepared by the action of phosphoric acid on solid sodium sulphide. It was dried over phosphorus pentoxide and purified by trap-to-trap distillation.

Sulphur dioxide: supplied by British Drug Houses Ltd. It was dried over phosphorus pentoxide, and purified by repeated freeze-pump-thaw cycles.

Oxygen: ultra-high purity grade, 99.95% minimum purity, supplied by the Matheson Company. It was used without further purification.

CHAPTER 3

DATA ANALYSIS.

3.1 INTRODUCTION.

Rate constants are determined in the flowing afterglow from the variation in reactant ion signal with added neutral reactant. The equations describing the reactant ion density are quite complex, and various groups have devised a number of analytical or numerical methods for solving them.[27,70,157-161] The treatment adopted here is based on that of Bolden et al.,[158] and Bohme et al.[70]

The various models used are described in section 3.2. A treatment based on an over-simplified model is first developed. This model, known as the "plug-flow" model, assumes that the carrier gas velocity is uniform throughout the flow tube, and that reaction with added neutral reactant is the only significant loss mechanism for the reactant ion. This model is then modified to take into account the actual hydrodynamic properties of the carrier gas flow, and to include radial ambipolar diffusion as a loss mechanism for reactant ions. A further modification is then made to include axial diffusion of reactant ions.

The distortion of flow patterns at the neutral reactant inlet jet has been neglected in these models. Section 3.3 describes the method used in making an empirical correction for inlet effects.

The computer program used to extract rate constants from the raw experimental data is described in section 3.4. Finally, in section 3.5, the accuracy of rate constants determined in the flowing afterglow is discussed.

3.2 THE FLOW ANALYSIS.

3.2.1 The Plug Flow Model

The decrease in concentration of the reactant ion A^+ as a consequence of addition of the neutral reactant B in the reaction

$$A^+ + B \rightarrow C^+ + D \qquad (3.1)$$

is given by

$$d[A^+]/dt = - k [A^+][B] \qquad (3.2)$$

where k is the binary rate constant for the reaction and $[A^+]$ and $[B]$ are the concentrations of A^+ and B respectively. If the axis of the flow tube is designated as the z axis, and if it is assumed that the carrier gas flow velocity v_o is constant and directed along the z axis, then (3.2) may be rewritten

$$v_o \frac{\partial[A^+]}{\partial z} = - k [A^+][B] \qquad (3.3)$$

where z is the distance from the point of neutral reactant addition.

All experiments in the flowing afterglow are performed with the neutral reactant present in far greater concentration than the reactant ion, and hence it may be assumed that $[B]$ is not affected by the reaction. Furthermore, it will be assumed that B is introduced uniformly over the cross section of the flow tube. Its concentration in the reaction zone will then be given by

$$[B] = Q/\pi a^2 v_o \qquad (3.4)$$

where Q is the rate of introduction of B in particles s^{-1}, and a is the radius of the tube. Equation (3.3) may now be

integrated to yield

$$\log_e ([A^+]/[A_o^+]) = - (k[B]/v_o) \int_o^L dz$$

$$= - QkL/\pi a^2 v_o^2 \qquad (3.5)$$

where L is the length of the reaction zone (the distance from the neutral reactant inlet to the tip of the nose cone), and $[A_o^+]$ the concentration of A^+ in the absence of any reaction.

Rate constants may be determined by observing the variation in $[A^+]$ when any one of the parameters Q, L, or v_o, in (3.5) is varied. In this work, the only parameter varied was the rate of neutral reactant addition, Q. Differentiating (3.5) one obtains

$$k = - (\pi a^2 v_o^2/L) (d \log_e [A^+] /dQ) \qquad (3.6)$$

The rate constant may then be determined from the slope of a plot of $\ln [A^+]$ vs. Q.

3.2.2 Non-uniform Velocity Profile and Radial Diffusion corrections

It has been assumed in the plug flow model that chemical reaction is the only loss mechanism for A^+ ions. This is not so. The concentration of A^+ ions will be subject to both radial and axial variation, and hence loss by diffusion will occur.

It was also assumed in the plug flow model that the carrier gas flow velocity is uniform. This is not so. At the pressures used in the flow tube, the carrier gas flow will be laminar with a few percent slip flow at the walls. Under these conditions the radial velocity profile is given by[162]

$$v (r,z) = (1/4\eta) . (a^2 - r^2 + 2sa) dp/dz \qquad (3.7)$$

where p is the pressure in the flow tube, η the viscosity of the carrier gas, and s the coefficient of slip. Cylindrical coordinates r, θ , z are used, with the z axis, as before, being the axis of the flow tube. The distance d required for such flow to fully develop is given by [163]

$$d = 0.227\ aR_e \qquad (3.8)$$

where R_e is the Reynolds number of the gas flow. For helium at room temperature with a flow rate of 180 $cm^3 atm.s^{-1}$, d is 12 cm.

It has been found experimentally[164] that for a wide variety of gases in copper tubes

$$s = 1.38\mu_1 / p \qquad (3.9)$$

where μ_1 is the mean free path in cm in the gas at a pressure of 1 torr.

The average flow velocity of the gas $\bar{v}(z)$, will be given by

$$\bar{v}(z) = \frac{\int_0^a 2\pi r v(r,z)\ dr}{\pi a^2}$$

$$= \frac{a^2}{8\eta}\left(1 + 5.52\mu_1/pa\right)\frac{dp}{dz} \qquad (3.10)$$

Substituting (3.10) into (3.7) to eliminate dp/dz gives

$$v(r,z) = w\bar{v}(z)\ (b - r^2/a^2)\ , \qquad (3.11)$$

where $w = 2/(1 + 5.52\mu_1/pa)$ (3.12)

and $b = 1 + 2.76\mu_1/pa$ (3.13)

The z-dependence of $\bar{v}$ will be neglected, since it does not enter into the analysis when a rate constant is

determined by varying Q.[70] The average flow velocity $\bar{v}$ is calculated using the equation

$$\bar{v} = \frac{F\ (cm^3 atm.s^{-1})}{\pi a^2\ (cm^2)} \cdot \frac{760\ torr\ atm.^{-1}}{p\ (torr)} \qquad (3.14)$$

where F is the experimentally-determined volume flow rate of the carrier gas at room temperature, and p the pressure measured at the mid-point of the reaction zone.

If $[A^+] = [A^+]\ (r, \theta, z)$ is the concentration of A^+ at some point (r, θ, z) in the flow tube, the continuity equation for A^+ is

$$(\partial[A^+]/\partial t) = -\nabla \cdot J + (\partial[A^+]/\partial t)_v \qquad (3.15)$$

where ∇ has its usual meaning of the vector operator $(\partial/\partial x, \partial/\partial y, \partial/\partial z)$, $(\partial[A^+]/\partial t)_v$ is the rate of change of $[A^+]$ due to volume formation or loss processes, and J is the ion current density given by

$$J = [A^+]\, v(r) - D_A \nabla[A^+] \qquad (3.16)$$

where D_A is the ambipolar diffusion coefficient of A^+ at some pressure p. Taking the divergence of (3.16) one obtains

$$\begin{aligned} \nabla \cdot J &= \nabla \cdot ([A^+]\, v(r)) - D_A \nabla^2 [A^+] \\ &= v(r)\, \partial [A^+]/\partial z - D_A \nabla^2 [A^+] \end{aligned} \qquad (3.17)$$

since $v(r)$ has only a z component. In the steady-state flowing afterglow $\partial[A^+]/\partial t$ is zero, so combination of (3.15) and (3.17) gives

$$D_A \nabla^2 [A^+] - v(r)\,(\partial[A^+]/\partial z) + (\partial[A^+]/\partial t)_v = 0 \qquad (3.18)$$

The volume formation and loss process which make up $(\partial[A^+]/\partial t)_v$ may include:

i) Loss by reaction with added neutral reactant.

ii) Loss by reaction with impurities.

iii) Loss by recombination.

iv) Loss by three-body association reactions.

v) Production by metastable-metastable reactions.

vi) Production by reverse reaction.

Experimental conditions can generally be chosen such that (i) is the only significant loss process. Hence $(\partial [A^+] / \partial t)_v = - k [A^+][B]$, using the same notation as in section 3.2.1.

Substituting for $(\partial[A^+] / \partial t)_v$ in (3.18), and transforming to cylindrical coordinates, one obtains

$$D_A \left\{ \frac{1}{r} \frac{\partial}{\partial r} \left(r \frac{\partial [A^+]}{\partial r} \right) + \frac{\partial^2 [A^+]}{\partial z^2} \right\} - v(r) \frac{\partial [A^+]}{\partial z} - k[A^+][B] = 0 \qquad (3.19)$$

To solve this equation, the term $\partial^2[A^+] / \partial z^2$, arising from axial diffusion of A^+, will be neglected for the present. It will also be assumed that the concentration of B is uniform at all points downstream of the neutral reactant inlet jet, and given by

$$[B] = Q / \pi a^2 \bar{v} \qquad (3.20)$$

Substituting for [B] and v(r) in (3.19) from (3.20) and (3.11) respectively, and dividing by $\bar{v}$ gives

$$\frac{D_A}{\bar{v}} \left\{ \frac{1}{r} \frac{\partial}{\partial r} \left(r \frac{\partial [A^+]}{\partial r} \right) \right\} - w \left(b - \frac{r^2}{a^2} \right) \frac{\partial [A^+]}{\partial z} - \frac{k Q [A^+]}{\pi a^2 \bar{v}^2} = 0 \qquad (3.21)$$

The dimensionless form of (3.21) is

$$\frac{1}{\rho} \frac{\partial}{\partial \rho} \left(\rho \frac{\partial y}{\partial \rho} \right) - (b - \rho^2) \frac{\partial y}{\partial u} - g^2 y = 0 \qquad (3.22)$$

where $y = [A^+] / [A_o^+]$, $\rho = r/a$, $u = D_A z / a^2 \bar{v} w$, and $g^2 = kQ / \pi \bar{v} D_A$

Equation (3.22) may now be solved by the method of separation of variables. If the substitution $y = R(\rho)Z(u)$ is made in (3.22), and the resulting equation divided by $(b - \rho^2)RZ$, one obtains

$$\frac{1}{R \rho (b - \rho^2)} \frac{d}{d\rho} \left(\rho \frac{dR}{d\rho} \right) - \frac{g^2}{b - \rho^2} = \frac{1}{Z} \frac{dZ}{du} \qquad (3.23)$$

Since the left hand side is a function of ρ only, and the right hand side a function of u only, each must be equal to the same constant, $-\kappa^2$ say (the separation constant). This leads to the two equations

$$\frac{d}{d\rho}\left(\rho\frac{dR}{d\rho}\right) + \{\kappa^2(b - \rho^2) - g^2\}R\rho = 0 \qquad (3.24)$$

and

$$\frac{dZ}{Z} = -\kappa^2 du \qquad (3.25)$$

Equation (3.24) is now in the Sturm-Liouville form and its lowest eigenvalue κ_o^2 may be determined by the Rayleigh-Ritz variational method.[165,166] Only the lowest eigenvalue, corresponding to the fundamental diffusion mode, need be considered since other workers have shown[27,159] that higher-order diffusion modes are rapidly attenuated. In the Rayleigh-Ritz variational method a trial function

$$R = \alpha(1 - \rho^2) + \beta(1 - \rho^2)^2 \qquad (3.26)$$

is assumed, where α and β are required to satisfy the equations

$$\int_o^1 \frac{\partial R}{\partial \alpha}\left\{\frac{d}{d\rho}\left(\rho\frac{dR}{d\rho}\right) + \rho(\kappa_o^2(b - \rho^2) - g^2)R\right\} d\rho = 0 \qquad (3.27)$$

$$\int_o^1 \frac{\partial R}{\partial \beta}\left\{\frac{d}{d\rho}\left(\rho\frac{dR}{d\rho}\right) + \rho(\kappa_o^2(b - \rho^2) - g^2)R\right\} d\rho = 0 \qquad (3.28)$$

Substitution for R from (3.26) in (3.27) and (3.28) leads, after some manipulation, to

$$\alpha\{6 + g^2 - \kappa_o^2(b - 0.25)\} + \beta\{4 + 0.75g^2 - \kappa_o^2(0.75b - 0.15)\} = 0 \qquad (3.29)$$

and

$$\alpha\{4 + 0.75^2 - \kappa_o^2(0.75b - 0.15)\} + \beta\{4 + 0.6g^2 - \kappa_o^2(0.6b - 0.1)\} = 0 \qquad (3.30)$$

A non-trivial solution of (3.29) and (3.30) exists if

$$\{6 + g^2 - \kappa_o^2(b - 0.25)\}\{4 + 0.6^2 - \kappa_o^2(0.6b - 0.1)\} = \{4 + 0.75g^2 - \kappa_o^2(0.75b - 0.15)\}^2 \qquad (3.31)$$

Expansion of this equation, neglecting terms in g^4, leads to a quadratic equation in κ_o^2. Solution of this equation in the normal manner gives κ_o^2 as a function of g^2 in the form

$$\kappa_o^2 = \delta + \gamma g^2 \qquad (3.32)$$

The eiginvalue components δ and γ, which are functions of b, are given by

$$\delta = \frac{1}{21}\left[m - \sqrt{(m^2 - 321)}\right] \qquad (3.33)$$

and

$$\gamma = -\frac{1}{21}\left[n - \frac{2mn + 6.41}{2\sqrt{(m^2 - 321)}}\right] \qquad (3.34)$$

where $$1 = (0.25-b)(0.1-0.6b)-(0.15-0.75b)^2 \qquad (3.35)$$

$$m = 1.6b - 0.4 \qquad (3.36)$$

and $$n = 0.025 - 0.075b \qquad (3.37)$$

The neglect of terms in g^4 in the expansion of (3.31) will not lead to serious error if the dimensionless term g^2 is less than 15.[159,160]

The eigenvalues in the form $\kappa_o^2 = \delta + \gamma g^2$ may now be substituted into (3.25). Integration of this equation between the limits z = 0 and z = L leads to, in the dimensional form,

$$\log_e \frac{Z}{Z_o} = -\left\{\frac{\delta}{w}\frac{D_A}{a^2} + \frac{\gamma k Q}{w\pi a^2 \bar{v}}\right\}\frac{L}{\bar{v}} \qquad (3.38)$$

If new eigenvalue components $\Delta=\delta/w$ and $\Gamma=\gamma/w$ are defined, the axial variation of $[A^+]$ may be written

$$\log_e \frac{[A^+]}{[A_o^+]} = -\left\{\frac{\Delta D_A}{a^2} + \frac{\Gamma k Q}{\pi a^2 \bar{v}}\right\}\frac{L}{\bar{v}} \qquad (3.39)$$

Differentiating (3.39) with respect to Q gives

$$k = -(\pi a^2 \bar{v}^2/\Gamma L)(d\log_e [A^+]/dQ) \qquad (3.40)$$

Comparing (3.40) with (3.6), it can be seen that inclusion of a radial diffusive loss term for A^+ has not

affected the expression for calculating k. The effect of the non-uniform velocity profile has been to multiply the rate constant obtained using the plug flow model by a factor of $1/\Gamma$, giving and increase of about 60% in k.

3.2.3 Axial Diffusion Correction

Loss of A^+ by radial diffusion and by reaction with added neutral reactant will lead to a gradient of $[A^+]$ in the axial direction, and hence axial diffusion of A^+ will take place. The equation describing the variation of $[A^+]$, taking axial diffusion into account, is equation (3.19) derived earlier. To separate the variables in this equation, the substitution $[A^+] = R(r)\,Z(z)$ is made. After dividing through by $D_A\, v(r) RZ$ one obtains

$$\frac{1}{v(r)Rr}\frac{d}{dr}\left(r\frac{dR}{dr}\right) - \frac{k[B]}{D_A v(r)} = \frac{1}{D_A Z}\frac{dZ}{dz} - \frac{1}{v(r)Z}\frac{d^2Z}{dz^2} \qquad (3.41)$$

The r-dependence of the last term is removed by replacing $v(r)$ with $\bar{v}$. Since the term d^2Z/dz^2 is small, the substitution of $\bar{v}$ for $v(r)$ should not lead to serious error. Equation (3.41) may then be separated to give

$$\frac{1}{r}\frac{d}{dr}\left(r\frac{dR}{dr}\right) + \left(\lambda^2 v(r) - \frac{k[B]}{D_A}\right)R = 0 \qquad (3.42)$$

and

$$\frac{1}{\bar{v}}\frac{d^2Z}{dz^2} - \frac{1}{D_A}\frac{dZ}{dz} - \lambda^2 Z = 0 \qquad (3.43)$$

where λ^2 is the separation constant. Substituting for $v(r)$ from (3.11) and putting $\rho = r/a$ in (3.42) one obtains

$$\frac{d}{d\rho}\left(\rho\frac{dR}{d\rho}\right) + \left(\lambda^2 w\bar{v}a^2(b - \rho^2) - \frac{k[B]a^2}{D_A}\right)R\rho = 0 \qquad (3.44)$$

This equation is exactly analogous to (3.24) solved earlier. Again, the dimensionless term $k[B]a^2/D_A$ is typically less than 15, and its square may be neglected. By analogy with

the solution of (3.24),

$$\lambda^2 = \{\Delta/a^2 + \Gamma k[B]/D_A\}\,\bar{v}^{-1}$$
$$= \{\Delta/a^2 + \Gamma kQ/\pi D_A a^2 \bar{v}\}\,\bar{v}^{-1} \qquad (3.45)$$

where Δ and Γ are the eigenvalue components found earlier, and $[B]$ has been replaced according to (3.20).

The solution of (3.43) is

$$\log_e(Z/Z_o) = [1 - (1 + 4\lambda^2 D_A^2/\bar{v})^{\frac{1}{2}}](\bar{v}/2D_A)L \qquad (3.46)$$

The expression to the $\frac{1}{2}$ power is expanded using the binomial theorem, retaining only the first three terms. This does not lead to serious error since the dimensionless term $4\lambda^2 D_A^2/\bar{v}$ is small, typically about 0.2. Substitution for λ^2 from (3.45) enables the axial variation of reactant ion concentration to be written

$$\log_e([A^+]/[A_o^+]) = -\left(\frac{\Delta D_A}{a^2} + \frac{\Gamma kQ}{\pi a^2 \bar{v}}\right)\frac{L}{\bar{v}}(1 - \varepsilon) \qquad (3.47)$$

where $\varepsilon = (\lambda^2/\bar{v})D_A^2$ (3.48)

The value of λ^2 and hence of ε is dependent on both k and Q. In calculating ε, an approximate value of k is first determined from (3.40). This value of k, together with an average value of Q, is used to calculate a value for λ^2 from (3.45). An average value of ε, denoted $\bar{\varepsilon}$, is then calculated by substituting the value of λ^2 in (3.48). The error introduced by these two approximations will be small since the term $\Gamma kQ / \pi D_A a^2 \bar{v}$ in (3.45) is typically less than one-fifth of the term Δ/a^2.

Differentiating (3.47) with respect to Q gives

$$k = -[\pi a^2 \bar{v}^2/\Gamma L(1 - \varepsilon)](d\log_e [A^+]/dQ) \qquad (3.49)$$

Equation (3.49) is the expression used to calculate rate constants in this work. Comparing (3.49) with (3.40), it can be seen that the effect of axial diffusion has been

to multiply the rate constant k by a factor of $(1/1-\varepsilon)$. This typically produces an increase in k of between 4% and 8%.

3.3 CORRECTION FOR INLET EFFECTS.

In the preceding treatment, it has been assumed that the concentration of the neutral reactant is uniform at all points downstream of the reactant inlet jet. In practice, this does not occur for it takes some time for the neutral reactant to diffuse into the buffer gas. Other effects occurring at the neutral reactant inlet jet are the disturbing of the reactant ion concentration profile by the inlet jet itself, and the presence of higher-order modes of diffusion of the reactant ion, although such modes are very rapidly attenuated by diffusion.

An empirical correction is made for these inlet effects by replacing L, the distance from the neutral reactant inlet jet to the tip of the nose cone, with L_{eff}, the effective reaction length. This effective reaction length is greater than the actual reaction length by an amount termed the "end correction." The end correction is expected to depend on the diffusion coefficient of the neutral reactant in the carrier gas. Since the diffusion coefficients of a number of atmospheric gases in hydrogen or helium are similar, lying in the range 450-650 cm^2 torr s^{-1}, the end correction is expected to be fairly insensitive to the nature of the reactant gas for reactions of small molecules in a hydrogen or helium carrier gas.[70]

However as diffusion coefficients are pressure-dependent, some variation of end correction with carrier gas pressure is expected.

The following method was used in this work to determine the end correction. Replacing L in (3.49) with L_{eff} and rearranging yields

$$d\log_e[A^+]/dQ = -k\Pi L_{eff}(1 - \varepsilon)/\pi a^2 \bar{v}^2 \qquad (3.50)$$

The left-hand side of this equation is directly proportional to L_{eff}, provided that the variation of ε and $\bar{v}$ with reaction length is small. If the value of $d \log_e [A^+]/dQ$ for a specific reaction is measured at several different reaction lengths, a linear plot of $d \log_e[A^+]/dQ$ vs. actual reaction length may be drawn. The intercept of this line with the reaction-length axis yields the effective reaction length and hence the end correction.

In practice, this was done as follows. The reaction chosen was the fast proton-transfer reaction

$$H_3^+ + CO \rightarrow HCO^+ + H_2 \qquad (3.51)$$

A third neutral reactant inlet jet was added to the flow tube. The CO reactant was added into the hydrogen afterglow containing H_3^+ as the dominant ion, through one of three identical inlet jets situated at distances of 51.3, 71.9, and 98.6 cm from the tip of the nose cone. The slope of a plot of $\log_e [H_3^+]$ vs. CO flow was determined for addition of CO through each of these inlet jets, and a plot of $d \log_e [H_3^+]/dQ$ vs reaction length constructed. From this plot, the value of the effective reaction length was obtained by extrapolation of the line to $d \log_e [H_3^+]/dQ = 0$. This procedure was carried out at a number of pressures in the range 0.2 - 0.6 torr.

Unfortunately, the process of extrapolating a straight line through only three points, each subject to several percent error, is not very satisfactory, and produces a large uncertainty in the effective reaction length. The value of the end correction determined by this method is 6 ± 6 cm. This degree of accuracy was insufficient to reveal any systematic dependence of the end correction on carrier gas pressure.

3.4 COMPUTER PROGRAM ION/RATES.

Rate constants were extracted from the raw experimental data by use of computer program ION/RATES. The program, listed in Appendix II, is written in Fortran IV language and is executed on a Burroughs B6718 computer.

Input data to the program comprises the characteristics of the carrier gas flow (flow velocity, pressure in the reaction zone, and mean free path in the carrier gas), the reaction length (which includes an empirical end correction), the average value of the neutral reactant flow, the ambipolar diffusion coefficient of the reactant ion, and pairs of values of reactant ion signal, $[A^+]$, and the corresponding neutral reactant flow rate, Q.

Ambipolar diffusion coefficients of the reactant ions are generally taken from references 69 and 167. Where experimental values are unavailable, a value of 900 cm^2 torr s^{-1} is assumed for ambipolar diffusion in helium, and a value of 550 cm^2 torr s^{-1} assumed for ambipolar diffusion in hydrogen. In any case, the value of the corrected rate constant is not particularly sensitive to the value of the

reactant ion diffusion coefficient. In a typical case, a variation of a factor of 2 in the diffusion coefficient of the reactant ion caused only a 7% variation in rate constant k.

The program evaluates the slope of a plot of $\log_e[A^+]$ vs. Q by a least-squares analysis of pairs of values of $\log_e[A^+]$ and Q. The eigenvalue components δ and γ are calculated from (3.33) and (3.34), and hence the eigenvalue components Δ and Γ are obtained by dividing δ and γ by w, defined according to (3.12). The first approximation to the rate constant, termed rate 1, is readily calculated by application of (3.40). This first value of the rate constant, rate 1, together with the average value of neutral reactant flow, BFLOW , is used to calculate the value of ε from (3.48). Substitution for ε in (3.49) then yields the corrected rate constant, termed rate 2.

3.5 ACCURACY OF RATE CONSTANT DATA.

Errors can enter a rate constant determination from two sources, either from uncertainties in the experimental measurement of the carrier gas flow velocity and the value of $d \log_e [A^+]/dQ$, or from the approximations made in the flow analysis.

The uncertainty in the measurement of the carrier gas flow velocity is about 5%, while the standard error in the least-squares value of $d \log_e [A^+]/dQ$ is generally between 1% and 5%. Since the carrier gas flow velocity term appears as a square in the expression for the rate constant, the uncertainty in the rate constant due to

these two sources of error is between 11% and 16%. In general, for a series of determinations of the rate constant for a specific reaction, individual values lie within about 12% of the mean.

The accuracy of a rate constant is further limited by the possibility of there being systematic errors in the solution of the flow equation. Errors introduced by neglecting higher-order terms in g^2 in the variational solution of the flow equations are small, provided that the condition laid down earlier, $g^2 \leqslant 15$, is met. Normally this condition is upheld for fast reactions. For values of $g^2 \leqslant 15$ Stock[159] found that the errors introduced into the eigenvalue components δ and γ are 0.4% and 1.5% respectively. More serious is the error involved in the end correction. The uncertainty of ± 6 cm in the effective reaction length leads to an error of about 11% in the rate constant.

In view of these factors, an absolute accuracy of no better than $\pm$ 30% is claimed for rate constants measured in this work. The relative accuracy of the rate constants is better than $\pm$ 16% however.

As a check on both the flow analysis and the calibration of the apparatus, the rate constant for the reaction of He^+ ions with N_2 was measured. The average value of the rate constant obtained was 1.1×10^{-9} cm^3 $molecule^{-1} s^{-1}$, in good agreement with a value of 1.2×10^{-9} $cm^3 molecule^{-1} s^{-1}$ determined by Dunkin et al.[68] in the flowing afterglow, using numerical methods to solve the flow equation. A value of $(1.0, + 0.3, - 0.2) \times 10^{-9}$ cm^3 $molecule^{-1}$ s^{-1} has been obtained using a drift tube-mass

spectrometer,[168] and a value of 1.45×10^{-9} cm^3 $molecule^{-1}$ s^{-1} determined by the stationary afterglow method.[51]

REACTIONS OF H_3^+ IONS WITH CYANIDE-CONTAINING NEUTRAL MOLECULES.

4.1 INTRODUCTION.

In this chapter, measurements of the rates of reaction of H_3^+ ions with the neutral molecules HCN, CH_3CN, ClCN, BrCN, ICN and C_2N_2 are reported. The study was undertaken with a view to comparing the experimentally-determined rate constants with those predicted by the various capture-rate theories, particularly the ADO theory.[131]

To compare measured reaction-rate constants with calculated capture-rate constants, it is essential that the percentage of capture collisions leading to reaction be known. Ideally, this percentage will be 100% i.e., the reaction efficiency will be unity. This is generally the case with proton-transfer reactions, which do not usually have activation energy barriers which decrease reaction efficiency. Also, since proton-transfer reactions require transfer of a particle which is heavy compared with the electron, they are unlikely to proceed at a rate greater than the capture rate, as can sometimes occur for charge transfer reactions proceeding by an electron jump mechanism. For these reasons, H_3^+ was chosen as the reactant ion. Hydrogen has a relatively low proton affinity, and thus H_3^+ readily undergoes proton transfer to many neutral species. The low mass of H_3^+ also ensures that the reduced mass of the ion-dipole pair varies only slightly for the range of neutral reactants studied.

Several comparisons have been made between experimentally-determined rate constants and those predicted by the ADO theory.[56,134,138] In particular, Schiff and Bohme [56] have found that, for proton transfer between ions of the type XH^+ and the neutral species NH_3 and HCN, the experimentally-determined rate constants exceed the predictions of the ADO theory by up to 40%. Both NH_3 and HCN have large permanent dipole moments of 1.47 D and 2.95 D respectively.[169] This result prompted the present study, in which all the neutral reactants, with the exception of C_2N_2, have large permanent dipole moments. These dipole moments are listed in table 4.1, along with the values of the average molecular polarizability, α, and the maximum component of the polarizability tensor, α_{max}. Although C_2N_2 does not possess a permanent dipole moment, it does have a quadrupole moment of -9.0×10^{-26} e.s.u. cm^2.[170]

TABLE 4.1

DIPOLE MOMENTS AND POLARIZABILITIES OF SOME CYANIDE-CONTAINING MOLECULES.

Molecule	μ_D, Debye[169]	$\alpha \cdot 10^{25}$, cm^3	$\alpha_{max} \cdot 10^{25}$, cm^3
HCN	2.95	25.9 [171]	39.2 [171]
CH_3CN	3.97	44.8 [172]	57.4 [172]
ClCN	2.80	41.63 [a]	67.7 [b]
BrCN	2.94	49.86 [a]	81.4 [b]
ICN	3.71	63.17 [a]	-
C_2N_2	0.	50.1 [171]	77.6 [171]

a. Values of Lippincott et al.,[173] calculated using the δ-potential function model.

b. Calculated by adding individual bond polarizabilities. See reference 174.

4.2 EXPERIMENTAL DETAILS AND RESULTS.

The reactions were carried out in a hydrogen carrier gas. Electron impact on hydrogen results in formation of H_2^+ ions having a Franck-Condon distribution of vibrational energies. These H_2^+ ions then react to give H_3^+ in the reaction

$$H_2^+ + H_2 \rightarrow H_3^+ + H \qquad (4.1)$$

which has a rate coefficient $k = 2.1 \times 10^{-9}$ cm^3 $molecule^{-1}s^{-1}$. [13]

The H_3^+ ions formed in reaction (4.1) are highly excited, due to both the initial vibrational excitation of the H_2^+ ions and the exothermicity of reaction (4.1). Several workers [175-179] have reported evidence for the presence of excited H_3^+, namely that the nature of the products of reaction of H_3^+ is dependent on the background gas pressure. The H_3^+ ions are de-excited by collisions with H_2 molecules, the rate constant for this process being 2.7×10^{-10} cm^3 $molecule^{-1}s^{-1}$. [180] In the flowing afterglow, the flow time between the electron gun and the neutral reactant inlet is several milliseconds, a period sufficiently long for all the H_3^+ to be de-excited to the ground state.

The hydrogen afterglow contains other ions in addition to H_3^+. Small amounts of H_5^+ are formed in the three-body reaction

$$H_3^+ + 2H_2 \rightarrow H_5^+ + H_2 \qquad (4.2)$$

In addition, some impurity ions are also present, the predominant ions being H_3O^+ and N_2H^+, formed chiefly by

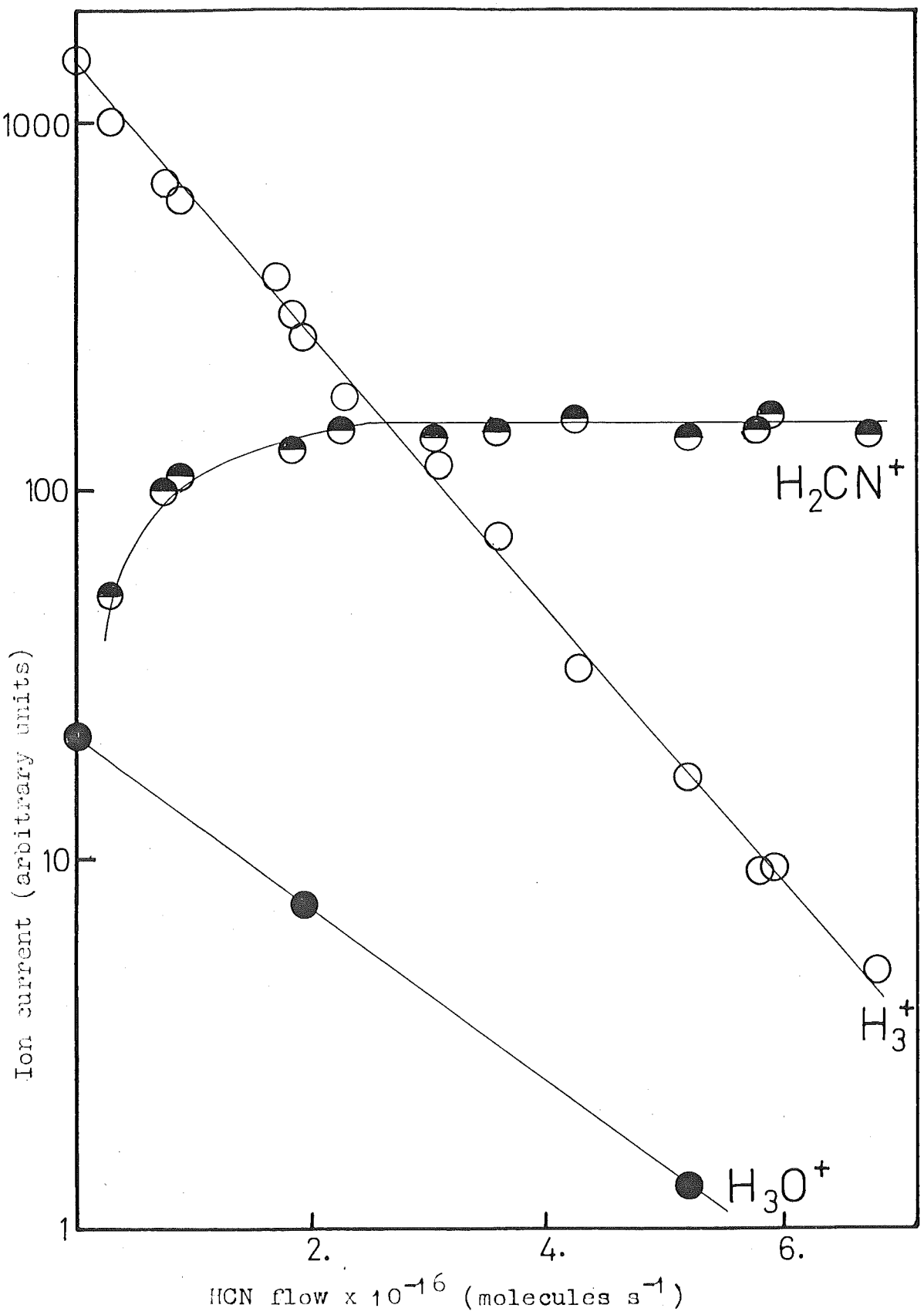

FIGURE 4.1 Ion currents vs. HCN flow rate for the reaction of H_3^+ with HCN.

proton transfer from H_3^+ to H_2O and N_2 impurities in the carrier gas. The magnitude of such impurity signals is always at least a factor of ten smaller than that of the H_3^+ ion signal before the neutral reactant is added.

Addition of the gaseous neutral reactants HCN, C_2N_2, and ClCN was straightforward. The vapour pressures of CH_3CN (liquid), BrCN (solid) and ICN (solid) are so low at 300K that it was necessary to dilute them with helium in order to achieve steady flow rates. This procedure has been outlined in chapter 2.1.3. The addition of ICN posed further problems. Since the vapour pressure of ICN at 300 K is only 1.1 torr,[181] very low concentrations of ICN in helium had to be used. At these low concentrations, the effect of impurities released from the walls of the gas-handling line becomes serious. Also, there was a tendency for ICN to condense out as the gas mixture passed through the needle valve. This problem was reduced by heating the needle valve. Because of these factors, the rate constant for the ICN reaction is probably reliable to within a factor of two only.

Addition of the neutral reactant XCN to the afterglow containing H_3^+ as the dominant ion results in a decrease in the H_3^+ signal and a concomitant increase in the $HXCN^+$ signal due to the proton-transfer reaction

$$H_3^+ + XCN \rightarrow HXCN^+ + H_2 \qquad (4.3)$$

Typical data is shown in figure 4.1 for the reaction

$$H_3^+ + HCN \rightarrow H_2CN^+ + H_2 \qquad (4.4)$$

The large discrepancy between the initial H_3^+ ion signal and the final H_2CN^+ ion signal is chiefly due to mass

discrimination in the ion sampling and detection systems. At higher flows of HCN than are shown in figure 4.1, the H_2CN^+ signal slowly declines as H_2CN^+ is removed in the three-body clustering reaction.

$$H_2CN^+ + HCN + H_2 \rightarrow H_2CN^+.HCN + H_2 \quad (4.5)$$

For all the reactions studied, the proton-transfer reaction (4.3) was the sole reaction channel observed. The semi-logarithmic decline of the H_3^+ ion signal with increasing XCN flow was observed to be linear over at least two-and-a-half decades in all cases.

The average values of the rate constants measured in this work, $k_{expt.}$, are listed in the first column of table 4.2. Only one of these rate constants appears to have been measured previously. Using the ICR method, Huntress et al.[182] have obtained a rate constant for reaction (4.4) of 8.0×10^{-9} cm^3 $molecule^{-1}s^{-1}$, in satisfactory agreement with the value of 7.0×10^{-9} cm^3 $molecule^{-1}s^{-1}$ measured in the present work.

4.3 COMPARISON OF EXPERIMENTAL AND THEORETICAL RATE CONSTANTS.

Capture rate constants for the reactions studied here have been calculated using the various classical theories of ion-molecule reactions described in chapter 1. These values are presented in table 4.2. The rate constants listed have been calculated using the Langevin Theory (k_L), the locked-dipole theory (k_{LD}), the ADO theory, $\overline{\cos\theta}$ model, using an average value for the polarizability of the neutral molecule (k_{ADO}), and the ADO theory using

the value of the maximum component of the polarizability tensor (k'_{ADO}). The final column of table 4.2 lists values of the ratio k_{expt}/k_{ADO}.

TABLE 4.2

RATE CONSTANTS [a] FOR PROTON TRANSFER FROM H_3^+ TO XCN AT 300K

XCN	$k_{expt.}$	k_L	k_{LD}	k_{ADO}	k'_{ADO}	k_{expt}/k_{ADO}
HCN	7.0	2.29	18.72	6.42	6.95	1.09
CH_3CN	7.3	2.95	24.67	8.45	8.84	0.86
ClCN	6.4	2.81	17.96	6.36	7.13	1.01
BrCN	4.2	3.05	18.79	6.69	7.54	0.63
ICN	4.2	3.42	23.20	8.15	-	0.52
C_2N_2	3.7	3.10	-	-	-	-

a All rate constants are in units of 10^{-9} cm^3 $molecule^{-1}s^{-1}$.

From table 4.2 it can be seen that, for all the polar molecules, the experimentally-determined rate constants are greater than the Langevin rate constants, but substantially smaller than the locked-dipole limit. Thus the permanent dipole does contribute to the long-range ion-molecule attraction, but the thermal rotational energy of the dipolar molecule is sufficient to prevent complete alignment of the dipole in the electric field of the ion.

The agreement between k_{expt} and k_{ADO} for the reactions of H_3^+ with HCN, CH_3CN, and ClCN is quite good, within the relative accuracy of the measured rate constants. The difference between the ADO rate constants calculated using the average polarizability and those calculated using the

maximum component of the polarizability tensor is small, less than the relative accuracy of rate constants measured in the flowing afterglow.

Schiff and Bohme[56] have observed that, for proton transfer from various ions of the type AH^+ to the neutral molecule HCN, the experimentally-determined rate constants exceed those predicted by the ADO theory by up to 40%. This observation is not supported by the results obtained in this work for proton transfer from H_3^+ to the highly polar neutral molecules HCN, CH_3CN, and ClCN. There is no apparent trend for the ratio $k_{expt.}/k_{ADO}$ to increase as the dipole moment of the neutral molecule increases in the series of reactions studied.

The measured rates of reaction of H_3^+ with BrCN and ICN are significantly less than those predicted by the ADO theory. It should be remembered, however, that the measured rate constant for the ICN reaction is probably reliable to within a factor of two only. This uncertainty is sufficient to account for the observed deviation from the prediction of the ADO theory. The rate constant for the BrCN reaction, however, is expected to have an absolute accuracy of $\pm$ 30%, and a relative accuracy of about $\pm$ 15%.

There are three possible reasons for the discrepancy between the measured and theoretical rate constants. These are: an unaccounted-for systematic error in the measured rate constant, too high a theoretical rate constant, or a reaction efficiency less than unity.

Condensation of the neutral reactant in the gas-handling line would tend to systematically lower the measured rate

constant. However rate constants have been measured using a number of different mixtures of BrCN in helium which cover a range of partial pressures of BrCN that are all well below the saturated vapour pressure of BrCN at room temperature. The observed rate constant shows no dependence on either the partial pressure of BrCN or the length of time elapsed since making up the mixture. It is unlikely therefore that condensation of BrCN is a problem.

It also seems unlikely that the rate constant given by the ADO theory is too great. The important parameters in determining the extent of locking-in of the dipole with the incoming ion are the dipole moment and polarizability of the neutral molecule. The dipole moment of BrCN is very close to that of HCN, while both the dipole moment and the polarizability of BrCN are not very different from those of ClCN. The measured rates of reaction of H_3^+ with HCN and ClCN are in close accord with the predictions of the ADO theory.

The size of the neutral molecule is another factor which might be expected to cause deviations from the ADO theory, since the theory treats both the ion and the neutral molecule as point particles. Sue and Bowers[134] have investigated the effect of the size of the neutral molecule on the rate of reaction for proton transfer from CH_5^+ to a series of alkyl chlorides. Even for the largest molecule studied, t-$C_3H_{11}Cl$, the measured rate was in good agreement with that predicted by the ADO theory. The larger size of the BrCN molecule, compared with say ClCN, is unlikely therefore to introduce error into the calculated ADO rate constants.

The third possible reason for the discrepancy between experiment and theory is a reaction efficiency less than unity. Although the great majority of proton-transfer reactions proceed on almost every collision, some have been observed to be less efficient. In particular, Solka and Harrison[183] report that for proton transfer from $CH_3SH_2^+$ to a variety of neutral substrates, the reaction efficiency drops sharply at low exothermicities (less than about 60 kJ mol^{-1}). Betowski et al.[184] have observed the same trend for proton-transfer reactions involving the neutral molecule H_2O. The model invoked by both groups to explain this trend is as follows. The proton transfer reaction

$$XH^+ + Y \rightarrow YH^+ + X \qquad (4.6)$$

is assumed to proceed via a proton-bound intermediate of the type $X...H^+...Y$. This intermediate may undergo unimolecular decay to products, the proton associating with Y, or decay back to reactants, the proton remaining associated with X. Decay into the product channel is increasingly favoured over decay back to reactants as the exothermicity of the proton transfer increases. Dependence of reaction efficiency on exothermicity is apparently fairly rare however. Schiff and Bohme[56] were not able to detect any trends in reaction efficiency with exothermicity in the series of proton-transfer reactions examined by them. Unfortunately, the exothermicity of the reaction of H_3^+ with BrCN is not known.

The molecule C_2N_2 does not possess a permanent dipole moment. It does have a quadrupole moment though, and this contributes to the long-range ion-molecule

attraction. The average quadrupole orientation theory gives a rate constant k_{AQO} of 3.24×10^{-9} cm^3 $molecule^{-1}s^{-1}$ for the reaction of H_3^+ with C_2N_2 at 300K. This is only slightly greater than the value of the Langevin rate constant (3.10×10^{-9} cm^3 $molecule^{-1}s^{-1}$), and indicates that the ion-quadrupole attraction is small compared with the ion-induced dipole attraction. The value of the ratio $k_{expt.}/k_{AQO}$ is 1.14. Agreement between theory and experiment is thus within the relative accuracy of the experimental measurement. If the average polarizability is replaced by the maximum component of the polarizability tensor in calculating the Langevin rate constant, a value of 3.86×10^{-9} cm^3 $molecule^{-1}s^{-1}$ is obtained. In this case the agreement between theory and experiment is better - $k_{expt.}/k_{theoretical} = 0.96$. However, the accuracy of the measured rate constant is such that a clear preference for either model cannot be made.

In summary, then, the ADO theory adequately accounts for the measured rates of reaction for the neutral molecules HCN, CH_3CN, and ClCN. Agreement between theory and experiment is not so good for the reactions of BrCN and ICN, but it seems possible that a low reaction efficiency, rather than error in the ADO rate constants, is responsible for this discrepancy. The AQO theory correctly predicts the rate of reaction of H_3^+ with C_2N_2, within the accuracy of the measured rate constant.

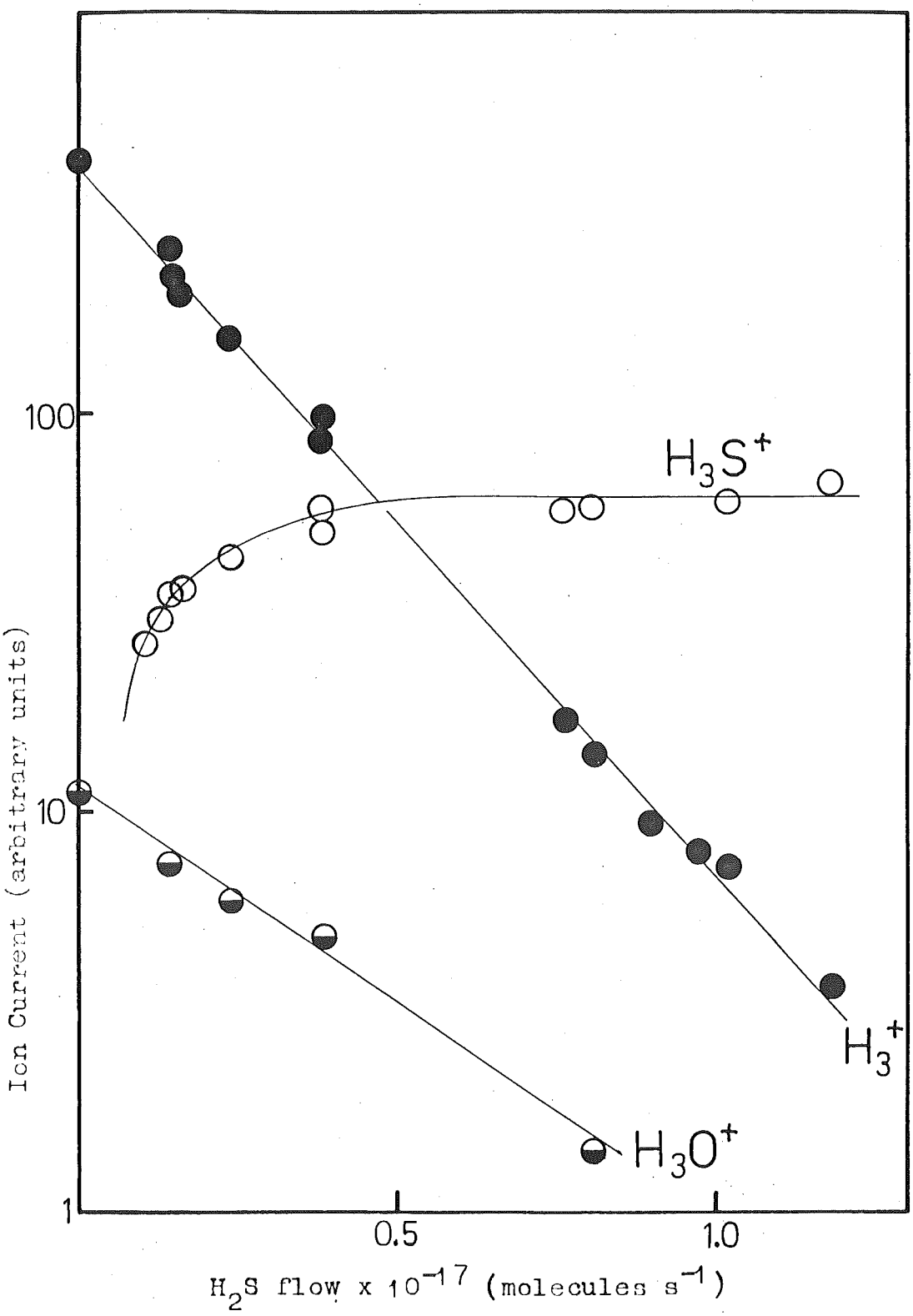

FIGURE 5.1 Ion currents vs. H_2S flow for the reaction of H_3^+ with H_2S.

CHAPTER 5

REACTIONS RELATED TO SULPHUR CHEMISTRY IN INTERSTELLAR CLOUDS.

5.1 H_3^+ WITH H_2S.

The reactant ion H_3^+ is established as the dominant ion in a hydrogen afterglow due to the fast reaction

$$H_2^+ + H_2 \rightarrow H_3^+ + H \qquad (5.1)$$

As discussed in chapter 4, it is expected that, in the flowing afterglow, the H_3^+ formed by reaction (5.1) will be completely de-excited by collisions to the ground state before the neutral reactant is added. Addition of H_2S to the hydrogen afterglow causes a decrease in the H_3^+ ion signal and an increase in the ion signals at m/e = 35 and 37, corresponding to formation of H_3S^+ in the reaction

$$H_3^+ + H_2S \rightarrow H_3S^+ + H_2 \qquad (5.2a)$$

Data for a typical run is shown in figure 5.1. Also shown is the decrease in the H_3O^+ impurity ion signal, due to the reaction

$$H_3O^+ + H_2S \rightarrow H_3S^+ + H_2O \qquad (5.3)$$

The measured rate constant for reaction (5.2a) is 3.4×10^{-9} cm^3 $molecule^{-1}s^{-1}$.

The reaction between H_3^+ and H_2S has been studied using ICR spectroscopy.[180] By varying the background gas pressure, the reaction was able to be studied as a function of the degree of excitation of H_3^+. For ground state H_3^+, the proton transfer reaction (5.2a) was the sole reaction channel observed. For excited H_3^+, however, the additional reaction channels

$$H_3^+ + H_2S \rightarrow H_2S^+ + H_2 + H \qquad (5.2b)$$

$$\rightarrow HS^+ + 2H_2 \qquad (5.2c)$$

were observed. The rate constant for the overall reaction (5.2) was found by ICR spectroscopy to be 3.7×10^{-9} cm^3 $molecule^{-1}s^{-1}$, independent of the degree of excitation of H_3^+.

5.2 HCO^+ WITH H_2S.

The reactant ion HCO^+ is produced by adding CO to the hydrogen afterglow. The reaction taking place is

$$H_3^+ + CO \rightarrow HCO^+ + H_2 \qquad (5.4)$$

The rate constant for reaction (5.4) is $1.4 \times 10^{-9} cm^3$ $molecule^{-1}s^{-1}$.[185] There is a small ion signal at m/e = 29, due to an N_2H^+ impurity, present before CO is added. Addition of CO should convert all the N_2H^+ ions to HCO^+ ions, since the reaction (5.5)

$$N_2H^+ + CO \rightarrow HCO^+ + N_2 \qquad (5.5)$$

is expected to be rapid as the proton affinity of CO is greater than that of N_2.[101]

Addition of H_2S to the afterglow containing HCO^+ as the dominant ion causes a decrease in the HCO^+ ion signal, and the appearance of ion signals due to H_3S^+. The semi-logarithmic decline of HCO^+ is linear for over two decades. The reaction taking place is

$$HCO^+ + H_2S \rightarrow H_3S^+ + CO \qquad (5.6)$$

The rate constant for reaction (5.6) has been found to be $1.4 \times 10^{-9} cm^3$ $molecule^{-1}s^{-1}$.

5.3 S^+, SO^+, AND SO_2^+ WITH H_2S.

The reactant ions S^+, SO^+, and SO_2^+ are formed by

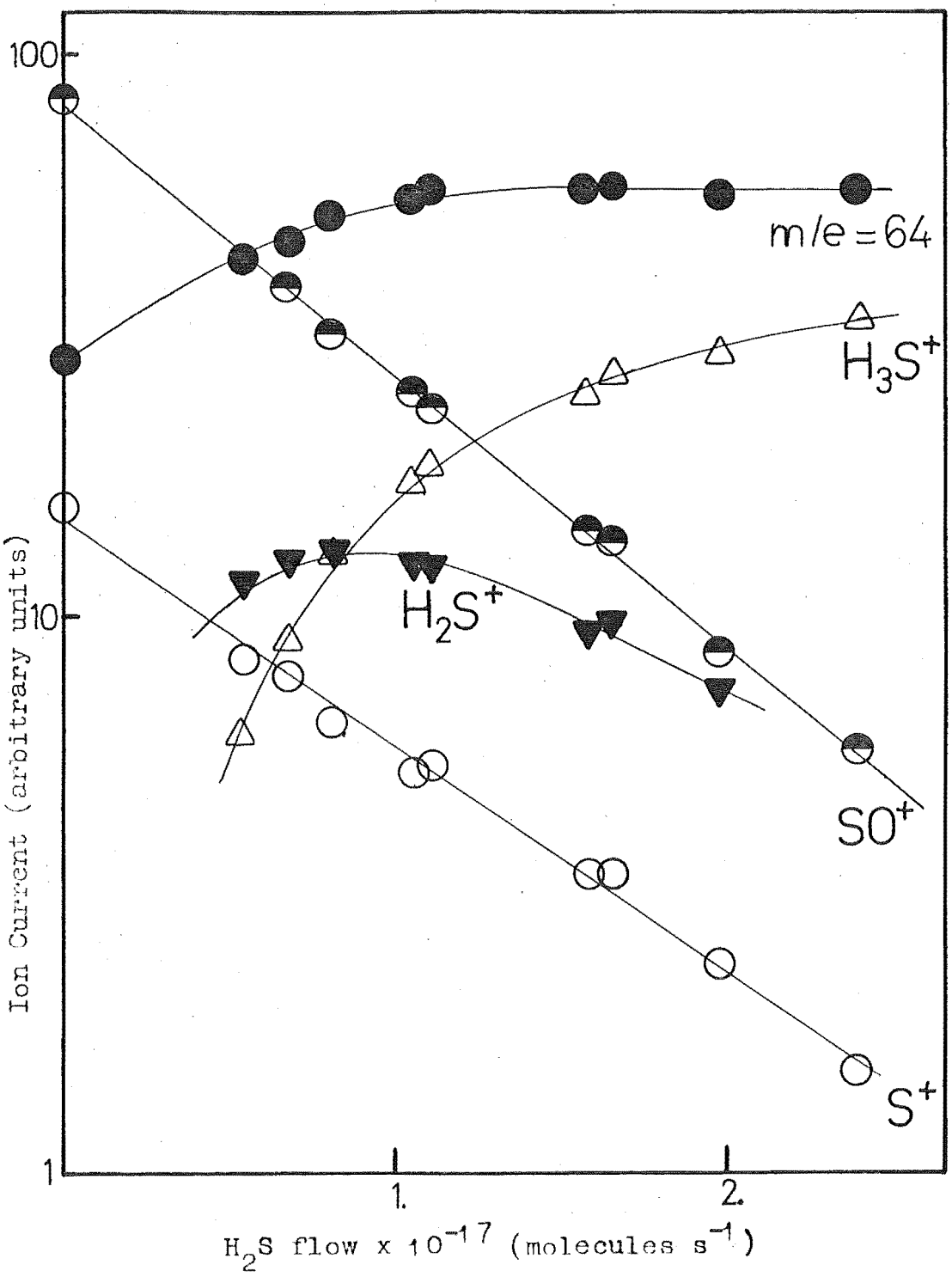

FIGURE 5.2 Ion currents vs. H_2S flow for the reaction of S^+ and SO^+ with H_2S.

adding SO_2 into a helium afterglow. Reaction of He^+ ions and He (2^3S) metastable atoms with SO_2 gives SO^+ as the dominant ion, together with smaller amounts of SO_2^+ and S^+.

All three reactant ions are rapidly removed by reaction with added H_2S. The measured rate constants for removal of S^+ and SO^+ are 8.3×10^{-10} cm^3 $molecule^{-1}s^{-1}$ and $9.4 \times 10^{-10} cm^3 molecule^{-1}s^{-1}$ respectively. Data for a typical run is shown in figure 5.2.

The ion signal at m/e = 64 is due to two different ionic species. In the absence of added H_2S, SO_2^+ is the only contributing ion. At high flows of H_2S however, the SO_2^+ is almost completely removed by reaction with H_2S and the m/e = 64 signal is due to the S_2^+ product ion. Identification of the ion at m/e = 64 at high H_2S flows as S_2^+ was made by examining the m/e = 66 ion signal due to the ^{34}S isotope of sulphur. The height of the m/e = 66 peak was found to be about 9% of that of the m/e = 64 peak, the natural abundance of the ^{34}S isotope being 4.4% of that of the ^{32}S isotope. The appearance of an S_2^+ product ion at the same mass as the SO_2^+ reactant ion precludes measurement of the rate of reaction of SO_2^+ with H_2S under the conditions in this work.

In addition to S_2^+, the H_2S^+ ion is produced by reaction of S^+, SO^+, and SO_2^+ with H_2S. This ion undergoes further reaction with H_2S:

$$H_2S^+ + H_2S \rightarrow H_3S^+ + HS \qquad (5.7)$$

The relationship between the reactant ions S^+, SO^+, and SO_2^+, and the product ions S_2^+ and H_2S^+, has been

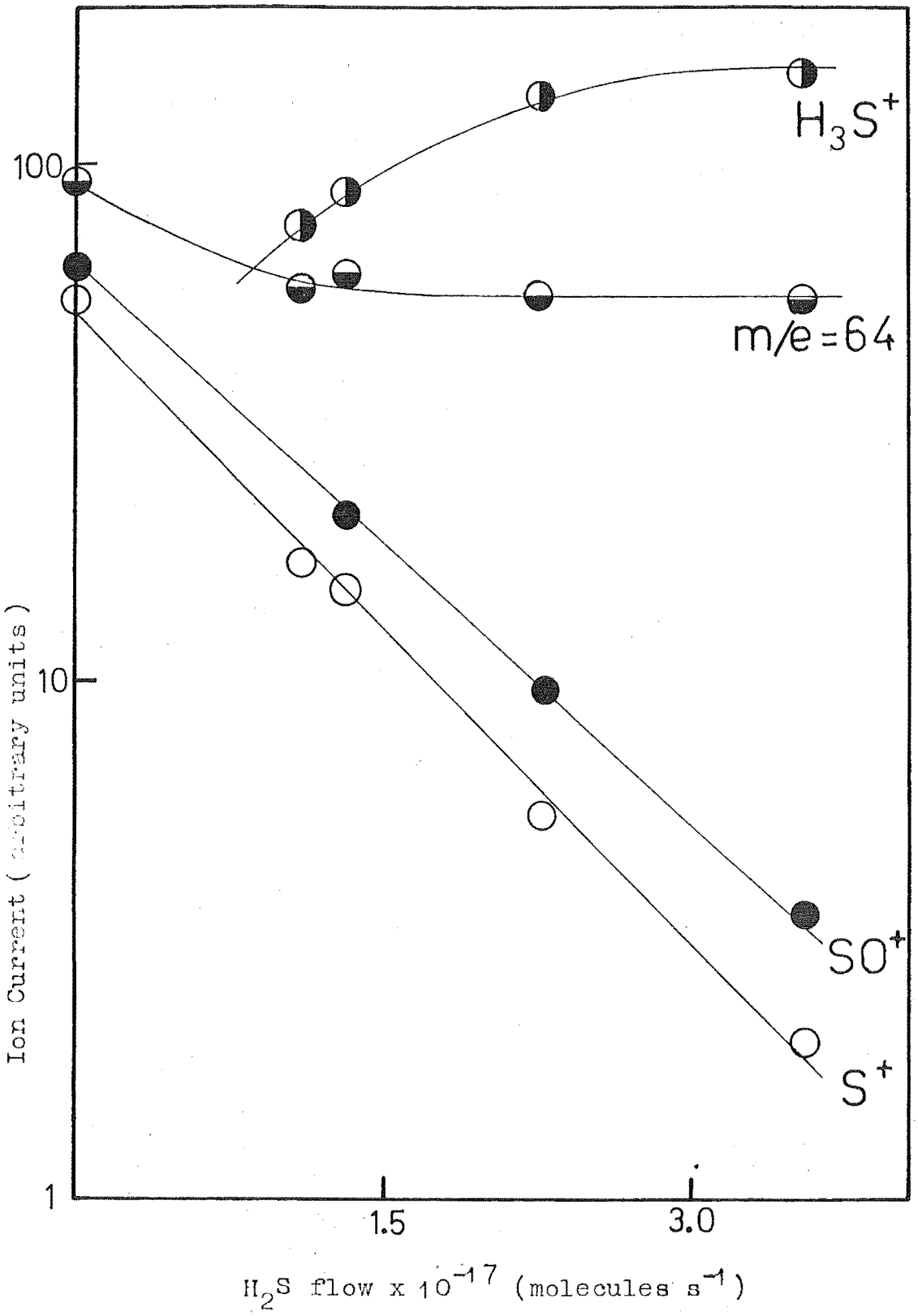

FIGURE 5.3 Ion currents vs. H_2S flow for the reaction of S^+ and SO^+ with H_2S. A small amount of argon has been added to the helium carrier gas.

determined in the following manner. Addition of a few percent of argon to the helium carrier gas upstream of the electron gun causes a change in the relative amounts of S^+, SO^+, and SO_2^+ formed when SO_2 is added to the afterglow. Figure 5.3 shows the data for a typical run in which argon has been added. (The secondary ion signal H_2S^+ has been omitted). By comparison with figure 5.2, it can be seen that the effect of the added argon is to decrease the initial SO^+ ion signal relative to the S^+ and SO_2^+ signals. Since the effect of added argon on the helium plasma is to convert $He(2^3S)$ metastable atoms in the afterglow to Ar^+ ions by the fast Penning reaction

$$He(2^3S) + Ar \rightarrow Ar^+ + He, \qquad (5.8)$$

the variation in the relative amounts of S^+, SO^+ and SO_2^+ formed with differing amounts of argon added to the helium carrier presumably reflects the different branching ratios for reaction of $He(2^3S)$ and Ar^+ with SO_2. Reactant ion-product ion relationships are identified by examining reactant-product ratios. For a specific reaction, the ratio of the final product ion signal to the initial reactant ion signal depends on the mass discrimination of the ion sampling and detecting system, and on the difference in the diffusive loss rates of the two types of ion. Provided that these two factors are kept almost constant, the product ion-reactant ion ratio is independent of the initial value of the reactant ion signal. In the reactions studied here, all possible ratios of the final product ion signals, $(H_3S^+)_f$ and $(S_2^+)_f$, to combinations of initial reactant ion signals $(S^+)_o$,

$(SO^+)_o$, and $(SO_2^+)_o$, were calculated for a number of different initial relative concentrations of the three reactant ions. Only two of these ratios did not show wide variation as the initial reactant ion relative concentrations were varied. The two ratios were $(H_3S^+)_f / \{(S^+)_o + (SO_2^+)_o\}$ and $(S_2^+)_f/(SO^+)_o$. From these observations it is inferred that the S_2^+ product is formed mainly from the SO^+ ion, while H_3S^+, and hence H_2S^+, is produced by reactions of S^+ and SO_2^+:

$$S^+ + H_2S \rightarrow H_2S^+ + S \qquad (5.9)$$

$$SO_2^+ + H_2S \rightarrow H_2S^+ + SO_2 \qquad (5.10)$$

However the possibility of formation of small amounts of S_2^+ from S^+ and SO_2^+, and/or H_2S^+ from SO^+ in minor reaction channels cannot be excluded.

The only possible exothermic reaction producing S_2^+ from SO^+ and H_2S is

$$SO^+ + H_2S \rightarrow S_2^+ + H_2O \qquad (5.11)$$

The observed rate constant for reaction of SO^+ with H_2S is 9.4×10^{-10} cm^3 $molecule^{-1}s^{-1}$. Comparing this rate with a value of 1.3×10^{-9} cm^3 $molecule^{-1}s^{-1}$ calculated using the ADO theory, it can be seen that the reaction proceeds with high efficiency ($\sim$ 75%) even though it involves considerable bond rearrangement. The extent of heavy-particle rearrangement may, however, be small if the ion-molecule pair achieve the relative orientation shown below during the collision.

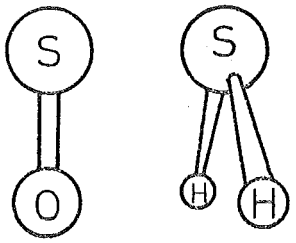

The observed charge-transfer reaction of S^+ with H_2S is interesting. Taking the ionization potentials of S and H_2S to be 10.356 eV [186] and 10.42 eV [187,188] respectively, the reaction is endothermic by 6.1 kJ mol^{-1} for the ground-state reactants. The maximum reaction rate constant k_r is given by an Arrehrius-type expression

$$k_r = k_c e^{-\Delta E/RT} \qquad (5.12)$$

where k_c is the rate constant for capture collisions and ΔE the endothermicity of reaction. Using a value of 1.41×10^{-9} cm^3 $molecule^{-1}s^{-1}$ given by the ADO theory for k_c, the maximum reaction rate constant at 300K given by (5.12) is 1.2×10^{-10} cm^3 $molecule^{-1}s^{-1}$. This value is significantly smaller than the measured value of 8.3×10^{-10} cm^3 $molecule^{-1}s^{-1}$. One possible reason for this enhanced reaction rate is the presence in the afterglow of long-lived excited states of the S^+ ion.

The low-lying excited states of the S^+ ion, and their excitation energies above the $S^+(^4S)$ ground state are

$^2D_{3/2}$	177.7	kJ mol^{-1}
$^2D_{5/2}$	178.0	" "
$^2P_{1/2}$	293.4	" "
$^2P_{3/2}$	294.0	" "

If the heats of formation of ground-state ionic and neutral species listed in reference 187 are adopted, the reaction

$$He^+ + SO_2 \rightarrow S^+ + 2O + He \qquad (5.13)$$

is exothermic by 297 kJ mol^{-1}. Thus both the ^2D and ^2P states of S^+ are energetically accessible in reaction (5.13).

Furthermore, transitions from these two states to the $^4S_{3/2}$ ground state of the S^+ ion are spin-forbidden, and thus the excited states might be expected to be long-lived.

The reactions of S^+ ions with H_2S have been studied in the mass spectrometer ion source by Ruska and Franklin,[189] and by Harrison,[190] and have also been studied using the ICR method by Huntress and Pinizzotto.[191] In all cases the S^+ reactant ions were produced by electron impact on H_2S. The overall rate constants for removal of S^+ by H_2S found by these three groups are 1.15×10^{-9}, 7.6×10^{-10}, and 5.3×10^{-10} cm^3 $molecule^{-1}s^{-1}$ respectively. Harrison, and Huntress and Pinizzotto, have found that the main products of reaction are H_2S^+ and S_2^+, formed in approximately equal amounts. In addition, Huntress and Pinizzotto have found that HS_2^+ is formed as a minor reaction product ($\sim$ 12%). Harrison has pointed out that the high rate constant of 1.15×10^{-9} cm^3 $molecule^{-1}s^{-1}$ measured by Ruska and Franklin is probably due to contribution from excited S^+ ions. Harrison has also attributed the observed curvature in his decays of S^+ concentration with time to the presence of excited S^+ ions. Huntress and Pinizzotto, however, claim that, in their experiment, any excited S^+ ions will have decayed to the ground state before reaction.

In order to investigate further the reaction of S^+ with H_2S, the reaction of He^+ with H_2S has been examined.

5.4 He^+ WITH H_2S.

Electron impact in a helium carrier gas produces He^+ ions and He (2^3S) and He(2^1S) metastable atoms. The 2^1S

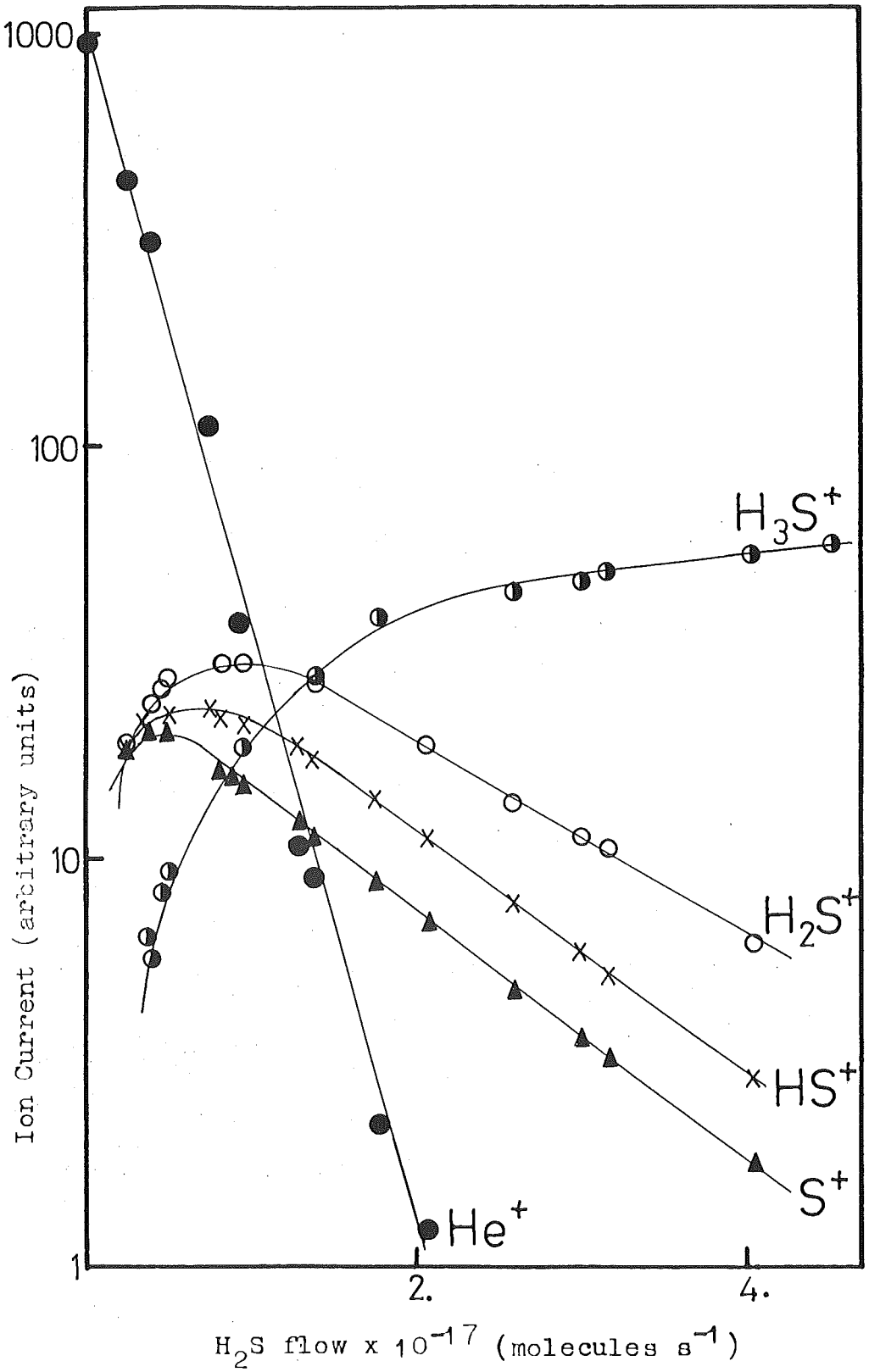

FIGURE 5.4 Ion currents vs. H_2S flow for the reaction of He^+ and $He(2^3S)$ with H_2S.

metastables are rapidly de-excited to the 2^3S state by superelastic collisions with electrons.[27] Typical data for the reaction sequence beginning with the reaction of He^+ and He (2^3S) with H_2S is shown in figure 5.4. No attempt has been made to distinguish between the products of reaction of He^+ and He (2^3S) with H_2S, although the most likely reaction channel for the He (2^3S) is the Penning ionization.

$$He\ (2^3S) + H_2S \rightarrow H_2S^+ + He + e \qquad (5.14)$$

The initial products of the reaction of He^+ and He (2^3S) with H_2S are S^+, HS^+, and H_2S^+. All three ions undergo secondary reactions with H_2S leading ultimately to H_3S^+ which becomes the dominant product ion at high flows of H_2S. In addition, small amounts of S_2^+, not shown in figure 5.4, are found. At the highest flows of H_2S shown in figure 5.4, the size of the S_2^+ peak is about 2% of that of the H_3S^+ peak.

The rate constant for the overall reaction of He^+ with H_2S is 3.0×10^{-9} cm^3 $molecule^{-1}s^{-1}$. Of more interest is the rate constant for the secondary reaction of S^+ with H_2S, which may be determined from that part of the S^+ curve which shows a linear decline, provided that the rate of production of S^+ in this region is small compared to its rate of removal. If the production rate of S^+ is comparable with its loss rate, the rate constant determined from the linear portion of the S^+ decline is properly regarded as a lower limit. From figure 5.4 it can be seen that the slope of the He^+ decline is much greater than that of the S^+ decline. Since the S^+ production rate is proportional to $[He^+]$, while the S^+ loss rate is proportional to

$[S^+]$, the S^+ production rate decreases much faster than the S^+ loss rate as the H_2S flow increases. By choosing a sufficiently high flow of H_2S then, it is possible to ensure that the S^+ production rate is negligible. The same considerations apply to the rates of the reactions of HS^+ and H_2S^+ with H_2S.

$S^+ + H_2S$

The linear portion of the S^+ decline corresponds to a rate constant for its removal by H_2S of 7.3×10^{-10} cm^3 $molecule^{-1}s^{-1}$. The only exothermic [a] reaction possible between ground-state S^+ and H_2S is

$$S^+ + H_2S \rightarrow S_2^+ + H_2 \qquad (5.15a)$$

The other possible reaction channels,

$$S^+ + H_2S \rightarrow H_2S^+ + S \qquad (5.15b)$$

$$S^+ + H_2S \rightarrow HS^+ + HS \qquad (5.15c)$$

are endothermic by 6.1 kJ mol^{-1} and 38 kJ mol^{-1} respectively. The small size of the S_2^+ peak indicates that (5.15a) is not a major reaction channel. Although an HS^+ peak is observed, it is probably a primary product of the reaction of He^+ with H_2S, rather than the product of the secondary reaction (5.15c), since no HS^+ was observed in the reaction of H_2S with S^+ produced from SO_2. The charge-transfer reaction (5.15b) is thus the major reaction channel.

A lower limit of 80% of the overall reaction can be placed on reaction channel (5.15b) because of the following observations. The primary products of the reaction of He^+

a. Except where otherwise stated, heats of reaction have been calculated using heats of formation listed in reference 187.

and He (2^3S), namely S^+, HS^+, and H_2S^+, all undergo further reaction with H_2S, and are converted almost entirely to H_3S^+ at high flows of H_2S. At low H_2S flow ($\sim 3 \times 10^{16}$ molecules s^{-1}), where the extent of secondary reactions is small, the S^+, HS^+, and H_2S^+ signals are approximately equal. Thus about 30% of the final H_3S^+ signal arises from reactions of S^+. Since at high H_2S flows the S_2^+ signal is only about 2% of the H_3S^+ signal, and the mass discrimination between m/e = 64 and peaks in the 32 - 35 mass range is no greater than a factor of three, reaction channel (5.15a) comprises less than 20% of the total reaction. The rate constant for reaction (5.15b) must then be at least 80% of the overall rate constant i.e., $5.8 \times 10^{-10} \leq k_{5.15b} \leq 7.3 \times 10^{-10}$ cm^3 $molecule^{-1}s^{-1}$. As discussed in section 5.3, this is significantly greater than is expected for a reaction which is endothermic by 6.1 kJ mol^{-1}.

It is postulated that the anomalously high rate constant $k_{5.15b}$ is due to the presence of excited S^+ ions. As the reaction

$$He^+ + H_2S \rightarrow S^+ + 2H + He \qquad (5.16)$$

is exothermic by 636 kJ mol^{-1}, both the ^2D and ^2P excited states of S^+ are energetically accessible in reaction (5.16).

The HS_2^+ ion was not observed in this work. Failure to detect it places an upper limit of 1% on the reaction channel observed by Huntress and Pinizzotto [191]

$$S^+ + H_2S \rightarrow HS_2^+ + H \qquad (5.15d)$$

The product distribution observed in this work (5.15a≤ 20%, 5.15b≥ 80%, and 5.15d < 1%) differs considerably from that observed by Harrison[190] (5.15a ~ 40-45% of total S^+ reaction), and by Huntress and Pinizzotto[191] (5.15a = 48%, 5.15b = 40%, 5.15d = 12%). This discrepancy may be another consequence of the presence of excited S^+. A variation in the amount of excited S^+ present would be expected to lead to a variation in the distribution of products of the $S^+ + H_2S$ reaction.

The possibility that excited states of S^+ may be present during reaction in the flowing afterglow has important implications for the measurement of the atmospherically-important reaction of S^+ with O_2. This will be discussed further in chapter seven.

$HS^+ + H_2S$

The linear portion of the HS^+ decline corresponds to a rate constant for removal of HS^+ by H_2S of 6.6×10^{-10} cm^3 $molecule^{-1}s^{-1}$.

Probable reaction channels are

$$HS^+ + H_2S \rightarrow H_2S^+ + HS \qquad (5.17a)$$

$$\rightarrow H_3S^+ + S \qquad (5.17b)$$

which are exothermic by 8kJ mol^{-1} and 111 kJ mol^{-1} respectively.

The reaction (5.17) has been studied by other groups. Huntress and Pinizzotto[191] have obtained a value of 7.8×10^{-10} cm^3 $molecule^{-1}s^{-1}$ for the overall rate constant for removal of HS^+ by H_2S, by the ICR method.

The two reaction channels

$$HS^+ + H_2S \rightarrow HS_2^+ + H_2 \qquad (5.17c)$$

$$\rightarrow H_2S_2^+ + H \qquad (5.17d)$$

were observed in addition to (5.17a) and (5.17b) above. The branching ratio was 5.17a = 55%, 5.17b = 35%, 5.17c = 8%, and 5.17d = 2%. Harrison[190] has measured a value of 1.22×10^{-9} cm^3 $molecule^{-1}s^{-1}$ for the overall rate constant for reaction (5.17), using the technique of ion-trapping in a mass spectrometer ion source. Only three reaction channels were identified, 5.17b = 74%, 5.17c = 21%, and 5.17d = 5%. Gupta et al.[123] have measured the rate constant for (5.17b) only, obtaining a value of 9×10^{-10} cm^3 $molecule^{-1}s^{-1}$.

In the present work, the reaction products HS_2^+ and $H_2S_2^+$ were not observed. Failure to observe these ions enables an upper limit of 2% the total reaction (5.17) to be placed on reaction channels (5.17c) and (5.17d).

The wide variation in reported values of both the overall reaction rate constant and the product distribution of reaction (5.17) could be a consequence of the presence of varying amounts of excited HS^+.

$H_2S^+ + H_2S$

Any H_2S^+ formed in the above reactions is removed in the reaction

$$H_2S^+ + H_2S \rightarrow H_3S^+ + HS \qquad (5.7a)$$

The rate constant for reaction (5.7a) measured in this work, 5.8×10^{-10} cm^3 $molecule^{-1}s^{-1}$, lies at the lower end of the range of values measured by other workers. These values

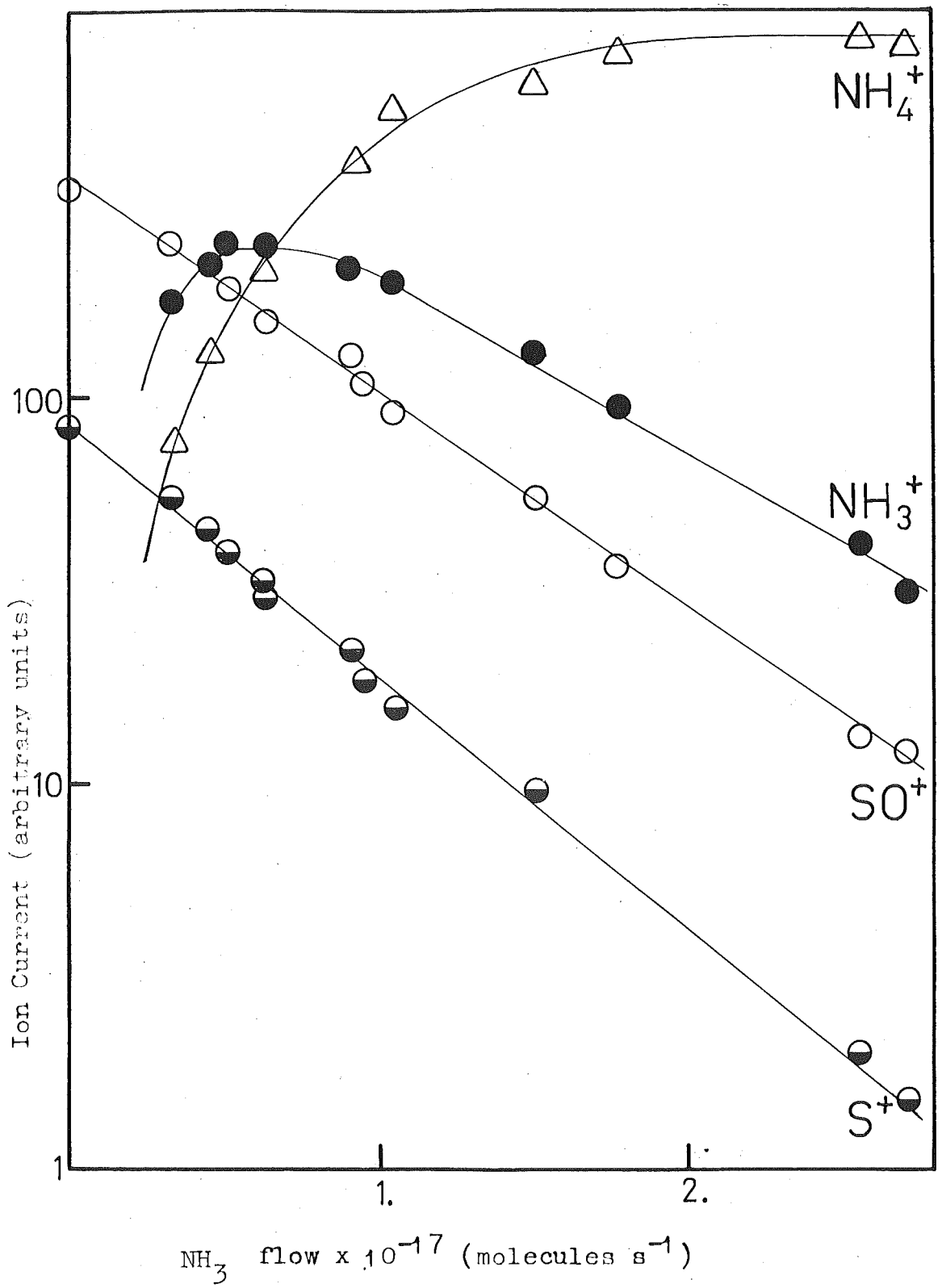

FIGURE 5.5 Ion currents vs. NH_3 flow for the reaction of S^+ and SO^+ with NH_3.

(in cm^3 $molecule^{-1}s^{-1}$) are 7.7×10^{-10}, [123] 9.2×10^{-10} [189] 7.2×10^{-10} [190], 5.9×10^{-10} [191], and 5.8×10^{-10}. [192] Huntress and Pinizzotto [190] also observed that a small fraction (~ 1.5%) of the total reaction proceeds via reaction (5.7b):

$$H_2S^+ + H_2S \rightarrow H_2S_2^+ + H_2 \qquad (5.7b)$$

If reaction (5.7b) occurs to the same extent in the flowing afterglow the amount of $H_2S_2^+$ thus produced would be below the level of detection. It has been suggested [191] that the wide variation of rate constants for reaction (5.7) may be due to the presence of excited H_2S^+.

5.5 S^+ AND SO^+ WITH NH_3.

The reactant ions S^+ and SO^+ were formed as before, by addition of SO_2 into the helium afterglow. Both the S^+ and SO^+ ion signals are reduced by the addition of NH_3; data for a typical run is shown in figure 5.5. The product initially formed is NH_3^+, produced in the charge-transfer reactions

$$S^+ + NH_3 \rightarrow NH_3^+ + S \qquad (5.18)$$

$$SO^+ + NH_3 \rightarrow NH_3^+ + SO \qquad (5.19)$$

The rate constants measured for reactions (5.18) and (5.19) are 1.4×10^{-9} cm^3 $molecule^{-1}s^{-1}$ and 1.3×10^{-9} cm^3 $molecule^{-1}$ s^{-1} respectively.

The NH_3^+ produced by charge transfer undergoes further reaction with added ammonia:

$$NH_3^+ + NH_3 \rightarrow NH_4^+ + NH_2 \qquad (5.20)$$

The linear portion of the NH_3^+ decline corresponds to a rate constant for (5.20) of 1.1×10^{-9} cm^3 $molecule^{-1}s^{-1}$. However, since the rate of decline of NH_3^+ is similar to that of the precursor ions S^+ and SO^+, there may be significant amounts of NH_3^+ still being formed at high NH_3 flows, and the rate constant for (5.20) is properly regarded as a lower limit.

At much higher NH_3 flows than are shown in figure 5.5, the NH_4^+ signal declines due to the three-body reaction

$$NH_4^+ + NH_3 + He \rightarrow NH_4^+ \cdot NH_3 + He \qquad (5.21)$$

The reaction of S^+ with NH_3 has been studied by Laudenslager and Huntress [193] by the ICR method. They obtained a value of 1.25×10^{-9} cm^3 $molecule^{-1}s^{-1}$ for the rate constant for (5.20), in reasonable agreement with the result obtained in this work. Laudenslager and Huntress found that the reaction proceeds via two channels:

$$S^+ + NH_3 \rightarrow NH_3^+ + S \quad 94\% \qquad (5.18a)$$

$$\rightarrow NH_2S^+ + H \quad 6\% \qquad (5.18b)$$

If reaction (5.18b) were occurring in the flowing afterglow, the production of NH_2S^+ would be expected to lead to curvature in the decline of the m/e = 48 ion signal due to SO^+, since both NH_2S^+ and SO^+ have the same mass. In the present work, the decline in the m/e = 48 ion signal has been observed to be linear over two decades. Failure to observe curvature in this ion signal enables an upper limit of 2% of the total reaction to be placed on reaction channel (5.18b). The different product distributions observed in the ICR and flowing afterglow experiments may be a further consequence of the presence of excited states of the S^+ ion. Variation in the relative amounts of excited S^+ present would be expected to cause a variation

in the distribution of the products of reaction of S^+.

The secondary reaction (5.20)

$$NH_3^+ + NH_3 \rightarrow NH_4^+ + NH_2 \qquad (5.20)$$

observed in the present work has been studied many times before. A number of results are collected in reference 190. Measured values of the rate constant range from 1.0×10^{-9} to 3.2×10^{-9} cm^3 $molecule^{-1}s^{-1}$, with an average value of 1.5×10^{-9} cm^3 $molecule^{-1}s^{-1}$. The lower limit for the rate constant measured in the present work is consistent with these results.

5.6 O^+ AND O_2^+ WITH H_2S.

The reactant ions O^+ and O_2^+ are produced by addition of O_2 into a helium afterglow. O^+ is formed in the fast reaction[55,158]

$$He^+ + O_2 \rightarrow O^+ + O + He \qquad (5.22)$$

O_2^+ is formed in the reaction [55]

$$He\ (2^3S) + O_2 \rightarrow O_2^+ + He + e \qquad (5.23)$$

and also in the slower reaction

$$O^+ + O_2 \rightarrow O_2^+ + O \qquad (5.24)$$

for which $k = 2 \times 10^{-11}$ cm^3 $molecule^{-1}s^{-1}$.[194] In studying the reaction of O^+, sufficient O_2 is added to the afterglow to completely remove the He^+ ions via the fast reaction (5.22). When studying the reaction of O_2^+, much higher flows of O_2 are used in order to remove all the O^+ ions via the slow reaction (5.24), since the O^+ ions would otherwise provide a distributed source of O_2^+ in the reaction zone.

Both the O^+ and O_2^+ ion signals are decreased by the addition of H_2S. The only product ion formed initially

is H_2S^+, produced in the charge-transfer reactions

$$O^+ + H_2S \rightarrow H_2S^+ + O \qquad (5.25)$$

$$O_2^+ + H_2S \rightarrow H_2S^+ + O_2 \qquad (5.26)$$

The rate constants measured for reactions (5.25) and (5.26) are 1.6×10^{-9} cm^3 $molecule^{-1}s^{-1}$ and 1.4×10^{-9} cm^3 $molecule^{-1}s^{-1}$ respectively.

The H_2S^+ initially formed undergoes further reaction with H_2S thus:

$$H_2S^+ + H_2S \rightarrow H_3S^+ + HS \qquad (5.7a)$$

The rate constant for (5.7) measured in this section of the present work is 6.8×10^{-10} cm^3 $molecule^{-1}s^{-1}$, in satisfactory agreement with the value of 5.8×10^{-10} cm^3 $molecule^{-1}s^{-1}$ determined earlier in section 5.4.

5.7 C^+ AND CO^+ WITH SO_2.

The reactant ions C^+ and CO^+ are formed by the addition of CO into a helium afterglow. The reactions involved, and their rate constants, are

$$He^+ + CO \rightarrow C^+ + O + He \qquad (5.27)$$

$$k = 1.7 \times 10^{-9} \text{ cm}^3 \text{ molecule}^{-1}\text{s}^{-1} \quad [55]$$

and

$$He\ (2^3S) + CO \rightarrow CO^+ + He + e \qquad (5.28)$$

$$k = 1.1 \times 10^{-10} \text{ cm}^3 \text{ molecule}^{-1}\text{s}^{-1} \quad [195]$$

If sufficiently high flows of CO are used, any N_2^+ initially present as an impurity at m/e = 28 should be converted to CO^+ in the reaction

$$N_2^+ + CO \rightarrow CO^+ + N_2 \qquad (5.29)$$

$$k = 7.0 \times 10^{-11} \text{ cm}^3 \text{ molecule}^{-1}\text{s}^{-1} \quad [196]$$

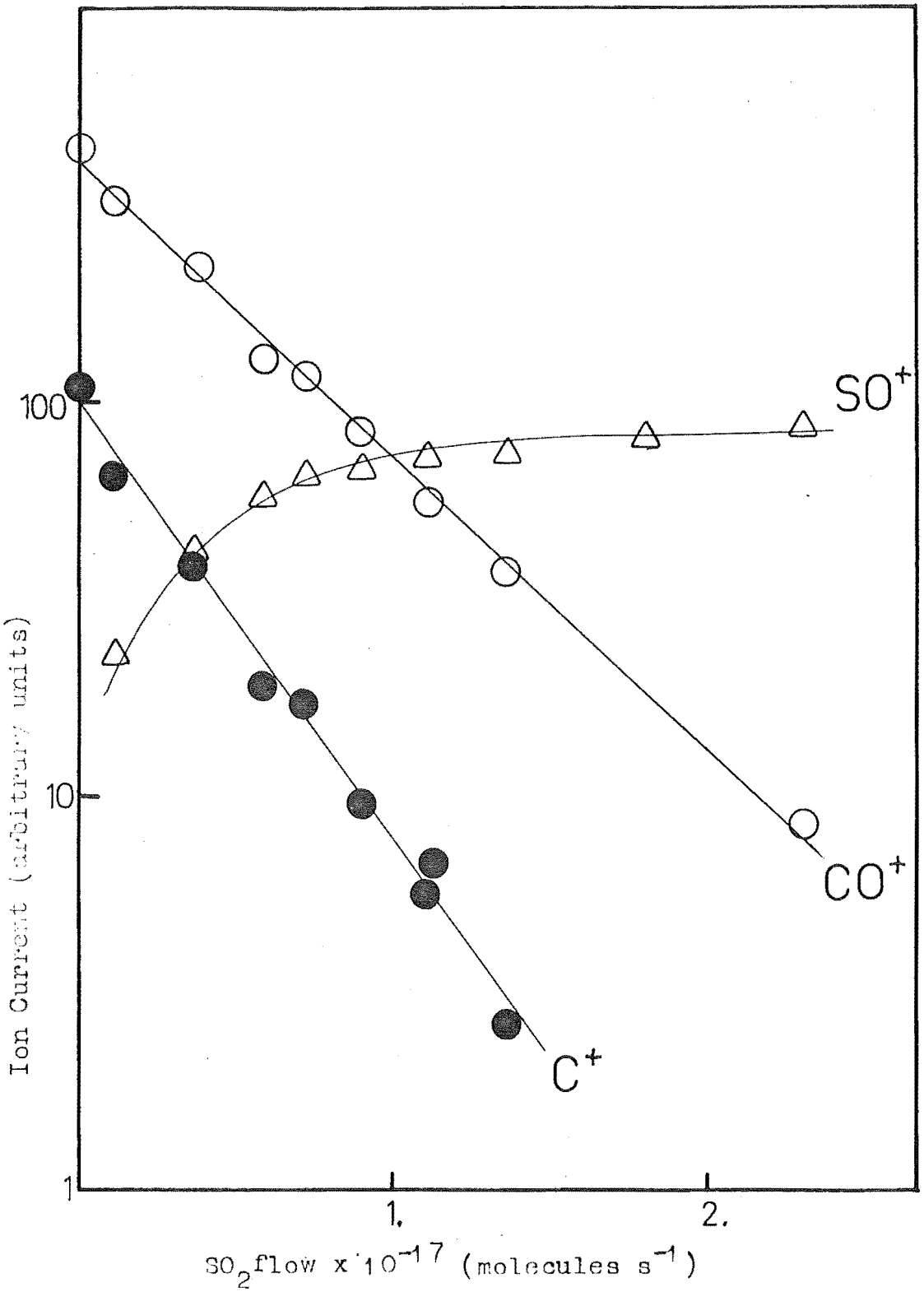

FIGURE 5.6 Ion currents vs. SO_2 flow for the reaction of C^+ and CO^+ with SO_2.

Typical data for the reaction of C^+ and CO^+ with SO_2 is shown in figure 5.6. Not included in this figure is the weak SO_2^+ ion signal observed; at the highest flows of SO_2, the SO_2^+ signal has a value of about 2% of that of the SO^+ ion signal shown.

Of the two product ions observed, SO^+ and SO_2^+, the SO_2^+ must arise exclusively from the reaction of CO^+, since the charge-transfer reaction between C^+ and SO_2 is endothermic by 107 kJ mol^{-1}. The sole reaction channel observed for reaction between C^+ and SO_2 is thus

$$C^+ + SO_2 \rightarrow SO^+ + CO \qquad (5.30a)$$

The rate constant for this reaction is 2.4×10^{-9} cm^3 $molecule^{-1}s^{-1}$.

The reaction channel

$$C^+ + SO_2 \rightarrow CO^+ + SO \qquad (5.30b)$$

is exothermic by 257 kJ mol^{-1}. If reaction (5.30b) were to occur, the CO^+ thus produced would lead to curvature in the decline of the CO^+ ion signal. Failure to observe such curvature enables an upper limit of 5% of the total C^+ reaction to be placed on reaction channel (5.30b).

Three other exothermic reaction channels are available for reaction between C^+ and SO_2:

$$C^+ + SO_2 \rightarrow CO_2^+ + S \qquad (5.30c)$$

$$\rightarrow CS^+ + O_2 \qquad (5.30d)$$

$$\rightarrow S^+ + CO_2 \qquad (5.30e)$$

None of these channels are observed. This result is hardly surprising in view of the considerable molecular rearrangement involved.

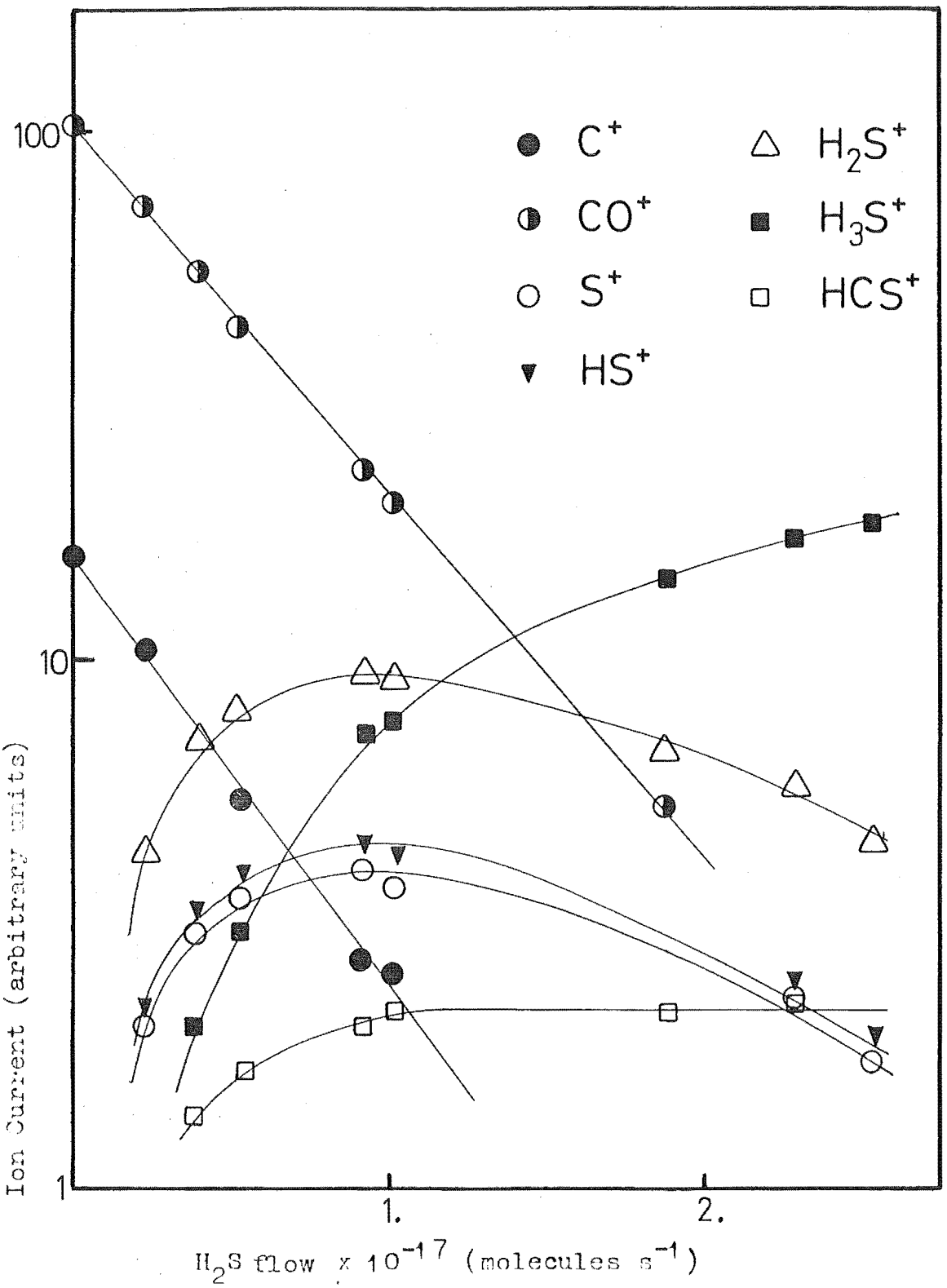

FIGURE 5.7 Ion currents vs. H_2S flow for the reaction of C^+ and CO^+ with H_2S.

The reaction between CO^+ and SO_2 is observed to proceed via two channels:

$$CO^+ + SO_2 \rightarrow SO^+ + CO_2 \qquad (5.31a)$$

$$\rightarrow SO_2^+ + CO \qquad (5.31b)$$

The rate constant for the overall reaction between CO^+ and SO_2 is 1.7×10^{-9} cm^3 $molecule^{-1}s^{-1}$. The branching ratio between the two channels may be calculated by comparing the SO_2^+ signal with that fraction of the SO^+ signal derived from CO^+, making allowance for mass discrimination. The decrease in sampling efficiency between masses 48 and 64 is unlikely to be greater than a factor of three, and hence it can be concluded that 95 - 98% of reaction (5.31) proceeds via channel a.

5.8 C^+ AND CO^+ WITH H_2S.

The reactant ions C^+ and CO^+ are formed by reaction of CO with the active species in a helium afterglow, as described in section 5.7. The ion signals resulting from addition of H_2S to the afterglow containing C^+ and CO^+ ions are shown in figure 5.7.

Both C^+ and CO^+ react rapidly with H_2S. The primary products of the reaction are S^+, HS^+, H_2S^+, and HCS^+. The ions S^+, HS^+, and H_2S^+ then undergo further reactions with H_2S to ultimately produce H_3S^+.

To distinguish between the products of the reactions of C^+ and CO^+ with H_2S, the energy of the ionizing electrons was lowered to about 24V. In this case, electron impact in the helium carrier results in formation of He (2^3S) and He (2^1S) metastable atoms, but no He^+ ions. Subsequent

addition of CO results in production of CO^+, but no C^+.

The product ions initially formed when H_2S is added to the afterglow containing CO^+ ions only are S^+, HS^+, and H_2S^+. The reactions involved are

$$CO^+ + H_2S \rightarrow S^+ + H_2 + CO \qquad (5.32a)$$

$$\rightarrow HS^+ + HCO \qquad (5.32b)$$

$$\rightarrow H_2S^+ + CO \qquad (5.32c)$$

The rate constant for the overall reaction between CO^+ and H_2S is 1.4×10^{-9} cm^3 $molecule^{-1}s^{-1}$.

The product ion HCS^+ arises exclusively from the reaction of C^+ ions with H_2S. Comparison of the final HCS^+ ion signal with the initial C^+ ion signal, allowing for mass discrimination effects, indicates that the reaction channel

$$C^+ + H_2S \rightarrow HCS^+ + H \qquad (5.33a)$$

accounts for 20-25% of the total reaction between C^+ and H_2S. Other reaction channels were not conclusively identified. Formation of any of the observed product ions S^+, HS^+, or H_2S^+ from C^+ cannot be ruled out on energetic grounds since the reactions

$$C^+ + H_2S \rightarrow S^+ + CH_2 \qquad (5.33b)$$

$$\rightarrow HS^+ + CH \qquad (5.33c)$$

$$\rightarrow H_2S^+ + C \qquad (5.33d)$$

are all exothermic. The occurrence of any one of these reactions should manifest itself as a change in the ion signal profile of the corresponding product ion when changing from a plasma containing CO^+ ions only to one containing both CO^+ and C^+. However, since the C^+ ion signal is considerably smaller than the CO^+ ion signal,

this effect is small and is overshadowed by variation in the mass discrimination of the ion sampling and detection system. The rate constant for the overall reaction between C^+ and H_2S is 1.8×10^{-9} cm^3 $molecule^{-1}$ s^{-1}.

The reaction between C^+ and H_2S has been studied by Huntress et al.[182], who determined a value of 2.0×10^{-9} cm^3 $molecule^{-1}$ s^{-1} for the overall rate constant, and found that the reaction proceeds via two channels :

$$C^+ + H_2S \rightarrow HCS^+ + H \quad 72\% \qquad (5.33a)$$

$$\rightarrow H_2S^+ + C \quad 28\% \qquad (5.33b)$$

The reaction between CO^+ and H_2S to produce S^+,

$$CO^+ + H_2S \rightarrow S^+ + H_2 + CO \qquad (5.32a)$$

is exothermic by 50 kJ mol^{-1}. Since the first excited state of S^+ lies 178 kJ mol^{-1} above the ground state of S^+, only ground-stste S^+ can be formed in reaction (5.32a). The reaction between ground-state S^+ and H_2S is expected to be slow. Unfortunately, at the time of performing these experiments, the sensitivity of the ion detection system was so low that it was not possible to follow the S^+ decline over a range sufficiently large to determine a rate constant for its removal. The sensitivity of the ion detection system has since been improved, and preliminary studies indicate that the rate constant for reaction between H_2S and S^+ formed in reaction (5.32a) is signif_ icantly lower than the rate constant reported for the reaction between H_2S and S^+ in sections 5.2 and 5.3, which may have involved a contribution from excited states of the S^+ ion.

5.9 SULPHUR CHEMISTRY IN INTERSTELLAR CLOUDS.

As mentioned in the first chapter , the interstellar gas clouds are composed chiefly of hydrogen. Any H_2^+ produced by cosmic-ray ionization is converted to H_3^+. Proton transfer from H_3^+ to neutral species is then important in initiating ion-molecule reaction schemes.

One of the most abundant molecules, after hydrogen, in many interstellar clouds is CO. This molecule is rapidly protonated by H_3^+:

$$H_3^+ + CO \rightarrow HCO^+ + H_2 \qquad (5.5)$$

$$k = 1.5 \times 10^{-9} cm^3 \text{ molecule}^{-1} s^{-1}. \quad [185]$$

The HCO^+ ion may also be formed in the rapid reaction

$$CO^+ + H_2 \rightarrow HCO^+ + H \qquad (5.34)$$

$$k = 2.0 \times 10^{-9} \text{ cm}^3 \text{ molecule}^{-1} s^{-1} \quad [197]$$

and, under some conditions, in the chemiionization reaction[198]

$$O + CH \rightarrow HCO^+ + e \qquad (5.35)$$

Since the HCO^+ ion does not undergo further reaction with the dominant neutral species H_2, He, and CO, its abundance is expected to be relatively high. The important loss mechanism for HCO^+ is proton transfer to minor neutral constituents of the interstellar clouds.

The He^+ ion is another important ion in interstellar clouds. It is produced by cosmic-ray ionization of He and, since it does not undergo rapid reaction with H_2,[55] it is relatively abundant. An important loss mechanism for He^+ is the reaction

$$He^+ + CO \rightarrow C^+ + O + He \qquad (5.27)$$

Since the reactions of C^+ with the dominant neutral species H_2 and CO are endothermic, the C^+ ion is not destroyed very rapidly. It is one of the more abundant ions in interstellar clouds, and is thought to play an important role in the creation and destruction of many neutral species.

Few interstellar cloud ion densities have been measured. Herbst and Klemperer[199] have calculated steady-state abundances of several ions in dense clouds, using a model based on ion-molecule reactions. Their model indicates that C^+, HCO^+, and possibly O_2^+ are the dominant ions in dense interstellar clouds.

Sulphur-containing compounds were not included in the model of Herbst and Klemperer. Oppenheimer and Dalgarno [200] have proposed a scheme, including both ion-molecule and atom-molecule reactions, to account for the creation and destruction of the observed sulphur-containing molecules. The observed molecules are CH, OCS, H_2CS, H_2S, and SO. In the scheme of Oppenheimer and Dalgarno, the Langevin model was used to estimate the rates of those ion-molecule reactions for which laboratory measurements were unavailable.

In dense interstellar clouds, appreciable ionizing radiation cannot penetrate, and Oppenheimer and Dalgarno have suggested that sulphur is mainly neutral. Their proposed mechanism for formation of H_2S is

$$H_3^+ + S \rightarrow H_2S^+ + H \qquad (5.36)$$

followed by charge exchange reactions to give neutral H_2S.

They suggested that the important reactions leading to the removal of H_2S are

$$HCO^+ + H_2S \rightarrow H_3S^+ + CO \qquad (5.6)$$

and

$$C^+ + H_2S \rightarrow HCS^+ + H \qquad (5.33a)$$

Other reactions which may be important for removing H_2S are

$$C^+ + H_2S \rightarrow H_2S^+ + C \qquad (5.33d)$$

$$H_3^+ + H_2S \rightarrow H_3S^+ + H_2 \qquad (5.2)$$

and

$$O_2^+ + H_2S \rightarrow H_2S^+ + O_2 \qquad (5.26)$$

Reactions (5.2) and (5.6) do not destroy H_2S, but serve only to recycle it, since H_2S is regenerated in the reaction

$$H_3S^+ + e \rightarrow H_2S + H \qquad (5.26)$$

The rate constants measured in this work for reactions (5.6) and (5.33) are reasonably close to the value of 1×10^{-9} cm^3 $molecule^{-1}s^{-1}$ adopted by Oppenheimer and Dalgarno for the rates of both reactions. The assumption made by these authors that the rates of (5.6) and (5.33) are comparable is confirmed.

In the model of Oppenheimer and Dalgarno, the chief loss mechanism for S^+ is the reaction

$$S^+ + O_2 \rightarrow SO^+ + O \qquad (5.37)$$

for which Fehsenfeld and Ferguson[201] have determined a rate constant of 2.0×10^{-11} cm^3 $molecule^{-1}s^{-1}$ by the flowing afterglow method. This value may be too high if there were significant amounts of excited S^+ present in the flowing afterglow, as suggested earlier in this chapter.

If this is so, the fast reaction

$$S^+ + NH_3 \rightarrow NH_3^+ + S \qquad (5.18a)$$

may provide an important loss process for S^+, even though NH_3 is much less abundant than O_2.

Although attempts to detect SO_2 in interstellar clouds have so far been unsuccessful,[202] this molecule is included in Oppenheimer and Dalgarno's reaction scheme. It is formed in the reaction

$$SO + OH \rightarrow SO_2 + H \qquad (5.38)$$

and destroyed in the reaction

$$C^+ + SO_2 \rightarrow SO^+ + CO \qquad (5.30a)$$

The value of 1×10^{-9} cm^3 molecule^{-1}s^{-1} adopted for the rate of reaction (5.30a) is not too different from the value of 2.4×10^{-9} cm^3 molecule^{-1}s^{-1} determined in this work.

The new laboratory measurements reported in this chapter are not sufficiently different from the rate constants adopted by Oppenheimer and Dalgarno to produce any major changes in these authors' sulphur-chemistry scheme. However the reaction

$$O_2^+ + H_2S \rightarrow H_2S^+ + O_2 \qquad (5.26)$$

which was ignored by Oppenheimer and Dalgarno, is sufficiently fast to provide an important loss mechanism for H_2S in clouds in which the oxygen abundance is high.

CHAPTER 6.

REACTIONS RELATED TO CYANIDE CHEMISTRY IN INTERSTELLAR CLOUDS.

6.1 H_2CN^+ WITH NH_3.

Addition of HCN into a hydrogen afterglow results in formation of H_2CN^+ due to the fast reaction

$$H_3^+ + HCN \rightarrow H_2CN^+ + H_2 \qquad (6.1)$$

Addition of NH_3 to the afterglow containing H_2CN^+ as the dominant ion results in a decrease in the ion signal at m/e = 28 due to H_2CN^+, and the appearance of an ion signal at m/e = 18 due to NH_4^+. The reaction taking place is

$$H_2CN^+ + NH_3 \rightarrow NH_4^+ + HCN \qquad (6.2)$$

The measured rate constant for reaction (6.2) is 2.4×10^{-9} cm^3 $molecule^{-1}s^{-1}$. At higher flows of NH_3, the NH_4^+ ion is removed in the three-body clustering reaction

$$NH_4^+ + NH_3 + H_2 \rightarrow NH_4^+ \cdot NH_3 + H_2 \qquad (6.3)$$

Reaction (6.2), together with most of the other reactions reported in this chapter, has been studied recently by Huntress et al.,[182] using the ICR method. Their value of the rate constant for this reaction is 2.2×10^{-9} cm^3 $molecule^{-1}s^{-1}$. Schiff et al.[121] have determined a lower limit of 1.5×10^{-9} cm^3 $molecule^{-1}s^{-1}$ for the rate constant for reaction (6.2) in the flowing afterglow.

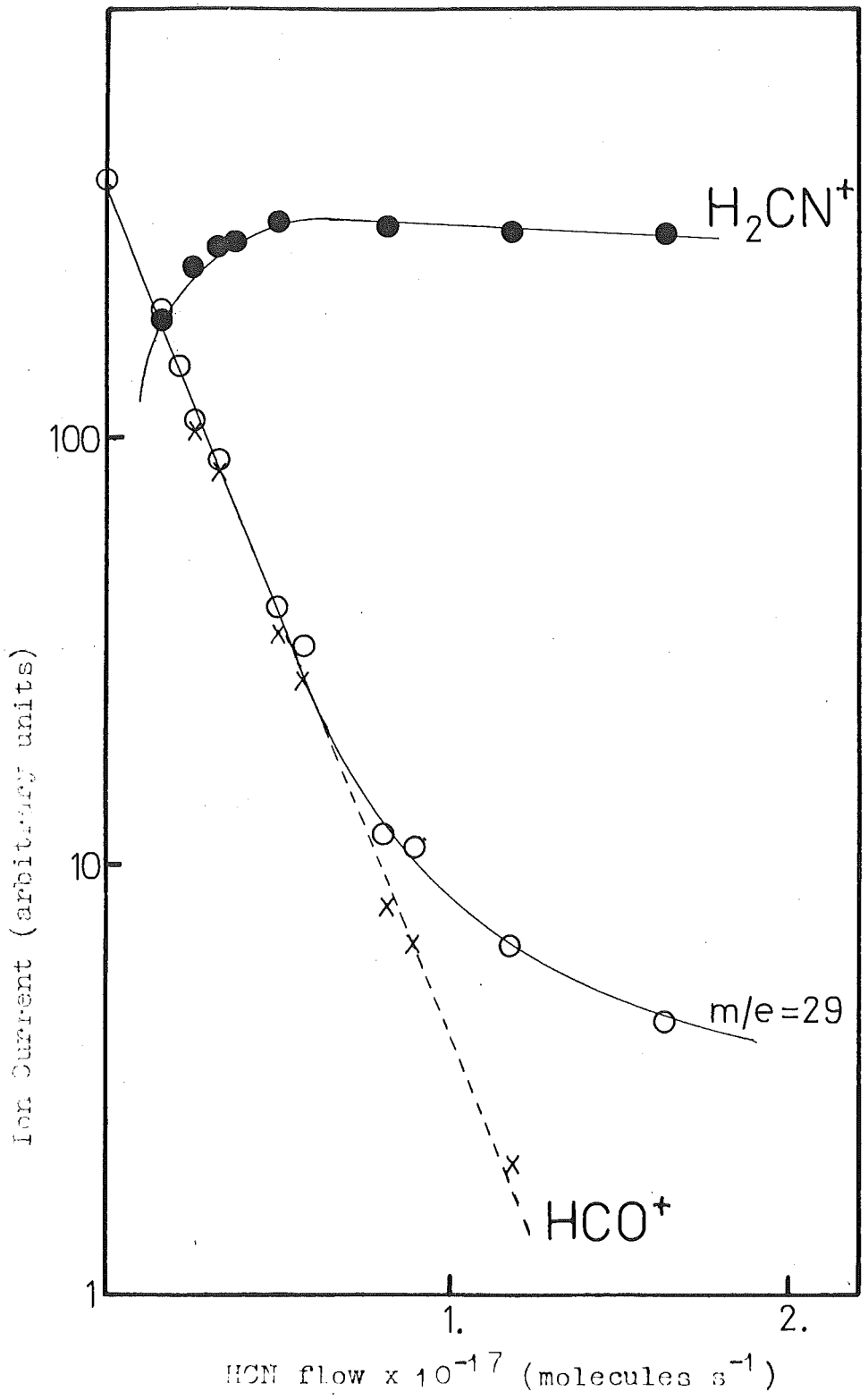

FIGURE 6.1 Ion currents vs. HCN flow for the reaction of HCO^+ with HCN.

6.2 HCO^+ + HCN.

The reactant ion HCO^+ was formed as described in the previous chapter, by addition of CO into a hydrogen afterglow. The ion signals resulting from addition of HCN to the afterglow containing HCO^+ as the dominant ion are shown in fig. 6.1.

The only primary reaction taking place is the proton-transfer reaction

$$HCO^+ + HCN \rightarrow H_2CN^+ + CO \qquad (6.4)$$

Not shown in fig. 6.1 is the ion signal due to $H_2CN^+.HCN$ formed at high HCN flows in the secondary reaction

$$H_2CN^+ + HCN + H_2 \rightarrow H_2CN^+.HCN + H_2 \qquad (6.5)$$

The ion signal at m/e = 29 is due to two different species: the reactant ion HCO^+, and isotopes of the product ion H_2CN^+. There are three isotopes of H_2CN^+ which contribute to the ion signal at m/e = 29. These are $^2H\,^1H\,^{12}C\,^{14}N^+$, $^1H_2\,^{13}C\,^{14}N^+$, and $^1H_2\,^{12}C\,^{15}N^+$. The size of the H_2CN^+ ion signal at m/e = 29 due to these three isotopic species is 1.49% of that of the H_2CN^+ ion signal at m/e = 28. (Isotopic abundances, relative to the isotope of lowest mass, are: ^2H 0.016%; ^{13}C 1.08%; ^{15}N 0.38%). To obtain the true HCO^+ decline, it is necessary to subtract the H_2CN^+ contribution to the ion signal at m/e = 29. This procedure results in a linear decline of the semilogarithmic plot of HCO^+ vs HCN flow for over two decades. The slope of this decline yields a value for the rate constant for reaction (6.4) of 4.0×10^{-9} cm^3 molecule^{-1}s^{-1}.

The rate constant measured by Huntress et al.[182] for reaction (6.4) is 3.5×10^{-9}cm^3 molecule^{-1}s^{-1}.

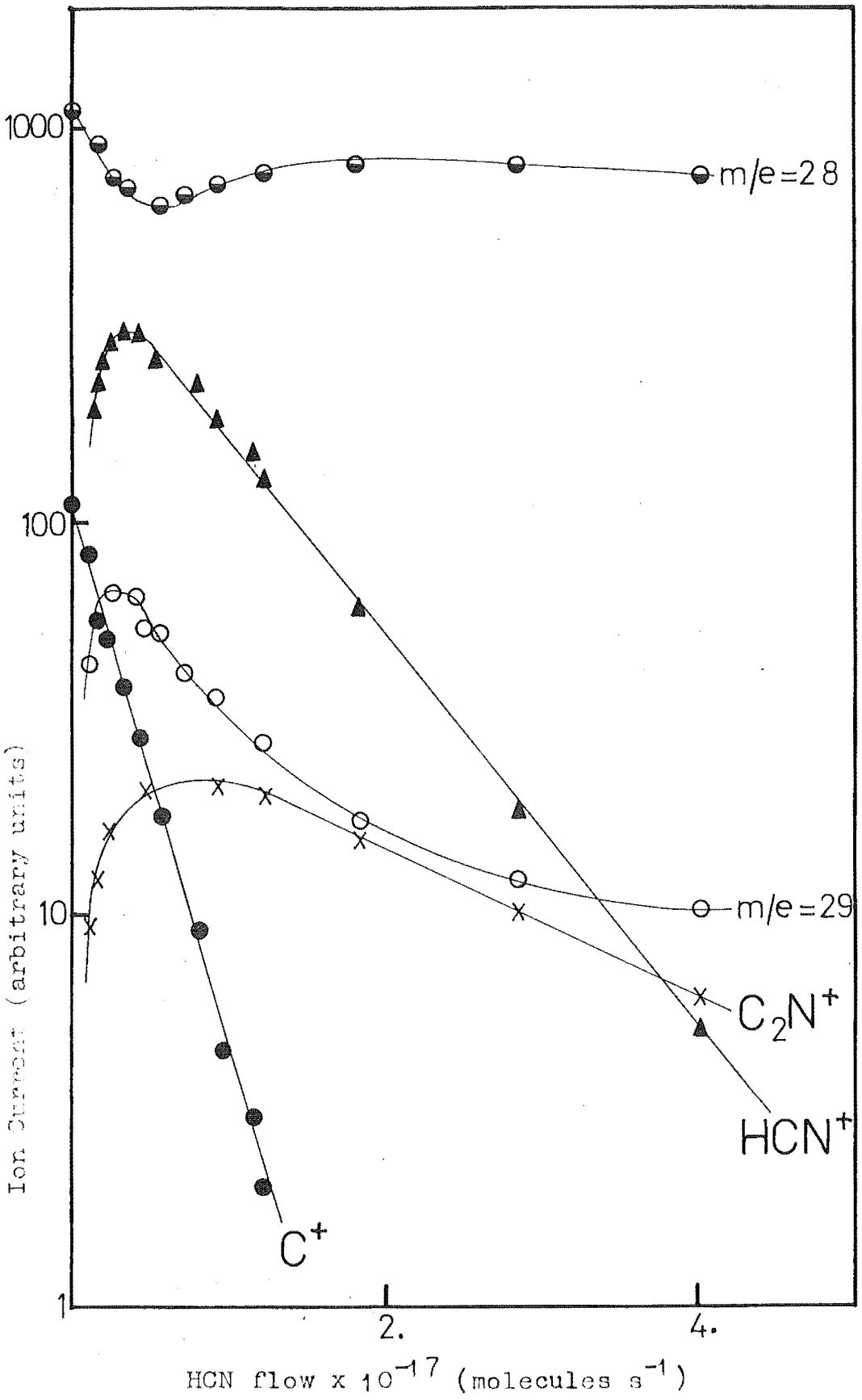

FIGURE 6.2 Ion currents vs. HCN flow for the reaction of C^+ and CO^+ with HCN.

The observation that reaction (6.4) is rapid establishes that the proton affinity (P.A.) of HCN is greater than that of CO. A value of 594.5 ± 8.8 kJ mol^{-1} for P.A. (CO) may be deduced from the data of Matthews and Warneck [203] for the heat of formation of HCO^+. Hence P.A. (HCN) > 585.7 kJ mol^{-1}, and adopting the values[187] of 135. kJ mol^{-1} for ΔH_f (HCN) and 1530 kJ mol^{-1} for ΔH_f (H^+), it may be deduced that $\Delta H_f(H_2CN^+)$ < 1079 kJ mol^{-1}. This is in disagreement with one of Gallegos and Kisser's[204] determinations of $\Delta H_f(H_2CN^+)$ = 1096 kJ mol^{-1}, but consistent with another of their values of 1059 kJ mol^{-1}, and is also consistent with the value of 1033 kJ mol^{-1} determined by Franklin et al.[205]

6.3 C^+ WITH HCN.

The reactant ion C^+, together with the CO^+ ion, is produced by addition of CO into a helium afterglow, as described in the previous chapter.

Figure 6.2 shows typical data for the sequence of reactions beginning with the reaction of HCN with the ions CO^+ and C^+. Both ions react rapidly with HCN. The CO^+ reacts via two channels:

$$CO^+ + HCN \rightarrow HCO^+ + CN \qquad (6.6a)$$

$$\rightarrow HCN^+ + CO \qquad (6.6b)$$

The initially-formed HCO^+ and HCN^+ ions both react further with HCN+

$$HCO^+ + HCN \rightarrow H_2CN^+ + CO \qquad (6.4)$$

and

$$HCN^+ + HCN \rightarrow H_2CN^+ + CO \qquad (6.7a)$$

The curvature in the decline of the m/e = 29 signal is again due to a contribution to this ion signal by isotopes of HCN, as discussed in the preceding section.

The decline in the m/e = 28 ion signal due to removal of CO^+ in reaction (6.6) is masked by an increase in the m/e = 28 ion signal due to production of H_2CN^+ in reactions (6.4) and (6.7a), all the CO^+ ultimately being converted to H_2CN^+. Fig. 6.2 shows that the H_2CN^+ ion signal at high HCN flows does not balance exactly the initial CO^+ ion signal. This discrepancy is presumably due to removal of H_2CN^+ in the three-body reaction

$$H_2CN^+ + HCN + He \rightarrow H_2CN^+.HCN + He \qquad (6.5)$$

and also possibly due to a difference in diffusion coefficients for CO^+ and H_2CN^+ leading to a greater diffusive loss of H_2CN^+ compared with CO^+.

The only reaction taking place between C^+ and HCN is

$$C^+ + HCN \rightarrow C_2N^+ + H \qquad (6.8)$$

The C_2N^+ thus produced undergoes further reaction with HCN:

$$C_2N^+ + HCN \rightarrow \text{products} \qquad (6.9)$$

However the products of this reaction could not be identified.

It was not possible to determine a rate constant for the reaction between CO^+ and HCN, due to interference from the H_2CN^+ product ion at m/e = 28. The rate constant measured for the reaction of C^+ with HCN, reaction (6.8), is 2.8×10^{-9} cm^3 $molecule^{-1}s^{-1}$. The value obtained by Huntress et al.[182] for this reaction is 3.2×10^{-9} cm^3 $molecule^{-1}s^{-1}$.

The rate constant for reaction (6.8) has also been measured by Inoue and Cottin.[206] The reaction was studied in a mass spectrometer ion source, where the C^+ ion was produced by electron impact on HCN. The measured rate constant for reaction (6.8) was 1.3×10^{-9} cm^3 $molecule^{-1}s^{-1}$. Inoue and Cottin's measurement is not a thermal-energy rate constant however, due to acceleration of the ion in the repeller field of the mass spectrometer ion source. It represents instead an average value of the rate constant over a range of ion energies from thermal to the ion exit energy. The ion-source pressure was not measured directly in these experiments, but was deduced from total ionization measurements. This procedure can lead to error as was pointed out by Gupta et al.[123]

The linear portion of the HCN^+ decline yields a rate constant for reaction (6.7a) of 9.6×10^{-10} cm^3 $molecule^{-1}s^{-1}$.

$$HCN^+ + HCN \rightarrow H_2CN^+ + CN \qquad (6.7a)$$

Harrison and Thynne [207] have obtained a value of 6.0×10^{-10} cm^3 $molecule^{-1}s^{-1}$ for the rate constant for reaction (6.7a), using the pulsed mass-spectrometer ion source method. However many of the early results of Harrison et al. have been shown[123] to be in error because of errors in measurement of the ion-source pressure. Reaction (6.7a) has also been studied at non-thermal energies by Inoue and Cottin,[206] who measured a rate constant for the reaction of 1.2×10^{-9} cm^3 $molecule^{-1}s^{-1}$, and also observed a second reaction channel

$$HCN^+ + HCN \rightarrow C_2N_2H^+ + H \qquad (6.7b)$$

Their measured rate constant for reaction (6.7b) is $3.2 \times$

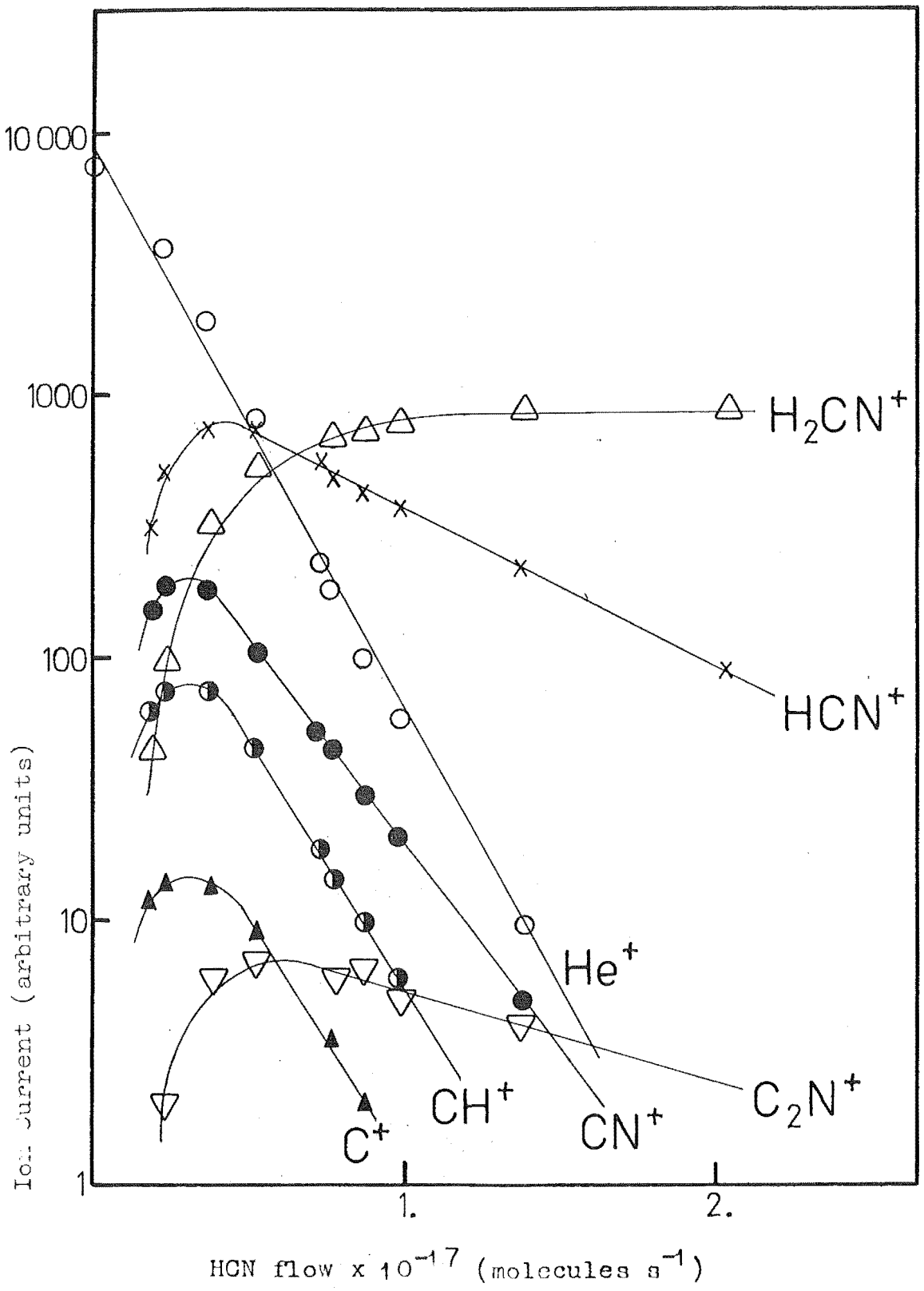

FIGURE 6.3 Ion currents vs. HCN flow for the reaction of He^+ and $He(2^3)$ with HCN.

10^{-11} cm^3 $molecule^{-1}s^{-1}$. The same workers measured a rate constant of 1.5×10^{-11} cm^3 $molecule^{-1}s^{-1}$ for the reactiom

$$C_2N^+ + HCN \rightarrow C_3N_2^+ + H \qquad (6.9)$$

The rate constant measured in the present work for the removal of C_2N^+ by reaction with HCN is 3.1×10^{-10} cm^3 $molecule^{-1}s^{-1}$. Discrepancies between the results of Inoue and Cottin and the present flowing afterglow results are presumably due to the non-thermal distribution of ion energies encountered in the mass spectrometer ion source.

6.4 He^+ WITH HCN.

As discussed in chapter 5, the dominant active species in a helium afterglow are He^+ ions and He (2^3S) metastable atoms, present in approximately equal amounts. The ion signals resulting from addition of HCN to a helium afterglow are shown in figure 6.3. No attempt has been made to distinguish between the products of reaction of He^+ and He (2^3S). It is likely, however, that the main reaction channel for reaction between He^+ ions and HCN is dissociative charge transfer, while He (2^3S) metastable atoms react predominantly by Penning ionization.

The measured rate constant for removal of He^+ by reaction with HCN is 3.9×10^{-9} cm^3 $molecule^{-1}s^{-1}$. The main products of dissociative charge transfer are CN^+ and CH^+, together with smaller amounts of C^+. The reactions producing these ions are

$$He^+ + HCN \rightarrow CN^+ + H + He \qquad (6.10a)$$

$$\rightarrow CH^+ + N + He \qquad (6.10b)$$

$$\rightarrow C^+ + N + H + He \qquad (6.10c)$$

Branching ratios were not determined, due to the complications caused by secondary reactions, and the presence of He (2^3S) metastable atoms. All three product ions of reaction (6.10) undergo further reaction with HCN. Probable reaction channels for CN^+ and CH^+ are

$$CN^+ + HCN \rightarrow HCN^+ + CN \qquad (6.11a)$$

$$CH^+ + HCN \rightarrow H_2CN^+ + C \qquad (6.12a)$$

$$\rightarrow C_2N^+ + H_2 \qquad (6.12b)$$

The reaction between C^+ and HCN, investigated earlier, is

$$C^+ + HCN \rightarrow C_2N^+ + H \qquad (6.8)$$

The linear portions of the CN^+ and CH^+ declines correspond to rate constants for their removal by HCN of 2.8×10^{-9} cm^3 $molecule^{-1}s^{-1}$ and 3.2×10^{-9} cm^3 $molecule^{-1}s^{-1}$ respectively. However, as the rates of removal of CN^+ and CH^+ are similar to the rate of removal of their precursor ion He^+, there may be significant amounts of CN^+ and CH^+ produced in the reaction zone, and the rate constants derived should be considered a lower limit.

In addition to the ion signals shown in fig. 6.3, a weak N^+ signal ($<$ 1% of total product ion signal) was observed. A small N^+ signal was present even in the absence of HCN, presumably due to reaction between He^+ ions and an N_2 impurity. The N^+ signal increases slightly and then decreases as increasing amounts of HCN are added. The

reactions involved are probably

$$He^+ + HCN \rightarrow N^+ + CH + He \qquad (6.13)$$

$$N^+ + HCN \rightarrow HCN^+ + N \qquad (6.14)$$

The HCN^+ formed in reactions (6.11) and (6.14), and in the Penning reaction

$$He\ (2^3S) + HCN \rightarrow HCN^+ + He + e \qquad (6.15)$$

reacts further with HCN as already discussed.

$$HCN^+ + HCN \rightarrow H_2CN^+ + CN \qquad (6.7a)$$

The linear portion of the HCN^+ decline corresponds to a rate constant for reaction (6.7a) of 1.0×10^{-9} cm^3 $molecule^{-1}s^{-1}$, in good agreement with the value of $9.6 \times 10^{-10} cm^3$ $molecule^{-1}s^{-1}$ obtained in the section 6.3.

The reaction between He^+ and HCN has been studied by Huntress et al.[182] An overall rate constant of 3.1×10^{-9} cm^3 $molecule^{-1}s^{-1}$ was obtained for removal of He^+ by reaction with HCN. The observed branching ratios were

$$He^+ + HCN \rightarrow CN^+ + H + He \quad 47\% \qquad (6.10a)$$

$$\rightarrow CH^+ + N + He \quad 21\% \qquad (6.10b)$$

$$\rightarrow C^+ + N + H + He \quad 25\% \qquad (6.10c)$$

$$\rightarrow N^+ + CH + He \quad 7\% \qquad (6.10d)$$

$$\rightarrow HCN^+ + He \quad < 1\% \qquad (6.10e)$$

The secondary reactions (6.11) and (6.12) have been studied by Inoue and Cottin.[206] They report that the reaction taking place between CN^+ and HCN is

$$CN^+ + HCN \rightarrow C_2N_2^+ + H \qquad (6.11b)$$

for which a rate constant of 1×10^{-10} cm^3 $molecule^{-1}s^{-1}$ was measured. Two reaction channels were observed for the reaction between CH^+ and HCN:

$$CH^+ + HCN \rightarrow C_2N^+ + H_2 \qquad (6.12b)$$

$$\rightarrow C_2NH^+ + H \qquad (6.12c)$$

The measured rate constants for reactions (6.12b) and (6.12c) are 4.3×10^{-10} cm^3 $molecule^{-1}s^{-1}$ and 2.3×10^{-10} cm^3 $molecule^{-1}s^{-1}$ respectively.

As pointed out earlier, the results of Inoue and Cottin were obtained at non-thermal energies, and agreement with the present thermal-energy results is not expected.

6.5 HCN^+ WITH H_2.

Attempts to form the HCN^+ reactant ion by charge transfer to HCN are complicated by the subsequent reaction of HCN^+ with HCN. For example, if HCN^+ is formed by adding HCN to an argon afterglow, addition of sufficient HCN to completely remove the Ar^+ ions results in almost complete removal of the HCN^+ ion. The same problem is encountered if HCN is added to a helium afterglow. Consequently, when studying the reactions of HCN^+, it is not possible to completely remove the ion producing HCN^+ before the neutral reactant is added, and some production of HCN^+ in the reaction zone is unavoidable. This leads to pronounced curvature in the semilogarithmic decline of HCN^+ with increasing H_2 flow. A rate constant may be derived from the initial part of the HCN^+ decline, but such a rate constant must be regarded as a lower limit, due to production of HCN^+ in the reaction zone.

A further problem was encountered when HCN^+ is produced in a helium carrier gas. Considerable amounts of CN^+ are produced by reaction of HCN with the active species in the afterglow. When the neutral reactant H_2 is added,

HCN^+ is formed in the reaction

$$CN^+ + H_2 \rightarrow HCN^+ + H \qquad (6.16)$$

which is rapid. (Huntress et al.[182] report a value of 1.22×10^{-9} cm^3 $molecule^{-1}s^{-1}$ for the rate constant for reaction (6.16)). Production of HCN^+ via reaction (6.16) contributes to the curvature in the HCN^+ decline.

Addition of H_2 to the afterglow containing HCN^+, along with substantial amounts of H_2CN^+, results in a decrease in the HCN^+ ion signal and a slight increase in the H_2CN^+ ion signal due to the reaction

$$HCN^+ + H_2 \rightarrow H_2CN^+ + H \qquad (6.17)$$

The rate constants obtained from the initial slope of the HCN^+ decline show a strong dependence on the flow of the reactant ion parent gas, which determines the extent of HCN^+ production in the reaction zone. Measured rate constants range from 9.8×10^{-10} cm^3 $molecule^{-1}s^{-1}$ to 7×10^{-11} cm^3 $molecule^{-1}s^{-1}$. Thus a value of 9.8×10^{-10} cm^3 $molecule^{-1}s^{-1}$ may be taken as a lower limit for the rate constant for reaction (6.17). This result is consistent with a value of 9.5×10^{-10} cm^3 $molecule^{-1}s^{-1}$ for the rate constant of reaction (6.14) measured by Huntress et al.[182]

6.6 CYANIDE CHEMISTRY IN INTERSTELLAR CLOUDS.

The mechanism of HCN formation in dense interstellar clouds is somewhat uncertain. The mechanism proposed by Herbst and Klemperer[199] is initiated by the reaction:

$$C^+ + NH_3 \rightarrow CNH_2^+ + H \qquad (6.18a)$$

followed by the dissociative recombination

$$CNH_2^+ + e \rightarrow CNH + H \qquad (6.19)$$

Herbst and Klemperer adopted a value of 2×10^{-9} cm^3 $molecule^{-1}s^{-1}$ for the rate constant for (6.18a), and an electron recombination coefficient of $1 \times 10^{-6} cm^3 s^{-1}$ for reaction (6.19) was assumed.

Schiff et al.[121] have investigated the reaction between C^+ and NH_3 in the flowing afterglow. Although the rate constant for the reaction was found to be 2.3×10^{-9} cm^3 $molecule^{-1}s^{-1}$, close to the value adopted by Herbst and Klemperer, reaction (6.18a) was found to be a minor reaction channel ($\sim$ 5%). The major reaction channel ($\sim$ 95%) was found to be the charge-transfer reaction

$$C^+ + NH_3 \rightarrow NH_3^+ + C \qquad (6.18b)$$

Reaction (6.18) has also been studied by Huntress et al.[182] who found that (6.18a) and (6.18b) were both major reaction channels ($\sim$ 49% each). In addition, a minor ($\sim$ 2%) channel was observed:

$$C^+ + NH_3 \rightarrow HNC^+ + H_2 \qquad (6.18c)$$

The overall rate constant was found to be 2.3×10^{-9} cm^3 $molecule^{-1}s^{-1}$.

The rate constants measured in the present work pertain to the loss processes for HCN. As discussed in chapter 5, the important ions in dense interstellar clouds are H_3^+, HCO^+, C^+, and He^+. These react with HCN as follows:

$$H_3^+ + HCN \rightarrow H_2CN^+ + H_2 \qquad (6.1)$$

$$HCO^+ + HCN \rightarrow H_2CN^+ + CO \qquad (6.4)$$

$$C^+ + HCN \rightarrow C_2N^+ + H \qquad (6.8)$$

$$He^+ + HCN \rightarrow CN^+ + H + He \qquad (6.10a)$$

$$\rightarrow CH^+ + N + He \qquad (6.10b)$$

$$\rightarrow C^+ + N + H + He \qquad (6.10c)$$

$$\rightarrow N^+ + CH + He \qquad (6.10d)$$

$$\rightarrow HCN^+ + He \qquad (6.10e)$$

The measured rate constants for these reactions, together with the rate constants adopted by Herbst and Klemperer, (k_{HK}), are collected in table 6.1.

TABLE 6.1

RATE CONSTANTS [a] RELATED TO PRODUCTION AND LOSS PROCESSES FOR HCN IN INTERSTELLAR CLOUDS.

Reaction	$k_{expt.}$ [b]	k_{HK} [c]	Reaction number [d]
$H_3^+ + HCN \rightarrow H_2CN^+ + H_2$	7.0	2.0	(6.1)
$H_2CN^+ + NH_3 \rightarrow NH_4^+ + HCN$	2.4	Not considered	(6.2)
$HCO^+ + HCN \rightarrow H_2CN^+ + CO$	4.0	1.0	(6.4)
$C^+ + HCN \rightarrow C_2N^+ + H$	2.8	2.0	(6.8)
$He^+ + HCN \rightarrow$ products	3.9	Not considered	(6.10)
$HCN^+ + H_2 \rightarrow H_2CN^+ + H$	≥ 0.98	2.0	(6.17)

a. All rate constants are in units of $10^{-9}cm^3molecule^{-1}s^{-1}$.

b. Rate constants measured in the present work.

c. Rate constants adopted in the model of Herbst and Klemperer.

d. Reactions numbered as in the text.

The CN^+ and HCN^+ ions produced in reactions (6.10a) and (6.10e) react rapidly with H_2 to form H_2CN^+:

$$CN^+ + H_2 \rightarrow HCN^+ + H \qquad (6.16)$$

$$HCN^+ + H_2 \rightarrow H_2CN^+ + H \qquad (6.17)$$

The H_2CN^+ formed in reaction (6.17), and in reactions (6.1) and (6.4) will react to regenerate HCN as follows

$$H_2CN^+ + NH_3 \rightarrow NH_4 + HCN \qquad (6.2)$$

$$H_2CN^+ + e \rightarrow HCN + H \qquad (6.20)$$

Since electron-ion recombination coefficients for polyatomic ions are generally $10^{-7} cm^3\ s^{-1}$ or greater,[208] and since the electron density is likely to be greater than the number density of NH_3,[199] the electron-ion recombination (6.20) will be the dominant process removing H_2CN^+ and reforming HCN. Consequently reactions (6.1), (6.4), and (6.10 a, e) do not destroy HCN, but only recycle it. The important reactions leading to the destruction of HCN are (6.8) and (6.10 b,c,d). Reaction (6.8) will dominate, since C^+ is probably more abundant than He^+.

Reaction (6.10) was not included in the model of Herbst and Klemperer. Also, the measured rate of reaction (6.8) is greater than the value adopted by these authors. Hence the Herbst-Klemperer model tends to underestimate the loss rate of HCN. If the results of Schiff et al.[121] are correct, the model overestimates the production rate of HCN by a factor of 20, and the proposed mechanism would appear to be inadequate in explaining the amount of HCN observed.[199] If the branching ratio for reaction (6.18)

measured by Huntress et al.[182] is correct, the model over-estimates the rate of production of HCN by a factor of two only. The branching ratio of (6.18) is thus a crucial factor in assessment of this model.

It is interesting to note that reaction (6.18) seems likely to produce HNC rather than HCN. Although the species HNC has been observed terrestrially only in an argon matrix at 4K,[209] ab initio calculations[210] of its molecular properties suggest that the HNC molecule is responsible for the galactic emission line observed by Snyder and Buhl.[211] Although HNC has an energy 61 kJ mol^{-1} above that of HCN, there is a considerable ($\sim$ 146 kJ mol^{-1}) activation energy barrier to the isomerization.[212] A possible mechanism for conversion of HNC to HCN is

$$AH^+ + HNC \rightarrow H_2CN^+ + A \qquad (6.21)$$

$$H_2CN^+ + e \rightarrow HCN + H \qquad (6.20)$$

$$\rightarrow HNC + H$$

where HCO^+ is the most probable proton donor AH^+. The calculations of Pearson and Schaefer[212] indicate that the linear structure (I) for H_2CN^+ is more stable by $\sim$300 kJ mol^{-1} than a structure of the type (II)

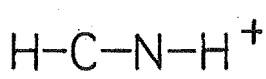

(I)

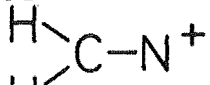

(II)

Dissociative recombination of the linear H_2CN^+ ion (I) might be expected to produce both HCN and HNC.

An alternative mechanism for HCN formation has been suggested by Watson,[105] and others (see reference [121]). The reactions involved are

$$CH_3^+ + N \rightarrow H_2CN^+ + H \qquad (6.22)$$

$$CH_3^+ + N \rightarrow HCN^+ + H_2 \qquad (6.23)$$

Reaction (6.23) will be followed by (6.17) producing H_2CN^+.

Dissociative recombination of H_2CN^+ produced in (6.17) or (6.22) produces HCN. Reactions (6.22) and (6.23) have not been studied in the laboratory, although a number of condensation reactions of CH_3^+ have been observed to proceed with elimination of H_2.[213] Although the N atom is fairly abundant in interstellar clouds, the abundance of CH_3^+, and even the mechanism of its formation, is uncertain. Although the reaction

$$CH_2^+ + H_2 \rightarrow CH_3^+ + H \qquad (6.24)$$

is rapid,[214] the ion CH_2^+, the precursor to CH_3^+, is probably formed in the slow radiative association reaction[215]

$$C^+ + H_2 \rightarrow CH_2^+ + h\nu \qquad (6.25)$$

The experiments of Fehsenfeld et al.[120] indicate that the rate of (6.25) may be very low, $\sim 4 \times 10^{-17}$ cm^3 $molecule^{-1}s^{-1}$. This is significantly lower than the value of 10^{-15} cm^3 $molecule^{-1}s^{-1}$ estimated by Black and Dalgarno.[215]

CHAPTER 7

CONCLUSION.

7.1 SUMMARY OF RESULTS AND CONCLUSIONS.

In chapter 4, the reactions between H_3^+ ions and neutral reactants of the general formula XCN were examined. In all cases the proton-transfer reaction

$$H_3^+ + XCN \rightarrow HXCN^+ + H_2 \qquad (7.1)$$

was the only reaction channel observed, and was found to be rapid. The experimentally-determined rate constants for reaction of H_3^+ with HCN, CH_3CN, and ClCN were in good agreement with the rate constants predicted by the ADO theory, at least within the relative accuracy of the experimental measurements. The agreement between theory and experiment for the reaction of H_3^+ with BrCN and ICN was not so good, but it seems possible that a low reaction efficiency, rather than error in the ADO rate constants, is responsible for the discrepancy. The measured rate constant for the reaction of H_3^+ with C_2N_2 agreed with that predicted by the AQO theory, to within the relative accuracy of the measured rate constant.

Chapters 5 and 6 report the results of a study of a number of reactions pertaining to the formation and destruction of sulphur-containing molecules and of HCN in interstellar clouds. The rate constants and product distributions observed for reactions of the sulphur-containing compounds were compared with values adopted in the model proposed by Oppenheimer and Dalgarno.[200]

The differences were not so great as to cause any major changes to the model. Measured rate constants and product distributions pertaining to the destruction of HCN in interstellar clouds have been compared with those adopted in the model of Herbst and Klemperer.[199] Again, the differences were not great. However, some doubt is cast on the validity of the Herbst-Klemperer mechanism by the conflicting results of Huntress [182], and Schiff et al.[121] for the rate of the reaction producing CNH_2^+ :

$$C^+ + NH_3 \rightarrow CNH_2^+ + H \qquad (7.2)$$

A re-investigation of this reaction is currently underway in this department.

The rate constant measured for the reaction

$$S^+ + H_2S \rightarrow H_2S^+ + S \qquad (7.3)$$

was found to be fairly large, in spite of the endothermicity of the reaction. This indicates that there may be significant amounts of long-lived excited states of the S^+ ion present in the flowing afterglow. If there are metastable S^+ ions present in the flowing afterglow, then conclusions concerning the occurrence of S^+ in the ionosphere which were based on the flowing afterglow measurement of the reaction between S^+ and O_2 [201] would have to be revised as follows.

Sampling of the ionosphere by rocket-borne mass spectrometers has revealed the presence of ions at masses 32 and 34 at altitudes between 74 and 86km.[216] These ion signals are thought to be due to S^+ ions. Fehsenfeld and Ferguson [201] have measured the rate of the reaction

$$S^+ + O_2 \rightarrow SO^+ + O \qquad (7.4)$$

Their measured value of the rate constant of 1.6×10^{-11} cm^3 molecule $^{-1}s^{-1}$ yields a loss rate for S^+ ions in the ionosphere via reaction (7.4) of at least 4×10^2 $cm^{-3}s^{-1}$ at 80 km. To account for the observed S^+ density of about 10^2 cm^{-3}, a production rate for S^+ of 4×10^4 $cm^{-3}s^{-1}$ is required. This rate exceeds the total ion production rate in the D region of the ionosphere. If, however, the measurement of the rate of reaction (7.3) involved a contribution from excited S^+ ions, the calculated ionospheric loss rate for S^+ may be too great. A lower value for the loss rate would of course mean that the rate of production need not be as great as required by the calculations of Fehsenfeld and Ferguson.

7.2 SUGGESTIONS FOR FURTHER WORK.

An investigation of the rates of reaction of unambiguously-identified ground-state S^+ ions is called for. A suitable source of S^+ reactant ions is the reaction

$$CO^+ + H_2S \rightarrow S^+ + CO + H_2 \qquad (7.5a)$$

$$\rightarrow S^+ + H_2CO \qquad (7.5b)$$

Since reactions (7.5a) and (7.5b) are exothermic by 50 kJ mol^{-1} and 59 kJ mol^{-1} respectively, only the ground state of the S^+ ion is energetically accessible in these reactions. The reaction of ground-state S^+ with O_2 is of particular importance.

Many ion-molecule reactions of relevance to interstellar molecule formation mechanisms remain to be studied. In particular, the mechanism proposed by Watson [105] for the

formation of H_2CN^+,

$$CH_3^+ + N \rightarrow H_2CN^+ + H \qquad (7.6)$$

has not yet been investigated in the laboratory. The flowing afterglow technique is ideally suited to the study of reactions of such unstable neutral reactants as N atoms. These atoms could be produced by dissociation of N_2 (or a dilute mixture of N_2 in an inert carrier such as helium) in a microwave discharge, and their concentration determined by titration with NO. [217] Since the reactions between CH_3^+ and N_2, such as

$$CH_3^+ + N_2 \rightarrow N_2^+ + CH_3 \qquad (7.7a)$$

$$\rightarrow N_2H^+ + CH_2 \qquad (7.7b)$$

$$\rightarrow NCH_2^+ + NH \qquad (7.7c)$$

etc.

are highly endothermic, the presence of any undissociated N_2 should not interfere with the measurement of the rate constant for reaction (7.6). The CH_3^+ reactant ion is produced as one of the dominant ions in the reaction between He^+ and CH_4. [158]

The formaldehyde molecule has been detected in interstellar clouds, [111] and the mechanism of its formation is uncertain. The scheme proposed by Herbst and Klemperer [199] is the slow radiative association

$$HCO^+ + H_2 \rightarrow H_3CO^+ + h\nu \qquad (7.8)$$

followed by electron-ion recombination

$$H_3CO^+ + e \rightarrow H_2CO + H \qquad (7.9)$$

A rate constant of 2×10^{-17} cm^3 $molecule^{-1}s^{-1}$ was assumed for reaction (7.8). However the work of Fehsenfeld et al. [120] suggests that the rate of reaction (7.8) may be

lower, about 10^{-18} cm^3 $molecule^{-1}s^{-1}$. The question of H_2CO production is closely connected with the mechanism for its removal though. If the loss rate of H_2CO is significantly lower than assumed in the Herbst-Klemperer model, the burden on its production rate is eased. The reactions considered by Herbst and Klemperer for the removal of H_2CO are

$$H_3^+ + H_2CO \rightarrow H_3CO^+ + H_2 \qquad (7.10)$$

$$HCO^+ + H_2CO \rightarrow H_3CO^+ + CO \qquad (7.11)$$

$$C^+ + H_2CO \rightarrow HC_2O^+ + H \qquad (7.12a)$$

all of which were assumed to proceed at the Langevin rate of 1-2 x 10^{-9} cm^3 $molecule^{-1}s^{-1}$. Only one of these reactions appears to have been studied in the laboratory. Karpas and Klein [218] have determined a value of 8.2 x $10^{-10}cm^3$ $molecule^{-1}s^{-1}$ for the rate constant for the reaction

$$C^+ + H_2CO \rightarrow CH_2^+ + CO \qquad (7.12b)$$

using the ICR method. It is suggested that the reactions (7.10) to (7.12) be studied in the flowing afterglow, together with the reactions of He^+ and O_2^+ with H_2CO, which may also be important in removing H_2CO in interstellar clouds. The handling of the neutral reactant H_2CO may pose some problems; because of the tendency of formaldehyde to polymerize, it will be necessary to heat the formaldehyde handling line to about 100° C. [219]

Dalgarno et al.[220] have proposed an alternative scheme for the production of H_2CO in interstellar clouds.

The ion H_2CO^+ produced in the reaction

$$CH_3^+ + O \rightarrow H_2CO^+ + H \qquad (7.13)$$

then undergoes charge transfer with metal atoms present:

$$H_2CO^+ + M \rightarrow M^+ + H_2CO \qquad (7.14)$$

The reaction (7.13) does not appear to have been studied in the laboratory. It may be studied in the flowing afterglow using the same procedure as recommended for the study of the reaction of CH_3^+ with N atoms. A known flow of O atoms may be generated by adding just sufficient NO to a flow of partially dissociated N_2 to convert all the N atoms to O atoms in the reaction [216]

$$N + NO \rightarrow N_2 + O \qquad (7.15)$$

ACKNOWLEDGEMENTS.

I should like to thank my supervisor, Dr. M.J.McEwan, for his help and encouragement during the course of this work. I am also grateful to Dr. C.G. Freeman, who acted as my supervisor during Dr. McEwan's absence overseas, for many helpful discussions.

My thanks are also due to the technical staff of the Chemistry Department for the construction of much of the apparatus, and to Mrs K. Dunlop, who typed this manuscript.

I gratefully acknowledge the award of a University Grants Committee Post-graduate scholarship.

REFERENCES.

1. P. Langevin, Ann. Chim. Phys., Series 8, 5, 245 (1905).
2. J.J. Thomson, Phil. Mag., 24, 209 (1912).
3. A.J. Dempster, Phil. Mag., 31, 438 (1916).
4. H.D. Smyth, Phys. Rev., 25, 452 (1925).
5. T.R. Hogness and E.G. Lunn, Phys. Rev., 26, 44 (1925)
6. H. Gutbier, Z. Naturforsch, 12a, 499 (1957).
7. T.R. Hogness and R.W. Harkness, Phys. Rev., 32 , 784 (1928).
8. W. Bleakney, Phys. Rev., 41, 32 (1932).
9. A.O. Nier, Rev. Sci. Instr., 18, 398 (1947).
10. M.M. Mann, A. Hustrulid, and J.T. Tate, Phys. Rev., 58, 340 (1940).
11. G.C. Eltenton, Nature, 141, 975 (1938).
12. H. Eyring, J.O. Hirschfelder, and H.S. Taylor, J. Chem. Phys., 4, 479 (1936).
13. M.T. Bowers, D.D. Elleman, and J. King, J. Chem., Phys., 50, 4787 (1969).
14. P. Warneck, J. Chem. Phys., 46, 502 (1967).
15. B.G. Reuben and L. Friedman, J. Chem. Phys., 37, 1636 (1962).
16. A.G. Harrison, A. Ivko, and T.W. Shannon, Can. J.Chem., 44, 1351 (1966).
17. V.L. Tal'roze and A.K. Lyubimova, Doklady Akad. Nauk SSSR, 86, 909 (1952), per Chem. Abstr., 47, 2590f (1953).
18. D.P. Stevenson and D.O. Schissler, J. Chem. Phys., 23, 1353 (1955).
19. G.G. Meisels, W.H. Hamill, and R.R. Williams, J. Chem. Phys., 25, 790 (1956).
20. F.H. Field, J.L. Franklin, and F.W. Lampe, J. Am. Chem. Soc., 79, 2419 (1957).
21. G. Gioumousis and D.P. Stevenson, J. Chem. Phys., 29, 294 (1958).
22. F.H. Field and J.L. Franklin, Electron Impact Phenomena and the Properties of Gaseous Ions, pp.217-224 (Academic Press, New York, 1957).

23. F.W. Lampe, J.L Franklin, and F.H. Field, Prog. Reaction Kinetics, 1, 67 (1961).

24. D.P. Stevenson, in Mass Spectrometry (C.A. McDowell,ed.), p. 589 (McGraw-Hill, New York, 1963).

25. P.J. Ausloos (ed.), Ion-Molecule Reactions in Gases. (Advances in Chemistry Series, No. 58, American Chemical Society, Washington, 1966).

26. E.E. Ferguson, Advan. Electron. Electron Phys., 24, 1 (1968).

27. E.E. Ferguson, F.C. Fehsenfeld, and A.L. Schmeltekopf, Advan. At. Mol. Phys., 5, 1 (1969).

28. E.W. McDaniel, V. Cermak, A. Dalgarno, E.E. Ferguson, and L. Friedman, Ion-Molecule Reactions. (Wiley, New York, 1970).

29. J.L. Franklin (ed.), Ion-Molecule Reactions. (Plenum Press, New York, 1972).

30. M.T. Bowers and T. Su, Advan. Electron. Electron Phys., 34, 223 (1973).

31. V.L. Tal'roze and E.L. Frankevich, Russian J. Phys. Chem., 34, 1275 (1960).

32. C.W. Hand and H. von Weyssenhoff, Can. J. Chem., 42, 195 (1964).

33. T.W. Shannon, F. Meyer, and A.G. Harrison, Can. J. Chem. 43, 159 (1965).

34. K.R. Ryan and J.H. Futrell, J. Chem. Phys. 42, 824 (1965).

35. K.R. Ryan, J.H. Futrell, and C.D. Miller, Rev. Sci. Instr., 37, 107 (1966).

36. F.H. Field and M.S.B. Munson, J. Am. Chem. Soc., 87, 3289 (1965).

37. K. Hiraoka and P. Kebarle, J. Chem. Phys., 63, 394 (1975).

38. A.J. Cunningham, J.D. Payzant, and P. Kebarle, J.Am. Chem. Soc., 94, 7627 (1972).

39. P. Kebarle, R.M. Haynes, and S.K. Searles, in ref. 25, p. 210.

40. P. Kebarle, in Ions and Ion Pairs in Organic Reactions (M. Szwarc, ed.), Vol. 1.p.27 (Wiley, New York,1972).

41. A.A. Herod and A.G. Harrison, Int. J. Mass Spectrom.Ion Phys., 4, 415 (1970).

42. R.F. Bonner, G. Lawson, and J.F.J. Todd, Int. J. Mass Spectrom.Ion Phys, 10, 197 (1973).

43. P.G. Miasek and J.L. Beauchamp, Int. J. Mass Spectrom.Ion Phys., 15, 49 (1974).

44. V.L. Tal'roze and G.V. Karachevtsev, Advan. Mass Spectrom., 3, 211 (1966).

45. T.F. Moran and L. Friedman, J. Chem. Phys., 42, 2391 (1965).

46. T.W. Shannon and A.G. Harrison, J. Chem. Phys., 43, 4206 (1965).

47. V. Cermak and Z. Herman, Nucleonics, 19, 106 (1967). See also J.H. Futrell and T.O. Tiernan, J. Chem. Phys., 39, 2539 (1963).

48. P.H.G. Dickinson and J. Sayers, Proc. Phys. Soc., 76, 137 (1960).

49. W.L. Fite, J.A. Rutherford, W.R. Snow, and V.A.J. van Lint, Disc. Far. Soc., 33, 264 (1962).

50. A.L. Schmeltekopf, E.E. Ferguson, and F.C. Fehsenfeld, J. Chem. Phys., 48, 2966 (1968)

51. J. Sayers and D. Smith, Disc. Far. Soc., 37, 167 (1964).

52. G.F.O. Langstroth and J.B. Hasted, Disc. Far. Soc., 33, 298 (1962).

53. P.H. Batey, G.R. Court, and J. Sayers, Planet.Space Sci., 13, 911 (1965).

54. M.J. Copsey, D. Smith, and J. Sayers, Planet.Space Sci., 14, 1047 (1966).

55. F.C. Fehsenfeld, A.L. Schmeltekopf, P.D. Goldan, H.I. Schiff, and E.E. Ferguson, J. Chem. Phys., 44, 4087 (1966).

56. H.I. Schiff and D.K. Böhme, Int. J. Mass Spectrom. Ion Phys., 16, 167 (1975).

57. V.M. Bierbaum and F. Kaufman, J. Chem. Phys., 61, 3804 (1974).

58. R.C. Bolden and N.D. Twiddy, Disc. Far. Soc., 53, 192 (1972).

59. J.P. Liddy, C.G. Freeman, and M.J. McEwan, Astrophys. Lett., 16, 155 (1975).

60. L.F. Phillips and H.I. Schiff, J. Chem. Phys., 37, 1233 (1962).

61. F. Kaufman, Ann. Geophys., 20, 106 (1964).

62. F.C. Fehsenfeld, A.L. Schmeltekopf, H.I. Schiff, and E.E. Ferguson, Planet. Space Sci., 15, 373 (1967).

63. F.C. Fehsenfeld, Can. J. Chem., 47, 1808 (1969).

64 P.D. Goldan, F.C. Fehsenfeld, H.I. Schiff, and E.E. Ferguson, J. Chem. Phys., 44, 4095 (1966).

65. E.E Ferguson, F.C. Fehsenfeld, P D. Goldan, A.L. Schmeltekopf, and H.I. Schiff, Planet. Space Sci., 13, 823 (1965).

66. F.C. Fehsenfeld, J. Chem. Phys., 63, 1686 (1975).

67. F.C. Fehsenfeld, D.L. Albritton, J.A. Burt, and H.I. Schiff, Can. J. Chem., 47, 1793 (1969).

68. D.B. Dunkin, F.C. Fehsenfeld, A.L. Schmeltekopf, and E.E. Ferguson, J. Chem. Phys., 49, 1365 (1968).

69. M. McFarland, D.L. Albritton, F.C. Fehsenfeld, E.E. Ferguson, and A.L. Schmeltekopf, J. Chem Phys., 59, pp. 6610, 6620 (1973).

70. D.K. Bohme, R.S. Hemsworth, H.W. Rundle, and H I. Schiff, J. Chem. Phys., 58, 3504 (1973).

71. R.S. Hemsworth, H. W. Rundle, D. K. Bohme, H.I. Schiff, and F.C. Fehsenfeld, J. Chem , Phys., 59, 61 (1973).

72. G. Gray, Advan.Chem. Phys., 19, 141 (1971).

73. J.D. Baldeschwieler and S.D. Woodgate, Acc. Chem. Res., 3, 114 (1971).

74. J.L. Beauchamp, Ann. Rev. Phys., Chem., 22,527 (1971).

75 L R. Anders, J.L. Beauchamp, R.C. Dunbar, and J.D. Baldeschweiler, J. Chem. Phys., 45, 1062 (1966).

76. J.L. Beauchamp and S.E. Buttrill, J. Chem. Phys., 48, 1783 (1968).

77. L.R. Anders, J. Phys. Chem., 73, 469 (1969).

78 R.P. Clow and J.H. Futrell, Int. J. Mass Spectrom. Ion Phys., 4, 165 (1970).

79. V.G. Anicich and M.T. Bowers, Int. J. Mass Spectrom. Ion Phys., 13, 359 (1974).

80. T. McAllister, Int. J. Mass Spectrom. Ion Phys., 8, 162 (1972).

81. V.G. Anicich and M.T. Bowers, Int. J. Mass Spectrom. Ion Phys., 11, 329 (1973).

82. R.T. McIver, Rev. Sci. Instr., 41, 555 (1970).

83. T.B. McMahon and J.L. Beauchamp, Rev. Sci. Instr., 43, 509 (1972).

84. P.R. Kemper and M.T. Bowers, J. Chem. Phys., 59, 4915 (1973).

85. R.N. Varney, Phys. Rev. Lett., 5, 559 (1960).

86. W.S. Barnes, D.W. Martin, and E.W. McDaniel, Phys. Rev. Lett., 6, 110 (1961).

87. E.W. McDaniel, Collision Phenomena in Ionized Gases. (Wiley, New York, 1964).

88. E.C. Beatty and P.L. Patterson, Phys. Rev., 137, A346 (1965).

89. E.C. Beatty and P.L. Patterson, Phys. Rev., 170, 116 (1968).

90. D.L. Albritton, T.M. Miller, D.W. Martin, and E.W. McDaniel, Phys. Rev., 171, 94 (1968).

91. J.H. Schummers, G.M. Thomson, D.R. James, E. Graham, I.R. Gatland, and E.W. McDaniel, Phys. Rev., 7, 689 (1973).

92. Y. Kaneko, L.R. Megill, and J.B. Hasted, J. Chem. Phys., 45, 3741 (1966).

93. R.H. Neynaber, Advan. At. Mol. Phys., 5, 57 (1969).

94. C.G. Meisels, W.H. Hamill, and R.R. Williams, J. Phys. Chem., 61, 1456 (1957).

95. S.O. Thompson and O.A. Schaeffer, J. Am. Chem. Soc., 80, 553 (1958).

96. F.C. Fehsenfeld, A.L. Schmeltekopf, and E.E. Ferguson, J. Chem. Phys., 45, 1844 (1966).

97. L.M. Branscomb in Atomic and Molecular Processes (ed. D.R. Bates), Ch.4. (Academic Press, New York, 1962).

98. A.L. Farragher, F.M. Page, and R.C. Wheeler, Disc. Far. Soc., 37, 203 (1964).

99. L. Brewster-Young, E. Lee-Ruff, and D.K. Bohme, Can. J. Chem., 49, 979 (1971).

100. D.K. Bohme, E. Lee-Ruff, and L. Brewster-Young, J. Am. Chem. Soc., 94, 5153 (1972).

101. A.E. Roche, M.M. Sutton, D.K. Bohme, and H.I. Schiff, J. Chem. Phys., 55, 5480 (1971).

102. M.J. McEwan and L.F. Phillips, Chemistry of the Atmosphere. (Edward Arnold, London, 1975).

103. P.M. Banks and G. Cockarts, Aeronomy, Part B. (Academic Press, New York, 1973).

104. E.E. Ferguson, Rev. Geophys., 9, 997 (1971).

105. T.M. Donahue, Science, 159, 489 (1968).

106. Defense Nuclear Agency Reaction Rate Handbook (M.H. Bortner and T. Baurer, eds.), Ch. 18. (DASIAC, Santa Barbara, 1972).

107. F.C. Fehsenfeld, D.B. Dunkin, and E.E. Ferguson, Planet. Space Sci., 18, 1267 (1970).

108. F.C. Fehsenfeld and E.E. Ferguson, J. Geophys. Res., 76, 8453 (1971).

109. B.E. Turner in, Galactic and Extra-Galactic Radio Astronomy. (G.L. Verschuur and K.I. Kellerman, eds.) Ch. 9. (Springer-Verlag, New York, 1974).

110. A.C. Cheung, D.M. Rank, C.H. Townes, D.C. Thornton, and W.J. Welch, Phys. Rev. Lett., 21,1701 (1968); Nature, 221, 626 (1969).

111. L.E. Snyder, D. Buhl, B. Zuckerman, and P. Palmer, Phys. Rev. Lett., 22, 679 (1969).

112. P.M. Solomon, Phys. Today, 26, 32 (March,1973).

113. D.M. Rank, C.H. Townes, and W.J. Welch, Science, 174, 1083 (1971).

114. W.D. Watson and E.E. Salpeter, Astrophys. J., 174, 321 (1972).

115. P.M. Solomon and W. Klemperer, Astrophys. J., 178, 389 (1972).

116. E. Herbst and W. Klemperer, Astrophys. J., 185, 505 (1973).

117. W.D. Watson, Astrophys. J., 182, L73 (1973).

118. W.D. Watson, Astrophys. J., 183, L17 (1973).

119. F.C. Fehsenfeld, D.B. Dunkin, E.E. Ferguson, and D.L. Albritton, Astrophys. J., 183, L25 (1973).

120. F.C. Fehsenfeld, D.B. Dunkin, and E.E. Ferguson, Astrophys. J., 188, 43 (1974).

121. H.I. Schiff, R.S. Hemsworth, J.D. Payzant, and D.K. Bohme, Astrophys. J., 191, L49 (1974).

122. T.F. Moran and W.H. Hamill, J. Chem. Phys., 39, 1413 (1963).

123. S.K. Gupta, E.G. Jones, A.G. Harrison, and J.J. Myher, Can. J. Chem., 45, 3107 (1967).

124. L.P. Theard and W.H. Hamill, J. Am. Chem. Soc., 84, 1134 (1962).

125. L.W. Sieck and S.K. Searles, J. Chem. Phys., 53, 2601 (1970).

126. M.T. Bowers and J.B. Laudenslager, J. Chem. Phys., 56, 4711 (1972).

127. J.L. Beauchamp, D. Holtz, S.D. Woodgate, and S.L. Patt, J. Am. Chem. Soc., 94, 2798 (1972).

128. S.E. Buttrill, J. Chem. Phys., 58, 656 (1973).

129. J.V. Dugan and J.L. Magee, J. Chem. Phys., 47, 3103 (1967).

130. T. Su and M.T. Bowers, J. Chem. Phys., 58, 3027 (1973).

131. T. Su and M.T. Bowers, Int. J. Mass Spectrom. Ion Phys., 12, 347 (1973).

132. T. Su and M.T. Bowers, Int. J. Mass Spectrom. Ion Phys., 17, 211 (1975).

133. L. Bass, T. Su, W.J. Chesnavich, and M.T. Bowers, Chem. Phys. Lett., 34, 119 (1975).

134. T. Su and M.T. Bowers, J. Am. Chem. Soc., 95, 7609 (1973).

135. P.P. Dymerski and R.C. Dunbar, J. Chem. Phys., 57, 4049 (1972).

136. M.J. Henchman, Ann. Rept. Chem. Soc., 62, 39 (1963).

137. L. Bass, T. Su, and M.T. Bowers, to be published. See reference 138, footnote 34.

138. T. Su and M.T. Bowers, J. Chem. Phys., 60, 4897 (1974).

139. M.T. Bowers, T. Su, and V.G. Anicich, J. Chem. Phys., 58, 5175 (1973).

140. D.L. Smith and J.H. Futrell, Int. J. Mass Spectrom. Ion Phys., 10, 405 (1972/3).

141. J.V. Dugan and R.W. Palmer, Chem. Phys. Lett., 13, 144 (1971).

142. T. Su and M.T. Bowers, Int. J. Mass Spectrom. Ion Phys., 17, 309 (1975).

143. J.C. Light and J. Lin, J. Chem. Phys., 43, 3209 (1965).

144. J.C. Light, J. Chem. Phys., 40, 3221 (1964).

145. F.A. Wolf, J. Chem. Phys., 44, 1619 (1966).

146. Reference 29, p. 224.

147. H.S.W. Massey and E.H.S. Burhop, Electronic and Ionic Impact Phenomena, Chapters VII and VIII. (University Press, Oxford, 1952).

148. D.K. Bohme, J.B. Hasted, and P.P. Ong, J. Phys. B, 1, 879 (1968).

149. J.B. Laudenslager, W.T. Huntress, and M.T. Bowers, J. Chem. Phys., 61, 4600 (1974).

150. M.T. Bowers and D.D. Elleman, Chem. Phys. Lett, 16, 486 (1972).

151. A.J. Masson, K. Birkenshaw, and M.J. Henchman, J. Chem. Phys., 50, 4112 (1969).

152. R.H. Perry and C.H. Chilton (eds.), Chemical Engineer's Handbook (5 edition), section 5-11. (McGraw-Hill Kogakusha, Tokyo, 1973).

153. D. MacNair, Rev. Sci. Instr., 38, 124 (1967).

154. F.C. Fehsenfeld, Int. J. Mass Spectrom. Ion Phys., 16, 151 (1975).

155. P.F. Fennelly, J.D. Payzant, R.S. Hemsworth, and D.K. Bohme, J. Chem. Phys., 60, 5115 (1974).

156. C.A. Goy, D.H. Shaw, and H.O. Pritchard, J. Phys. Chem., 69, 1504 (1965).

157. R.W. Huggins and J.H. Cahn, J. Appl. Phys., 38, 180 (1967).

158. R.C. Bolden, R.S. Hemsworth, M.J. Shaw, and N.D. Twiddy, J. Phys., B., 3, 45 (1970).

159. H.M.P. Stock, J. Phys. B., 6, L86 (1973).

160. A.L. Farragher, Trans. Far. Soc., 66, 1411 (1969).

161. P.J. Ogren, J. Phys. Chem., 79, 1749 (1975).

162. E.H. Kennard, Kinetic Theory of Gases, p. 293. (McGraw-Hill, New York, 1938).

163. S. Dushman and J.M. Lafferty, Scientific Foundations of Vacuum Technique (2nd ed.), p 84. (Wiley, New York, 1962).

164. G.P. Brown and A. DiNardo, J. Appl. Phys., 17, 802 (1946).

165. P.M. Morse and H. Feshbach, Methods of Theoretical Physics, p. 736. (McGraw-Hill, New York,1953).

166. J. Irving and N. Mullineaux, Mathematics in Physics and Engineering, p. 394 (Academic Press, New York, 1959).

167. W. Lindinger and D.L. Albritton, J. Chem. Phys., 62, 3517 (1975).

168. J. Heimerl, R. Johnsen, and M.A. Biondi, J. Chem. Phys., 51, 5041 (1969).

169. A.L. McClellan, Tables of Experimental Dipole Moments. (Freeman, San Francisco, 1963).

170. M. Krause, U.S. Nat. Bur. Stand., Tech. Note 438 (1967).

171. Landolt-Bornstein, Zahlenwerte und Funktionen aus Physik, Chemie, Astronomie, Geophysik und Technik, (6 Auflage), I. Band, 3 Teil, 14 207 p 510 (Springer-Verlag, Berlin, 1951).

172. J. Applequist, J.R. Carl, and K.K. Fung, J. Am. Chem. Soc., 94,2952 (1972).

173. E.R. Lippincott, G. Nagarajan, and J.M. Stutman, J. Phys. Chem., 70, 78 (1966).

174. J.O. Hirschfelder, C.F. Curtiss, and R.B. Bird, Molecular Theory of Gases and Liquids, p. 947 (Wiley, New York, 1964).

175. J.J. Leventhal and L. Friedman, J. Chem. Phys., 50, 2928 (1969).

176. W.T. Huntress and M.T. Bowers, Int. J. Mass Spectrom. Ion Phys., 12, 1 (1973).

177. M.T. Bowers, W.J. Chesnavich, and W.T. Huntress, Int. J. Mass Spectrom. Ion Phys., 12, 357 (1973).

178. D.L. Smith and J.H. Futrell, Chem. Phys. Lett., 24, 611 (1974).

179. M.T. Bowers and D.D. Elleman, J. Am. Chem. Soc., 92, 1847 (1970).

180. J.K. Kim, L.P. Theard, and W.T. Huntress, Int. J. Mass Spectrom. Ion Phys., 15, 223 (1974).

181. Handbook of Chemistry and Physics, (52 ed.) D151 (Chemical Rubber Co., Cleveland, 1971).

182. W.T. Huntress, private communication.

183. B.H. Solka and A.G. Harrison, Twenty-first Annual Conference on Mass Spectrometry and Allied Topics, San Francisco, 1973. See also Chem. Phys. Lett., 26, 417 (1974).

184. D. Betowski, J.D. Payzant, G.I. MacKay, and D.K. Bohme, Chem. Phys. Lett., 31, 321 (1975).

185. J.A. Burt, J.L. Dunn, M.J. McEwan, M.M. Sutton, A.E. Roche, and H.I. Schiff, J. Chem. Phys., 52, 6062 (1970).

186. C.E. Moore, Atomic Energy Levels, U.S. Nat. Bur. Stand. Circ. 467, Vol. 1 (1949).

187. J.L. Franklin, J.G. Dillard, H.M. Rosenstock, J.T. Herron, K. Draxl, and F.H. Field, Ionization Potentials, Appearance Potentials, and Heats of Formation of Gaseous Positive Ions, U.S. Nat. Bur. Stand., NSRDS-NBS 26 (1969).

188. M.I. Al-Joboury and D.W. Turner, J. Chem. Soc., 4434 (1964).

189. W. Ruska and J.L. Franklin, Int. J. Mass Spectrom. Ion Phys., 3, 221 (1969).

190. A.G. Harrison, Int. J. Mass Spectrom. Ion Phys., 6, 297 (1971).

191. W.T. Huntress and R.F. Pinizzotto, J. Chem. Phys., 59, 4742 (1973).

192. L.Y. Wei and L.I. Bone, J. Phys. Chem., 78, 2527 (1974).

193. J.B. Laudenslager and W.T. Huntress, Int. J. Mass Spectrom. Ion Phys., 14, 435 (1974).

194. F.C. Fehsenfeld, P.D. Goldan, A.L. Schmeltekopf, and E.E. Ferguson, Planet. Space Sci., 13, 579 (1965).

195. R.C. Bolden, R.S. Hemsworth, M.J. Shaw, and N.D. Twiddy, J. Phys. B, 3, 61 (1970).

196. F.C. Fehsenfeld, A.L. Schmeltekopf, and E.E.Ferguson, J. Chem. Phys., 44, 4537 (1966); see also erratum, J. Chem. Phys., 46, 2019 (1967).

197. F.C. Fehsenfeld, A.L. Schmeltekopf, and E.E.Ferguson, J. Chem. Phys., 46, 2802 (1967).

198. A. Dalgarno, M. Oppenheimer, and R.S. Berry, Astrophys. J., 183, L21 (1973).

199. E. Herbst and W. Klemperer, Astrophys. J., 185, 505 (1973).

200. M. Oppenheimer and A. Dalgarno, Astrophys. J., 187, 231 (1974).

201. F.C. Fehsenfeld and E.E. Ferguson, J. Geophys. Res., 78, 1699 (1973).

202. T. Cato, J. Ellder, B. Hoglund, O.E.H. Rydbeck, B. Ronnang, and A. Sume, Astron. Astrophys., 21, 435 (1972).

203. C.S. Matthews and P. Warneck, J. Chem. Phys., 51, 854 (1969).

204. E.J. Gallegos and R.W. Kisser, J. Phys. Chem., 51, 854 (1969).

205. J.L. Franklin, V.H. Diebler, R.M. Reese, and M.Krauss, J. Am. Chem. Soc., 80, 298 (1958).

206. M. Inoue and M. Cottin, Adv. Mass Spectrom., 3, 339 (1966).

207. A.G. Harrison and J.C.J. Thynne, Can. J. Chem., 45, 1321 (1967).

208. J.N. Bardsley and M.A. Biondi, Adv. At. Mol. Phys., 6, 1 (1970).

209. D.E. Milligan and M.E. Jacox, J. Chem. Phys., 39, 712 (1963).

210. P.K. Pearson, G.L. Blackman, H.F. Schaefer, B.Roos, and U. Wahlgren, Astrophys. J., 184, L19 (1973).

211. L.E. Snyder and D. Buhl, Bull. A.A.S., 3, 388 (1971).

212. P.K. Pearson and H.F. Schaefer, Astrophys. J., 192, 33 (1974).

213. W.T. Huntress, R.F. Pinizzotto, and J.B. Laudenslager, J. Am. Chem. Soc., 95, 4107 (1973).

214. J.K. Kim, L.P. Theard, and W.T. Huntress, J. Chem. Phys., 62, 45 (1975).

215. J.H. Black and A. Dalgarno, Astrophys. Lett., 15, 79 (1973).

216. R.S. Narcisi in "Planetary Electrodynamics" (eds. S.C. Coroniti and J. Hughes), p. 447 (Gordon and Breach, New York, 1969).

217. F. Kaufman, J. Chem. Phys., 28, 992 (1958).

218. Z. Karpas and F.S. Klein, Int. J. Mass Spectrom. Ion Phys., 16, 289 (1975).

219. G.P.R. Mack and B.A. Thrush, J. Chem. Soc. Far.I, 69, 208 (1973).

220. A. Dalgarno, M. Oppenheimer, and J.H. Black, Nature Phys. Sci., 245, 100 (1973).

APPENDIX I

DATA FOR INDIVIDUAL KINETIC RUNS

The following table contains data from individual kinetic runs, arranged as follows:

Column 1: Reaction number, as used in the text.

Column 2: Ionic and neutral reactants. The carrier gas is identified in parentheses.

Column 3: P, the pressure measured at the mid-point of the reaction zone, in torr.

Column 4: $\bar{v}$, the average linear flow velocity of the carrier gas, in cm s^{-1}.

Column 5: L, the actual length of the reaction zone, in cm.

Column 6: Gradient, the least-squares slope of the plot of $\log_e A^+$ vs. Q, where A^+ is the reactant ion signal, and Q the flow of the neutral reactant in molecules s^{-1}. Units of gradient are 10^{-17} s $molecule^{-1}$.

Column 7: k, the rate constant, corrected as described in chapter 3, in units of 10^{-9} cm^3 $molecule^{-1}s^{-1}$.

Reaction number	Reactants (Carrier)	P	$\bar{\nu}$	L	Gradient	k
(4.4)	H_3^+ + HCN	0.265	6420	49.5	8.61	7.27
	(H_2)	0.385	6380	49.5	8.39	6.95
		0.409	6400	49.5	8.30	6.91
	H_3^+ + CH_3CN	0.256	6720	51.3	7.22	6.48
	(H_2)	0.267	6700	51.3	9.31	8.35
		0.258	6300	51.3	8.81	6.88
		0.370	6200	51.3	8.98	6.86
		0.229	6300	51.3	10.3	8.23
		0.370	6400	51.3	8.23	6.69
	H_3^+ + ClCN	0.308	6330	51.3	8.37	6.68
	(H_2)	0.326	6440	51.3	7.76	6.39
		0.374	6280	51.3	7.88	6.18
		0.213	6470	51.3	7.83	6.65
		0.399	6420	51.3	7.63	6.23
	H_3^+ + BrCN	0.262	6350	51.3	5.76	4.47
	(H_2)	0.319	6140	51.3	4.53	3.47
		0.368	6260	57.3	5.40	4.20
		0.237	6270	51.3	5.98	4.77
		0.308	6290	51.3	5.39	4.09
	H_3^+ + ICN	0.334	6350	51.3	4.89	3.91
	(H_2)	0.329	6440	51.3	6.90	5.68
		0.291	430	51.3	3.69	3.01
	H_3^+ + C_2N_2	0.293	6470	49.5	4.01	3.46
	(H_2)	0.188	6410	49.5	4.34	3.73
		0.300	6600	49.5	4.24	3.78
(5.2)	H_3^+ + H_2S	0.413	6410	49.5	4.00	3.34
	(H_2)	0.334	6470	49.5	4.06	3.47

Reaction number	Reactants (Carrier)	P	$\bar{\nu}$	L	Gradient	k	
(5.6)	$HCO^+ + H_2S$	0.358	6430	49.5	1.73	1.45	
	(H_2)	0.331	6210	49.5	1.81	1.43	
(5.7)	$H_2S^+ + H_2S$	0.246	6740	49.5	0.518	0.492	a
	(He)	0.263	6710	49.5	0.660	0.622	b
		0.266	6880	49.5	0.745	0.731	b
		0.258	6930	49.5	0.667	0.679	b
		0.258	6920	49.5	0.546	0.546	c
		0.275	6880	49.5	0.616	0.605	c
(5.9)	$S^+ + H_2S$	0.246	6740	49.5	0.912	0.870	d
	(H_2)	0.267	6860	49.5	0.759	0.746	d
		0.252	6710	49.5	1.00	0.945	d
		0.273	6150	49.5	0.966	0.772	d
		0.258	6930	49.5	0.732	0.734	e
		0.275	6880	49.5	0.729	0.717	e

a. H_2S^+ produced by reaction of S^+ and SO_2^+ with H_2S

b. H_2S^+ produced by reaction of O^+ and O_2^+ with H_2S

c. H_2S^+ produced by reaction of He and He (2^3S) with H_2S

d. S^+ produced by reaction of He^+ with SO_2

e. S^+ produced by reaction of He^+ with H_2S

Reaction number	Reactants (Carrier)	P	$\bar{\nu}$	L	Gradient	k
(5.11)	$SO^+ + H_2S$	0.267	6860	49.5	0.910	0.897
	(He)	0.252	6720	49.5	1.04	0.981
		0.273	6150	49.5	1.01	0.804
		0.246	6740	49.5	1.11	1.06
(5.16)	$He^+ + H_2S$	0.256	6810	49.5	3.02	2.85
	(He)	0.258	6920	49.5	3.13	3.03
		0.279	6870	49.5	3.22	3.08
(5.17)	$HS^+ + H_2S$	0.258	6930	49.5	0.671	0.672
	(He)	0.275	6880	49.5	0.653	0.641
(5.18)	$S^+ + NH_3$	0.241	6780	49.5	1.50	1.45
	(He)	0.257	6670	49.5	1.39	1.30
		0.246	6750	49.5	1.47	1.41
(5.19)	$SO^+ + NH_3$	0.241	6780	49.5	1.28	1.25
	(He)	0.257	6670	49.5	1.34	1.25
		0.246	6750	49.5	1.44	1.38
(5.20)	$NH_3^+ + NH_3$	0.241	6780	49.5	1.28	1.25
	(He)	0.246	6750	49.5	1.06	1.02
(5.25)	$O^+ + H_2S$	0.258	6930	49.5	1.37	1.39
	(He)	0.263	6710	49.5	1.81	1.71

Reaction number	Reactants (Carrier)	P	$\bar{\nu}$	L	Gradient	k
(5.26)	$O_2^+ + H_2S$	0.258	6930	49.5	1.13	1.15
	(He)	0.263	6710	49.5	1.46	1.38
		0.266	6880	49.5	1.66	1.65
		0.258	6890	49.5	1.41	1.40
(5.30)	$C^+ + SO_2$	0.251	6520	49.5	2.75	2.52
	(He)	0.251	6470	49.5	2.60	2.33
		0.237	6400	49.5	2.60	2.28
(5.31)	$CO^+ + SO_2$	0.251	6520	49.5	2.04	1.85
	(He)	0.251	6470	49.5	1.86	1.65
		0.237	6400	49.5	1.69	1.48
	$C^+ + H_2S$	0.271	6830	49.5	1.79	1.75
	(He)	0.220	6900	49.5	1.69	1.72
		0.222	6980	49.5	1.72	1.79
		0.222	6980	49.5	1.73	1.80
	$CO^+ + H_2S$	0.271	6830	49.5	1.47	1.44
	(He)	0.220	6900	49.5	1.38	1.40
		0.222	6980	49.5	1.42	1.45
		0.222	6980	49.5	1.44	1.48

Reaction number	Reactants (Carrier)	P	$\bar{\nu}$	L	Gradient	k
(6.2)	$H_2CN^+ + NH_3$	0.460	6350	51.3	2.95	2.34
	(H_2)	0.610	6170	51.3	3.28	2.49
		0.287	6330	51.3	2.96	2.43
(6.4)	$HCO^+ + HCN$	0.280	6950	51.3	3.96	3.87
	(H_2)	0.362	6690	51.3	4.94	4.47
		0.262	6550	51.3	4.56	4.05
		0.386	6610	51.3	4.19	3.67
		0.492	6420	51.3	4.54	3.72
		0.362	6660	51.3	4.83	4.32
(6.7)	$HCN^+ + HCN$	0.222	6250	51.3	1.17	0.967 [a]
	(He)	0.229	6500	51.3	1.08	0.958 [a]
		0.225	6400	51.3	1.39	1.18 [b]
		0.232	6510	51.3	1.00	0.881 [b]
		0.235	6780	51.3	1.07	1.02 [b]
(6.8)	$C^+ + HCN$	0.222	6250	51.3	3.18	2.61
	(He)	0.229	6500	51.3	3.28	2.89
(6.9)	$C_2N^+ + HCN$	0.222	6250	51.3	0.409	0.336
	(He)	0.229	6500	51.3	0.322	0.285

a. HCN^+ formed by reaction of CO^+ with HCN

b. HCN^+ formed by reaction of He^+ and $He(2^3S)$ with HCN

Reaction number	Reactants (Carrier)	P	$\bar{\nu}$	L	Gradient	k
(6.10)	He^+ + HCN	0.225	6400	51.3	4.91	3.97
	(He)	0.228	6420	51.3	4.18	3.40
		0.198	6470	51.3	5.02	4.18
(6.11)	CN^+ + HCN	0.225	6400	51.3	3.65	2.94
	(He)	0.235	6780	51.3	2.72	2.58
(6.12)	CH^+ + HCN	0.225	6400	51.3	4.35	3.50
		0.235	6780	51.3	3.07	2.92
(6.17)	HCN^+ + H_2	0.186	6360	51.3	0.972	0.770
	(He)	0.180	6570	51.3	1.06	0.895
		0.175	6750	51.3	1.10	0.984
		0.251	6130	51.3	0.864	0.636
		0.286	6290	51.3	0.243	0.188

COMPUTER PROGRAM ION/RATES

```
C ***********************************************************************
C PROGRAM TO CALCULATE UP TO 10 RATE CONSTANTS OF ION MOLECULE REACTIONS
C AFTER LEAST SQUARES ANALYSIS OF RAW DATA.PROGRAM CORRECTS EACH VALUE
C OF K FOR PARABOLIC VELOCITY PROFILE WITH SLIP FLOW AND RADIAL
C DIFFUSION TO GIVE RATE1. RATE1 IS THEN CORRECTED FOR AXIAL DIFFUSION
C TO GIVE RATE2. AN EMPIRICAL END CORRECTION IS ASSUMED IN THE REACTION
C LENGTH TERM.
C ***********************************************************************$*****

      DIMENSION TITLE (70),DATE(70)
      DIMENSION RFLOW(25),SIGNL(25),ONSIG(25)
  200 FORMAT(1HO,8X,69(1H*))
  201 FORMAT(1HO,8X,70(1H-))
  202 FORMAT(1HO,'INPUT CHECK')
  203 FORMAT (1HO,//,5X,'TEMPERATURE',20X,G10.5,'DEG K',//,5X,'MEAN FREE
     *PATH',18X,G10.5,'CM',//,5X,'REACTION LENGTH',16X,G10.5,'CM',//)
  204 FORMAT(1HO,5X,'NUMBER OF REACTIONS',20X,I5,//)
  205 FORMAT(1HO,9X,70A1,/)
  206 FORMAT(1HO,5X,'REACTION TUBE PRESSURE',9X,G10.5,'TORR',/)
  207 FORMAT(1HO,5X,'DIFFUSION COEFFICIENT',10X,G10.5,'CM**2 PER SEC',/)
  208 FORMAT(1HO,5X,'AV.LINEAR VELOCITY OF CARRIER GAS',8X,G10.4,'CM PER
     * SEC',/)
  209 FORMAT(1HO,5X,'AV.FLOW OF NEUTRAL REACTANT',10X,G10.5,'PARTICLES P
     *ER SEC',/)
  210 FORMAT(1HO,5X,'ION SIGNAL (AMPS)',12X,'REACTANT FLOW(PARTICLES PER
     *SEC)')
  211 FORMAT(1HO,15X,'NUMBER OF POINTS FOR LEAST SQUARE ANALYSIS=',I5,/)
  300 FORMAT(70A1)
  310 FORMAT(1HO,5X,'SLIP FLOW FACTOR(B)=',G10.3,3X,'SLIP FLOW FACTOR(GA
     *MMA)=',G10.3,/)
  311 FORMAT(1HO,5X,'SLIP FLOW FACTOR(DELTA)=',G10.3,/)
  312 FORMAT(1HO,5X,'AXIAL DIFF CORRECTION FACTOR=',G10.3,//)
  313 FORMAT(1HO,//,5X,'RATE1=',G10.3,15X,'RATE2=',G10.3,//)
   30 FORMAT (1HO,8X,G10.3,20X,G10.3)
C
C ***********************************************************************
C READ IN DATA COMMON TO ALL REACTIONS FIRST : TEMPERATURE IN DEGREES K
C (TEMP)} MEAN FREE PATH IN CARRIER GAS AT 1 TORR AND 298 K IN CM
C (YMFP1)} REACTION LENGTH (INCLUDING END CORRECTION) IN CM (RLGTH)
C ALL DATA IN FREE FORMAT
C ***********************************************************************
      READ(5,/) TEMP,YMFP1,RLNGTH

C READ IN NUMBER OF REACTIONS (IN FIXED POINT AND FREE FORMAT) FOR WHICH
C K IS TO BE CALCULATED.
      READ(5,/)NREACT
C CHECK ALL INPUT DATA
      WRITE(6,200)

      WRITE(6,202)
      WRITE(6,200)
      WRITE(6,203) TEMP,YMFP1,RLNGTH
      WRITE(6,200)
      WRITE(6,204)NREACT
      WRITE(6,200)
      DO 800 IJ = 1,NREACT
C
C READ IN TITLE OF REACTION (I)
      READ(5,300)(TITLE(I) ,I=1,70)
C READ IN DATE OF REACTION
      READ(5,300)(DATE(I),I=1,70)
C ***********************************************************************
C READ IN VARIABLES WHICH APPLY TO EACH REACTION : PRESSURE IN REACTION
C TUBE IN TORR (PRESS)} AMBIPOLAR DIFFUSION COEFFICIENT OF REACTANT
C ION AT 298 K AND 1 TORR IN CM**2 PER SECOND (DIFCO)} AVERAGE LINEAR
C VELOCITY OF CARRIER GAS IN CM PER SECO D (FLOW)} AVERAGE FLOW RATE OF
C NEUTRAL REACTANT IN PARTICLES PER SECOND (BFLOW).
C ALL DATA IN FREE FORMAT
      READ(5,/) PRESS,DIFCO,FLOW,BFLOW
      DIFCO=DIFCO/PRESS
C READ IN NUMBER OF POINTS FOR WHICH LEAST SQUARES ANALYSIS TO BE DONE
C IN REACTION(I) IN FREE FORMAT AND FIXED POINT.
      READ(5,/) NUPNT
C READ IN CONSECUTIVE PAIRS OF VALUES OF NEUTRAL REACTANT FLOW IN
C PARTICLES PER SECOND (RFLOW(I)) AND ION SIGNAL IN AMPS (SIGNAL(I)).
C ALL DATA IN FREE FORMAT.
      READ(5,/)(RFLOW(I),SIGNL(I),I=1,NUPNT)
      DO 20 I=1,NUPNT
      ONSIG(I)=ALOG(SIGNL(I))
   20 CONTINUE
      WRITE(6,205)(TITLE(I),I=2,70)
      WRITE(6,201)
      WRITE(6,205)(DATE(I),I=2,70)
      WRITE(6,206)PRESS
      WRITE(6,207)DIFCO
      WRITE(6,208)FLOW
      WRITE(6,209)BFLOW
      WRITE(6,211)NUPNT
      WRITE(6,210)
      WRITE(6,201)
      WRITE(6,30)(SIGNL(I),RFLOW(I),I=1,NUPNT)
C
C PERFORM LEAST SQUARES ANALYSIS OF DATA.
C SLOPE = SLOPE} CEPT = INTERCEPT} SIGMA = STANDARD DEVIATION} COEF =
C CORRELATION COEFFICIENT} SDESLP = STANDARD ERROR IN SLOPE} SDEINT =
C SYANDARD ERROR IN INTERCEPT.
      CALL LEASSQ (RFLOW,ONSIG,NUPNT,SLOPE,CEPT,SIGMA,COEFF,SDESLP,SDEIN
     *T)
```

```
C CALCULATE FIRST VALUE OF K TO GIVE RATE 1,RATE 1 INCLUDES CORRECTION
C FOR PARABOLIC VELOCITY PROFILE WITH SLIP FLOW AND RADIAL DIFFUSION
C TRAD=RADIUS OF REACTION TUBE IN CM
      TRAD=4.74
      YMFP=YMFP1*SQRT(TEMP/298.)
      WSLIP=2./(1.+(5.52*YMFP/(PRESS*TRAD)))
      BSLIP=1.+(2.76*YMFP)/(PRESS*TRAD)
      AINT=(.25-BSLIP)*(.1-.6*BSLIP)-(.15-0.75*BSLIP)**2
      BINT=(1.6*BSLIP)-0.4
      CINT=(0.025)-(0.075*BSLIP)
      DEN=SQRT(BINT**2-32.*AINT)
      DEL=(1./(2.*AINT))*(BINT-DEN)
      GAM=-(1./(2.*AINT))*(CINT-((2.*BINT*CINT+6.4*AINT)/(2.*DEN)))
      DELTA=DEL/WSLIP
      GAMMA=GAM/WSLIP
      SLOPE=-SLOPE
      RATE1 =SLOPE*(3.1416*TRAD**2)*(FLOW**2)/(GAMMA*RLNGTH)
C CORRECTION FOR AXIAL DIFFUSION
      BCON=BFLOW/(3.1416*TRAD**2*FLOW)
      AXK= ((DELTA/(TRAD** 2)+(GAMMA*RATE1*BCON/DIFCO))/FLOW )
      AXCOR=(AXK/FLOW)*(DIFCO**2)
      RATE2=RATE1/(1.-AXCOR)
      WRITE (6,310)BSLIP,GAMMA
      WRITE(6,311)DELTA
      WRITE(6,312)AXCOR
      WRITE(6,200)
      WRITE(6,313)RATE1,RATE2
      WRITE(6,200)
  800 CONTINUE
      STOP
      END
```

```
      SUBROUTINE LEASSQ (RFLOW,ONSIG,NUPNT,SLOPE,CEPT,SIGMA,COEFF,SDESLP
     *,SDEINT)
C SUBROUTINE OBTAINS LEAST SQUARES FIT FOR ONSIG=SLOPE*RFLOW+CEPT AND
C RETURNS SLOPE,INTERCEPT,CORRELATION COEFF,STND DEVIATION,STND ERRORS
C IN SLOPE AND INTERCEPT.
      DIMENSION RFLOW(1),ONSIG(1)
  301 FORMAT(1HO,//,5X,'SLOPE=',G10.4,5X,'INTERCEPT=',G10.4,/)
  302 FORMAT(1HO,5X,'CORRELATION COEFF=',G10.4,5X,'STND DEVIATION=',G10.
     *4,/)
  303 FORMAT(1HO,5X,'STND ERROR SLOPE=',G10.4,6X,'STND ERROR INTERCEPT=!
     *,G10.4,//)
      ANUPNT=FLOAT(NUPNT)
      P=0.0
      Q=0.0
      R=0.0
      S=0.0
C SUMMATION OF P=RFLOW**2,Q=RFLOW,R=RFLOW*ONSIG,S=ONSIG
      DO 35 I=1,NUPNT
      P=P+RFLOW(I)*RFLOW(I)
      Q=Q+RFLOW(I)
      R=R+RFLOW(I)*ONSIG(I)
   35 S=S+ONSIG(I)
C CALCULATION OF SLOPE AND INTERCEPT
      DET=ANUPNT*P-Q*Q
      SLOPE=(ANUPNT*R-Q*S)/DET
      CEPT=(P*S-Q*R)/DET
C CALCULATION OF MEAN VALUE OF RFLOW(XBAR)AND ONSIG(YBAR)
      XBAR=Q/ANUPNT
      YBAR=S/ANUPNT
C CALCULATE SUMS FOR CORRELATION COEFFICIENT AND STND DEVIATION(SIGMA)
      SUMA=0.0
      SUMB=0.0
      SUMC=0.0
      DEV=0.0
      DO 40 I=1,NUPNT
      SUMA=SUMA+(RFLOW(I)-XBAR)*(ONSIG(I)-YBAR)
      SUMB=SUMB+(RFLOW(I)-XBAR)*(RFLOW(I)-XBAR)
      SUMC=SUMC+(ONSIG(I)-YBAR)*(ONSIG(I)-YBAR)
   40 DEV =(ONSIG(I)-SLOPE*RFLOW(I)-CEPT)**2+DEV
      COEFF=SUMA/SQRT(SUMB*SUMC)
      SIGM2=((SUMB*SUMC-SUMA*SUMA)/(SUMB*(ANUPNT-2.)))
      SDESLP=SQRT(SIGM2/SUMB)
      SDEINT=SQRT(SIGM2*(1./ANUPNT+XBAR*XBAR/SUMB))
      SIGMA=SQRT(DEV/(ANUPNT-1.))
      WRITE(6,301) SLOPE,CEPT
      WRITE(6,302)COEFF,SIGMA
      WRITE(6,303)SDESLP,SDEINT
      RETURN
      END
```

****

INPUT CHECK

****

TEMPERATURE 300.00 DEG K
MEAN FREEPATH .94000E-02CM
REACTION LENGTH 57.300 CM

****

NUMBER OF REACTIONS 1

****

H3+ + CLCN

28.9.75.B

REACTION TUBE PRESSURE .30800 TORR

DIFFUSION COEFFICIENT 1590.9 CM**2 PER SEC

AV.LINEAR VELOCITY OF CARRIER GAS 6330. CM PER SEC

AV.FLOW OF NEUTRAL REACTANT .50000E+17PARTICLES PER SEC

NUMBER OF POINTS FOR LEAST SQUARE ANALYSIS= 17

ION SIGNAL (AMPS)	REACTANT FLOW(PARTICLES PERSEC)
.240E-06	0.
.103E-06	.154E+17
.168E-07	.359E+17
.215E-07	.415E+17
.960E-07	.212E+17
.165E-07	.334E+17
.360E-07	.281E+17
.590E-08	.502E+17
.820E-09	.723E+17
.100E-09	.995E+17
.410E-07	.264E+17
.660E-08	.442E+17
.630E-09	.727E+17
.900E-10	.101E+18
.180E-10	.117E+18
.165E-09	.899E+17
.210E-07	.342E+17

SLOPE=-.8371E-16 INTERCEPT=-14.84

CORRELATION COEFF=-.9956 STND DEVIATION=0.2673

STND ERROR SLOPE= .2031E-17 STND ERROR INTERCEPT=0.1249

SLIP FLOW FACTOR(B)= 1.02 SLIP FLOW FACTOR(GAMMA)= 0.638

SLIP FLOW FACTOR(DELTA)= 3.72

AXIAL DIFF CORRECTION FACTOR= .288E-01

****

RATE1= .648E-08 RATE2= .667E-08

****

APPENDIX III

CIRCUIT DIAGRAMS

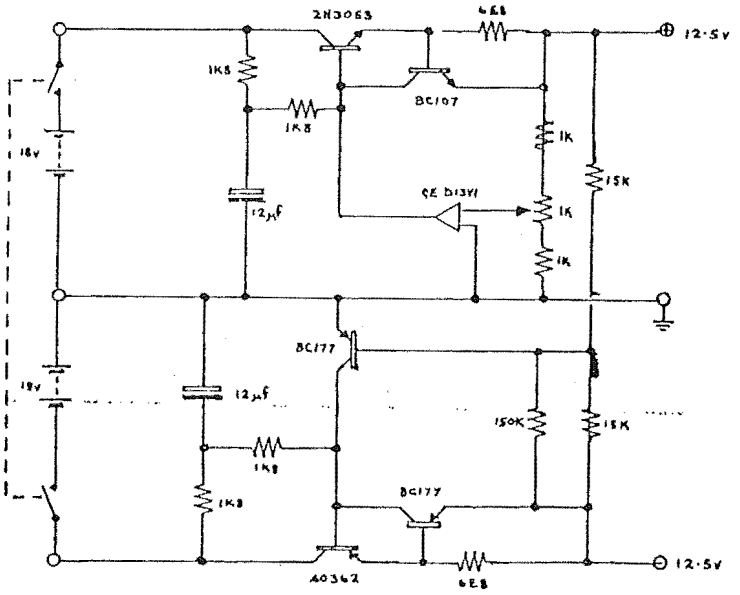

voltage regulator

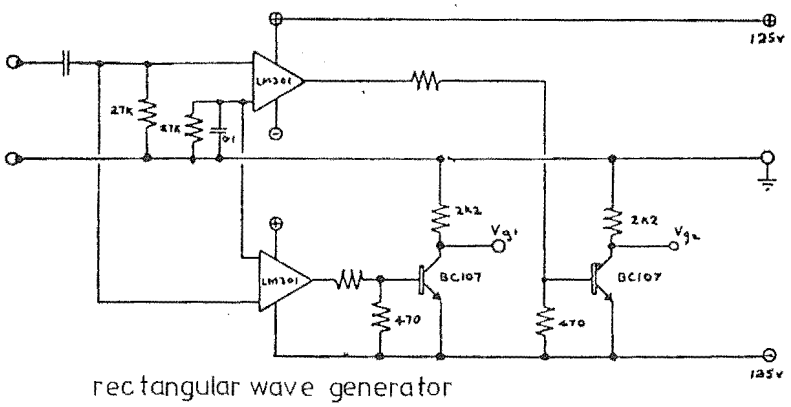

rectangular wave generator

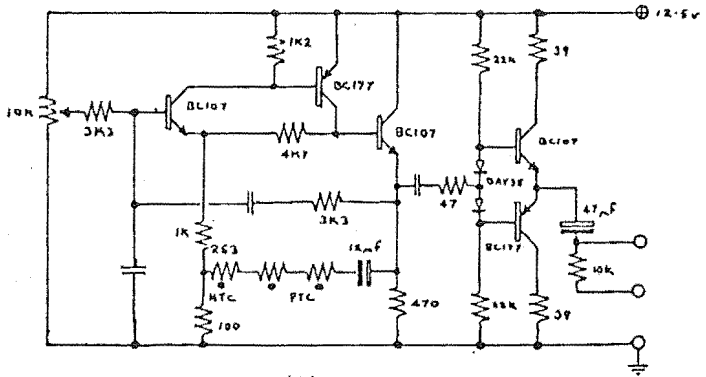

oscillator

IIIa. Control unit for P7D differential pressure transducer.

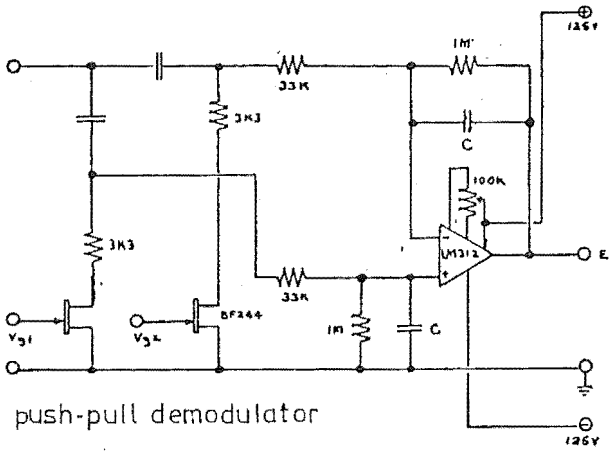

push-pull demodulator

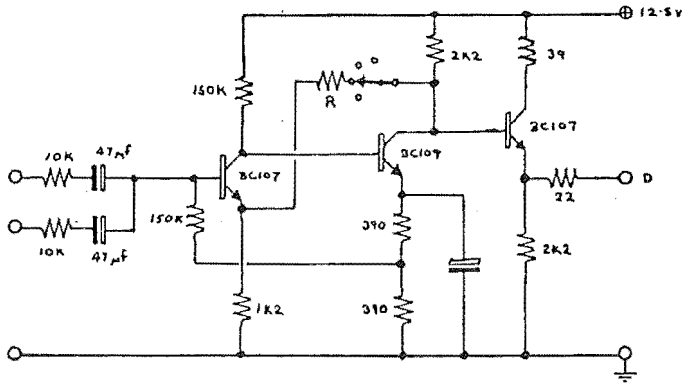

signal amplifier

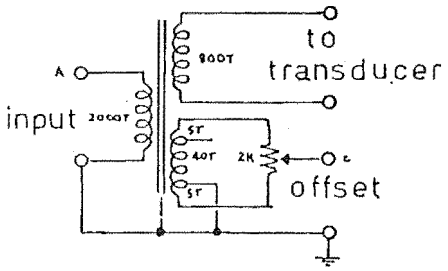

transformer connections

IIIa.(cont.) Control unit for the P7D differential pressure transducer.

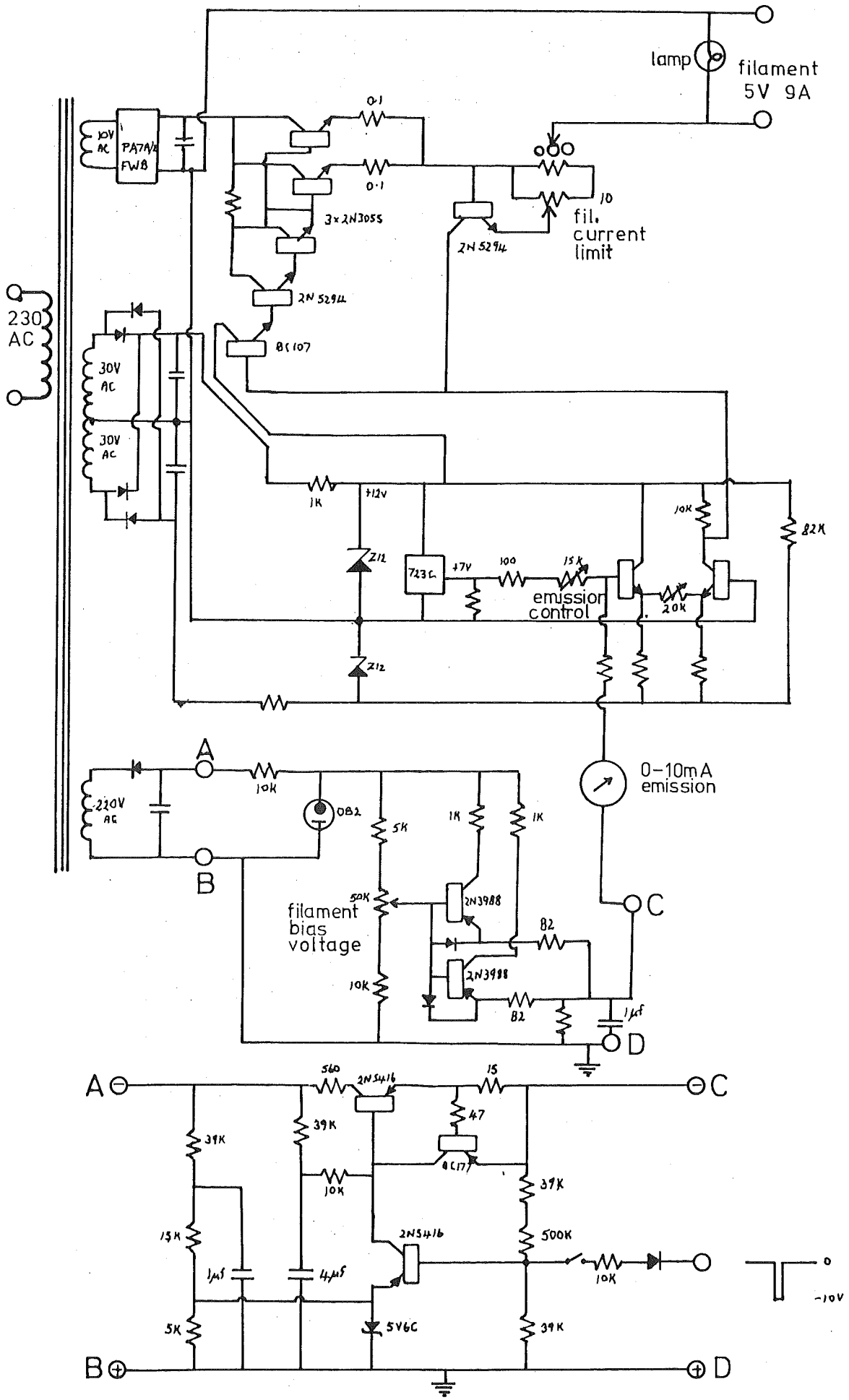

IIIb. Emission control unit.